

Descending Control of Limb Movements in *Drosophila melanogaster*

by

Cynthia Tien-Cynn Hsu

Department of Neurobiology
Duke University

Date: _____

Approved:

Vikas Bhandawat, Supervisor

Stephen G. Lisberger, Chair

Marc Sommer

Rebecca Yang

Dissertation submitted in partial fulfillment of
the requirements for the degree of Doctor
of Philosophy in the Department of
Neurobiology in the Graduate School
of Duke University

2016

ABSTRACT

Descending Control of Limb Movements in *Drosophila melanogaster*

by

Cynthia Tien-Cynn Hsu

Department of Neurobiology
Duke University

Date: _____

Approved:

Vikas Bhandawat, Supervisor

Stephen Lisberger, Chair

Marc Sommer

Rebecca Yang

An abstract of a dissertation submitted in partial
fulfillment of the requirements for the degree
of Doctor of Philosophy in the Department of
Neurobiology in the Graduate School of
Duke University

2016

Copyright by
Cynthia Tien-Cynn Hsu
2016

Abstract

Because the interactions between feedforward influences and feedback circuits are inextricably linked during many motor outputs (including but not limited to walking), the contribution of descending inputs to the generation of movements is difficult to study. Here we take advantage of the relatively small number of descending neurons (DNs) in the *Drosophila melanogaster* model system. We first characterize the number and distribution of the DN populations, then present a novel load free preparation, which enables the study of descending control in a context where sensory feedback can be reduced while the animal remains intact. Lastly we use *in-vivo* whole cell patch clamp electrophysiology to characterize the role of individual DN's in response to specific sensory stimuli and in relationship to movement. We find that there are approximately 1100 DN's in *Drosophila* that are distributed across six clusters. Input from these DN's is not necessary for coordinated motor activity, which can be generated by the thoracic ganglion, but is necessary for the specific combinations of joint movements typically observed in forward walking. Lastly, we identify a particular cluster of DN's that are tuned to sensory stimuli and innervate the leg neuromeres. We propose that a multi-layered interaction between these DN's, other DN's, and motor circuits in the thoracic ganglia enable the diverse but well-coordinated range of motor outputs an animal might exhibit.

Contents

Abstract	iv
List of Tables	ix
List of Figures	x
Acknowledgements	xvii
1. Introduction	1
1.1 Overview	1
1.2 Descending tracts are complex	3
1.3 Models of descending control.....	4
1.3.1 Command neuron model of descending control	4
1.3.2 Dynamical decision making and motor control.....	6
1.4 Role of central pattern generators (CPGs) in movement.....	7
1.5 The insect as a model system.....	9
1.5.1 The insect brain consists of two major structures	9
1.5.2 Anatomy of insect legs.....	10
1.5.3 Stance and swing phases are driven by coordination among multiple joints in a single leg	11
1.5.4 Coordination among legs	12
1.5.4.1 Straight line forward locomotion.....	12
1.5.4.2 Perturbations of feedback	13
1.6 Characterizing the logic of descending control.....	15

2. Anatomical organization of DNs.....	17
2.1 Overview and rationale	17
2.2 <i>Drosophila</i> have ~1,100 DNs distributed in six major clusters	19
2.2.1 <i>Drosophila</i> have ~1,100 DNs.....	19
2.2.2 DNs are organized in 6 clusters.....	20
2.2.2.1 b-Anterior clusters	22
2.2.2.2 <i>Pars Intercerebralis</i> cluster	23
2.2.2.3 Gnathal ganglia cluster	24
2.2.2.4 Superior Medial Protocerebrum (SMP) cluster	25
2.2.3 Assessing efficiency of backfilling technique for labeling DNs.....	25
2.3 Neuropil labeled by backfill from cervical connective.....	28
2.4 Distribution of DNs by neurotransmitter	31
2.4.1 Major excitatory (cholinergic) and inhibitory (GABAergic) neurotransmitters in the DN populations	33
2.4.2 Minor neurotransmitters	34
2.4.3 Neurotransmitters not accounted for and other caveats	36
2.5 Discussion.....	37
3. Characterization of load free leg movements	40
3.1 Overview and rationale	40
3.2 Methodology	41
3.3 Kinematics of load-free leg movements can be categorized into stop, initiation, and burst phases.....	43

3.4.1 Stops return to a small region with high probability, suggesting the stop position is mostly determined by passive muscle control.....	47
3.4.2 Movement initiation is driven primarily along the protraction/retraction axis	48
3.4.3 Bursting movement in different legs is controlled independently.....	50
3.5 Characterization of burst types	52
3.5.1 Discrete types of bursts are achieved via different combinations of joint movements	52
3.5.2 Bursts can be defined as repeating sequences of different states	57
3.6 Descending inputs are necessary for generating cycle to cycle variability	59
3.7 Structured movement in load free preparations is affected by activity in the brain	63
3.8 Activation of specific DNs changes the probability distribution of bursts observed in a subset of legs.....	70
3.9 Conclusions	74
4. The role of the AOTU DN cluster in descending control.....	76
4.1 Overview and rationale	76
4.2 Methodology	77
4.3 AOTU DNs subdivide into two clusters	78
4.3.1 Most if not all AOTU DNs in the ventral cluster are leg innervating.....	79
4.3.2 Wing innervating AOTU DN in dorsal cluster	84
4.5 AOTU DNs are broadly tuned to sensory information	86
4.6 Activity in the ventral cluster corresponds to movement initiation in the legs	90
4.7 Conclusions	92

5. Discussion	93
5.1 Drosophila have ~1100 DNs in at least six discrete clusters.....	93
5.1.1 Clusters of DNs express multiple neurotransmitter types.....	93
5.1.2 Number and organization of DNs across arthropods appears conserved.....	94
5.2 Descending control of limb movements is multi-layered.....	96
5.2.1 Some coordination between joints within a leg is generated at the level of the thoracic ganglia.....	96
5.2.2 Coordination across legs requires some form of feedback.....	97
5.2.2 DNs in the GNG	98
5.2.3 A subset of DNs tuned to sensory stimuli may be involved in movement initiation.....	99
5.2.4 Putative roles of DNs in other clusters.....	101
Appendix A: Neurotransmitter Specific DNs by Cluster.....	103
Appendix B: Neuronal activation and inactivation by P2X2 and ort	106
Appendix C: Visual stimuli	111
References	113
Biography	124

List of Tables

Table 1: Number of DNs per cluster in <i>Drosophila</i> versus other insects.....	21
Table 2 : Percent of DNs by neurotransmitter	36
Table 3 : Activation and inactivation of the midline gnathal ganglion (where the GNG cluster is located).....	64
Table 4 : Number of cycles observed during inactivation of the SMP cluster with histamine	66
Table 5 : Prothoracic cycle types in response to activation of SMP	67
Table 6 : Mesothoracic cycle types in response to activation of SMP	68
Table 7 : Mesothoracic cycle types in response to activation of SMP	69
Table 8 : Octopaminergic DNs labeled using Tdc2-Gal4.....	103
Table 9 : Serotonergic and Dopaminergic DNs labeled using Ddc-Gal4	103
Table 10 : Glutamatergic DNs labeled using VGlut-Gal4	104
Table 11 : GABAergic DNs labeled using a GABA antibody	104
Table 12 : Cholinergic DNs labeled by Cha-Gal4 driver	104

List of Figures

Figure 1: Segments, joints, and their respective degrees of freedom in an insect leg. (A) The four major limb segments in *Drosophila* and other insects. (B) Retraction (backwards motion) and protraction (forwards motion) occurs around the Thorax-Coxa joint, where the coxa attaches to the thorax. (C) Levation (upwards motion) and depression (downwards motion) occurs around the Coxa-Trochanter joint, located between the coxa and the femur. (D) Extension and flexion occurs around the femur-tibia joint. 11

Figure 2: *Drosophila* have ~1100 DNs distributed in 6 clusters. (A) Representative confocal image stacks showing the distribution of DN clusters. Maximum projection of dextran label (white) over the range specified, superimposed on a section of neuropil containing the representative anatomical markers (anti-nc82, purple). (B) Schematic illustrating the mean distribution of DNs in the 6 clusters. Each cluster is represented with a different color. Each dot represents approximately 10 DNs. 23

Figure 3 : Using a sparse genetic label to estimate the efficiency of labeling. E49-Gal4/tsh-Gal80;UAS-CD8GFP labels a small number of DNs which are distributed across five of the six clusters. (A) Retrograde labeling to identify the DNs in the brain. (B) GFP+ neurons labeled by the E49-Gal4 driver. (C) Merge showing colabeling (D) Inset showing the GNG cluster. Arrows indicate colabeling (GFP+ DNs). (E) Inset showing the colabeled DNs in the SMP cluster. (F), (G), and (H) are from a different brain. 27

Figure 4 : Pattern of neuropil labeling suggest distinct regions for sensory, associative, and motor processing. (A) Density of labeling for different neuropil regions. (B) Projections of a confocal stack show dextran labeling (white) and neuropil labeling (magenta). Regions marked in yellow are expanded in panels (C-G). (C) Sparse innervation of the lobula. (D) Sparse innervation of the anterior optic tubercle. (E) Sparse innervation of the lateral horn. (F) Dense innervation of the posterior ventrolateral protocerebrum, where optic glomeruli are found. (G) Dense innervation of AMMC and surrounding neuropil. For clarity, only a single representative 1 μ m slice is shown. The extent of the image stack is different for the images in (B-G). 30

Figure 5 : Strategy for labeling DNs with a given neurotransmitter. (A) Schematic illustrating that the subset of GFP+ neurons labeled by a Gal4 driver can be identified as DNs if they are also colabeled by retrograde labeling (yellow). Schematic illustrating that the subset of GFP+ neurons labeled by a Gal4 driver can be identified as DNs if they are also colabeled by retrograde labeling (yellow). (B-J) Projection of a confocal stack of a retrogradely labeled brain in which all cholinergic neurons are labeled using Cha-

Gal4,UAS-GFP (green). Retrograde label is in red. Cholinergic DNs are colabeled and appear yellow. (K-M) Close-up of the region in white square in (D), (G), and (J) show the co-labeled neurons 32

Figure 6 : Schematics showing distribution of DNs by neurotransmitter. (A) Distribution of cholinergic (red) and GABAergic DNs (green). Dots are in proportion to the fraction of DN of a given type. (B) Distribution of DNs which employ other (minor) neurotransmitters. Each dot represents a single DN. 34

Figure 7 : Autotracking in a load free preparation. (A) Diagram showing the preparation, in which the fly has fluorescent polyethelene spheres glued to its legs, is fixed to a foil, then illuminated and filmed from below. (B) Image of a fly with natural light, a 365 nm light, and a 420 nm light. (C) Image of the fly with a 365 nm and a 465 nm light conditions. (D) Background subtraction removes everything except the balls, which marks the tips of the legs. 42

Figure 8 : Movement can be separated into discrete phases on the basis of speed. (A) Bursting type movements (red) were time when speed exceeded an empirically set threshold (red dashed line). Slow initiation type movements were separated from burst movements on the basis of speed, if they occurred between a stop and a burst; initiation movements that followed a burst were identified as such if the below threshold speed was observed for at least 200 ms. (B) Representative example of a stop, initiation, and burst bout shown in blue, green, and red, respectively. The blue circle identifies the first timepoint during which the leg was stopped. (C) The distribution of stop accuracy, burst amplitude, and frequency. Amplitude and frequency of bursts overlaps with that which is typically seen in freely walking flies, as indicated by the grey boxes (Wosnitza, Bockemuhl et al. 2013). Boxes represent quartiles; outliers represent points outside the whiskers (more than three times the interquartile range)..... 46

Figure 9 : Stops return to a small region with high probability. Each color represents the 80% most likely stop positions for an individual fly (different flies represent different individuals). The irregular polygon outlined in gray represents the distribution of all XY positions observed in all flies for the leg in question. The dashed grey circle circle represents the theoretical region a leg might occupy, computed using the maximum distance between the leg and its associated CTr joint as the radius. 48

Figure 10 : Movement initiates along a stereotyped direction. (A) Representative examples of different movement initiation bouts observed in the right prothoracic leg. (B) Distribution of probability of movement in a particular trajectory during initaion represented in an angle wedge histogram. Each wedge represents 20°. The radius of the

circle represents 0.2. The solid gray circle represents the distribution that would be expected if all directions of motion were equally probable. (C) Resultant vector computed from the axis of the movement trajectories of individual flies. Each individual fly is represented by a different arrow. The magnitude of the arrow represents the relative magnitude of the vector. As in (B), the radius of the circle represents 0.2. 49

Figure 11 : Legs are under independent control. (A) Examples of time periods during which only one leg was bursting. For the first (left) two examples, 200 ms are plotted for each leg. For the third example, 417 ms are plotted. Each leg is drawn in a different color. Open circles represent the first timepoint plotted. (B) Number of legs bursting during times when at least one leg is bursting. (C) Examples periods of bursting in which individual legs do not maintain a constant phase relationship with each other. Symbols are the same as in (A). (D) Examples of legs in which bursts do maintain a constant phase relationship with each other. Symbols are the same as in (A)..... 51

Figure 12 : Characterizing different degrees of freedom displayed by the different limb segments of the fly's legs. (A) Diagram demonstrating how fixing different colored balls to different limb segments changes in the orientation of these limb segments with respect to the line parallel to the length of the fly (the tibia-flyaxis and the tarsus-flyaxis angles) could be computed. (B) Diagram demonstrating how the tarsus-coxa radius is computed and how it varies as a result of extension (filled circles, brown leg) or flexion (open circles, grey leg). (C) Diagram demonstrating how the tarsus-coxa radius is computed and how it varies as a result of extension (filled circles, brown leg) or flexion (open circles, grey leg). (D) Representative example of movement of the femur but not the tibia. (E) The tarsus-flyaxis angle and the tibia-flyaxis angle maintain a constant linear relationship with the femur-flyaxis angle, suggesting that any changes in the orientation of the tarsus and tibia relative to the flyaxis are the result of changes in the orientation of the femur. (F) The flexion angle remains constant because there is no movement of the tibia independent of the movement in the femur. (G) The tarsus-coxa radius remains constant, indicating no movement around the FTi axis. (H) Representative example of movement driven primarily by extension and flexion around the FTi joint. (I) The tibia-flyaxis angle changes even during periods when there is little change in the femur-flyaxis angle, indicating flexion and extension. The tarsus-flyaxis angle also has a similar relationship to the femur-flyaxis angle. (J) As predicted by (I), the angle of flexion is changing throughout the trajectory of the movement shown in (H). (K) Extension and flexion of the FTi-joint results in a large decrease in the distance of the tarsus from the coxa. (L) Representative example of movement with both protraction-retraction and flexion/extension. (M), (N), and (O) similar to (I), (J), and (K). 54

Figure 13 : Probability of states and state transitions. (A) Fraction of bursting time the fly spends in each of the eight states. n=number of legs for which data was obtained. Total time bursting in parentheses. (B) Probability of transitioning from State A (row) to State B (column). Number of legs same as in A. 56

Figure 14 : Bursts can be defined as repeating sequences of different states. (A) Two representative examples of the most common type of burst cycle, Ret-Pro-Ret, for the mesothoracic leg. The trajectories through x and y are shown as well as the change in state over time. (B) Two representative examples of another type of burst cycle, Ret-Flex-Pro, commonly observed in the mesothoracic leg. As in (A), the trajectories through x and y are shown as well as the change in state over time. (C) Example of a burst bout observed in the metathoracic leg where multiple cycle types were observed within a single bout, as a consequence of variability throughout the bout on a cycle by cycle basis. (D) Example of a burst bout observed in the metathoracic leg where there were several sequential repetitions of one cycle type (Ret-Pro), followed by several repetitions of a different cycle type (RetFlex-Pro-ProExt)..... 58

Figure 15 : The burst cycle types that make up 80% of the cycles observed in each leg. Each color represents a different state. n_c refers to the total number of cycles observed. 59

Figure 16 : Headless flies show a reduction in burst probability and burst diversity, but an increased probability of exhibiting atypical states. (A) For individual flies, probability of bursting was greatly reduced after severing the neck. This was true for both the meso and the meta legs. Probability of bursting in any of the four legs that were tracked was also reduced. (B) Representative example of the distribution of burst trajectories in one metathoracic leg in an individual fly, showing the reduction in the range of motion after the neck has been severed. (C) All of the burst bouts observed in the fly/leg shown in (B) after severing the neck. Colors represent different states. (D) Representative example of the burst bouts observed in a different fly after severing the neck. (E) Fraction of total bursting time spent in each state. 62

Figure 17 : Activation of moonwalking DNs. (A) Although activating the moonwalking DNs did not greatly perturb the probability of observing common cycles such as Ret-Pro and Flex-Ext, there was an increased probability of observing atypical cycles such as Ret-Pro-ProExt, Ret-Flex-Ext, Ret-Flex-ProExt, and Ret-Pro-Ext. The control data in this figure only includes the no drug trials recorded from the same individual flies. (B) There was no consistent change in the probability of protraction preceding retraction across individual flies..... 73

Figure 18 : AOTU DNs can be further subdivided into two clusters. (A) Representative Z-projection of the anterior half of a brain in which the retrograde label has been applied to the neck. The yellow square indicates the region shown in (B) and (C). (B) Zoomed in image of the AOTU cluster, illustrating the presence of two distinct clusters. The anterior optic tubercle outlined in yellow. Yellow arrowheads indicate the presence of two different tracts leading away from the AOTU cluster (suggesting a separate tract for the dorsal and the ventral subcluster). (C) Identical confocal stack as shown in (A) and (B), but recolored to show the colabeling between the Gal4 driver specific to AOTU DNs (e49-Gal4, shown in green) and the retrograde label identifying DNs (shown in red). Arrows represent dorsal (d) and ventral (v) cells labeled by the e49-Gal4 driver.79

Figure 19 : Representative examples of DNs in the ventral AOTU subcluster, showing that while the projections of DNs in this subcluster are heterogeneous, all innervate the LAL and the inferior slope. (A-C). Single cell fills of ventral AOTU DNs obtained through diffusion of neurobiotin into the cell during whole cell patch clamp recording. White represents the Z projection of the neurobiotin in the anterior portion of the brain. Purple represents a representative section of the neuropil (stained with nc-82) containing the reference markers shown in (D). (A), (B), and (C) represent different example neurons. The color with which their respective columns has been outlined corresponds to the color drawn in the schematics in (D), (H), (L), and (P). (D). Six representative cell fills for different ventral AOTU DNs are manually traced and shown superimposed on neuropil markers in a reference brain. Each color represents a different DN. (E-P). Same as (A-D), but for successively more posterior sections of the brain with corresponding reference neuropil markers as drawn in (H), (L), and (P). Scalebars in all panels represent 100 μ m. In (A-C) and (E-G), the dotted outline indicates the LAL. In (I-K) and (M-O), the dotted yellow line indicates the inferior slope. 80

Figure 20 : The pattern of leg neuromere innervation of DNs in the ventral AOTU subcluster could be subdivided into two types. (A) Schematic representation of a single cell fill of type v1. The darker the trace, the more anterior the projection in the brain and the more ventral projection in the thoracic ganglia. (B) Z projection of the confocal stack from which the schematic in (A) was obtained. The square with the dotted yellow outline represents the region used in (C). (C) The projection along the anterior to posterior axis of the mesothoracic ganglia, as outlined by the square with a dotted yellow line in (B). (D) Projection from the lateral view of the thoracic ganglia shown in (A). (E) Schematic representation of a single cell fill of type v2. Intensity of the trace represents the same as in (A). (F) Z projection of the confocal stack from which the schematic in (E) was obtained. The square with the dotted yellow outline represents the metathoracic ganglia, the region used in (G). (G) The projection along the anterior to

posterior axis of the metathoracic ganglia, as outlined by the square with a dotted yellow line in (E). (H) Representative slice through the axonal tract of the neuron shown in (F). (I) Representative slice showing the innervation of the leg neuromeres by the neuron shown in (F). In all panels, the scale bar represents 50 μm 82

Figure 21 : Denmark and synaptotagmin labeling for ventral clusters. (A) e49-Gal4>UAS-Denmark,synaptotagmin. The e49-Gal4 driver labeled three AOTU ventral DNs and one AOTU dorsal DN. White dashed lines outline the LAL. (B) Neurobiotin single cell fill of one of the two e49-v1 DNs, shown in green. Denmark shown in red. White rectangle represents the region magnified in panel (C). (C) Magnification of the region outlined by the white rectangle in panel (B), showing that the innervation of the e49-v1 DN in the inferior slope is probably axonal rather than dendritic. Colors are the same as in panel (B). In all three panels, the scale bar represents 50 μm 84

Figure 22 : Neurons in the dorsal AOTU subcluster innervate the accessory mesothoracic neuromere but not the legs. (A) Schematic representation of a single cell fill of type v1. The darker the trace, the more anterior the projection in the in the brain and the more ventral projection in the thoracic ganglia. (B) Z projection of the confocal stack from which the schematic in (A) was obtained. (C) Representative slice through the approximate midline of the fly, showing the innervation of the wing neuromere (outlined in dashed yellow). (D) Representative slice showing the lack of innervation in the leg neuromeres. 85

Figure 23 : Denmark labeling for e49-dorsal. (A) Single cell fill (green) of e49-Gal4>UAS-Denmark (Denmark shown in red). Z projection over the entire brain shows the colabeling (yellow) between the Denmark and the neurobiotin fill of the inferior slope on the posterior surface of the brain. The regions for which a subset of the stack were magnified in panels (B) and (C) are shown outlined in white. (B) Colabeling in the anterior optic tubercle of neurobiotin (green) and Denmark (red). Colabeling appears yellow and is indicated by the white arrows. (C) Colabeling in the anterior optic tubercle of neurobiotin (green) and Denmark (red). Colabeling appears yellow and is indicated by the white arrows. In all three panels, the scale bar represents 50 μm 86

Figure 24 : Comparison of how DNs in the AOTU cluster are tuned to sensory information but have heterogeneous responses to the same stimuli. (A) Responses of e49-dorsal. Gray trace in top panels are shown as the mean and STD of cells, where the data collected from each cell is averaged over all trials. Bottom panels contain the mean and STD of all moving (red) and non-moving (blue) trials. (B) e49-v1. Colors are the same as in (A). (C) e49-v2. Colors are the same as in (A). Stray capacitance current from noise

in the electrophysiology rig was observed at the offset of the mechanosensory stimulus. Movement of the legs was computed as a change in pixel intensity in the recorded video.	88
Figure 25 : DNs in the AOTU cluster respond to broad field stimuli (moving gratings) but not small field stimuli (such as an expanding square). However, these responses vary in magnitude.....	90
Figure 26 : Depolarization precedes movement initiation in e49-v2. (A) Individual representative movement bouts, lined up according to movement onset. (B) Average voltage and movement for one fly. (C) Mean and standard deviation in response for 4 flies.	91
Figure 27 : There is no relationship between activity in e49-dorsal and movement initiation. Left: average voltage and movement for one fly. Right: mean and standard deviation in response for 4 flies.	92
Figure 28 : Representative examples of the effect of (B) ATP and (C) His on neuronal activation and inactivation for a single cell. Each color represents a different trial. The Drug was delivered at time=0. Diagram in (A) illustrates where the position indicated by the variable X is located relative to the position of the pipette. This schematic is not drawn to scale.....	108
Figure 29 : Mean and SEM data for effects of ATP activation (A) and His inactivation (B). (A) For each neuron (n=6), the average response to ATP over the three trials recorded at each position of the drug pipette was computed. The peak response at each position was then normalized by the peak response overall. (B) Same as for (A), except that the peak refers to the lowest voltage (or the largest magnitude of hyperpolarization). n=5.	109
Figure 30 : Response of a GFP+ neuron in a fly of genotype <i>UAS-mCD8-GFP/+; VT50660/UAS-P2X2</i> to ATP. Time and position as indicated in the title.....	110
Figure 31 : Schematic showing the position of the screen relative to the fly. The screen is represented by the solid black line. Schematic not drawn to scale.....	111

Acknowledgements

This project would not have been possible without the continued mentorship of my advisor, Dr. Vikas Bhandawat, who has continued to provide me feedback through every step of the scientific process and through his mentorship helped me to achieve things that I would have otherwise thought I was not capable of. I would also like to thank Dr. Katherine Anne Tschida, a former postdoc in the lab who made seminal contributions to the initial stages of this process, especially troubleshooting the retrograde labeling and setting up the electrophysiology rig.

I would also like to thank my committee, Drs. Steve Lisberger, Marc Sommer, and Rebecca Yang, for their incredible insight, encouragement, and support.

I would also like to thank the personal support network which has simultaneously encouraged me while enforcing much needed breaks throughout the past six years, and provided me with incredible memories of my time in Durham and at Duke. This includes the incredibly supportive, open, and friendly community of graduate students, postdocs, and faculty that both Duke Neurobiology and Biology has provided me with, as well as friends that I have made through Shotokan karate and the local board game group.

In addition, I would like to thank everyone who has ever helped me to get to this point, especially those who helped me reach graduate school in the first place: Andrew

Steele, Jon Pierce-Shimomura, Michael Dickinson, Allan Wong, Alice Robie, Gregory E. Sims, Joel Sachs, and Ellen Simms. The faith, encouragement, and support that they all provided to me, though many years past, definitely provided a crucial bedrock to my persistence and endurance during the past six years.

Lastly, I would like to thank my family. My older sister, Vicky, who has always been there for me through all of my emotional ups and downs throughout the past thirty years and provided me with a sane, good-humored and objective voice during the times when it was desperately needed. My parents, for forgiving me for not going to medical school as well as being too busy to talk to them as often as they'd like during the past six years. And my boyfriend, Michael, who has never ceased to provide me with emotional (as well as some intellectual) support, in spite of my decision to move across country from him in order to learn electrophysiology in fruit flies.

1. Introduction

1.1 Overview

The ability to execute precise, well-timed and coordinated movements that can be flexibly adapted to changes in the environment is a complex procedure that requires integration of both feedforward control (from the brain to circuits in the body) and feedback control (from load, stretch, and proprioceptors in the limbs). Both feedforward and feedback control can alter the pattern of muscle activity by acting on local motor circuits, or central pattern generators (CPGs), which are neuronal networks characterized with intrinsic rhythmic activity.

A conserved feature of motor control across the animal kingdom is the anatomical separation between the circuits for feedforward and feedback control. Circuits that integrate sensory information and initiate movement are found in the brain, while those that control rhythm generation are found in spinal cord/ventral nerve cord/segmental ganglia (collectively called body ganglia). These two circuits are connected by descending neurons (DNs), which have their cell bodies in the brain and carry sensory processing and motor-related information to the body ganglia, and ascending neurons (ANs), which have their cell bodies in the body ganglia and carry motor-related and sensory feedback information to the brain. This anatomical separation represents a bottleneck in information processing, as the large number of neurons in the brain must converge onto a relatively small number of descending neurons, while the

small number of descending neurons must provide sufficient information to the CPGs to enable flexible but context appropriate motor output.

Although the DNs represent a bottleneck in information processing relative to the rest of the central nervous system, the information encoded in these neurons is still not well understood. This is largely because the neurons in the DN population are distributed over various regions throughout the brain, and thus receive a diversity of inputs and send projections along many different tracts. In addition, a significant fraction of the input received by DNs is recurrent, as it may include information from other descending tracts or ascending input from the body ganglia.

The *Drosophila* model system is a uniquely advantageous model for disentangling the diverse functions of the different DN tracts because it has an intermediate level of complexity. *Drosophila* have fewer neurons relative to mammalian systems but are still capable of a diversity of behavioral outputs. This diversity includes behaviors that can involve either coordinated or independent control of multi-jointed limbs, and be executed in response to a diversity of sensory modalities. In addition to its intermediate level of complexity, the *Drosophila* system has the advantage of the availability of many genetic tools, which enable reproducible identification and manipulation of neurons across individuals in a population. When combined with their relatively small number of neurons, the *Drosophila* system becomes an incredibly powerful model for elucidating the relative contributions of individual DNs.

1.2 Descending tracts are complex

In mammals, there are two major descending pathways originating in the brainstem. The first group, the ventromedial brainstem pathways, includes tectospinal tracts from the midbrain, lateral and medial vestibulospinal tracts, and the reticulospinal and bulbospinal projections from the pontine and medullary reticular formation. The ventromedial tracts terminate in the ventromedial intermediate zone of the spinal cord and have functions that include postural control for the head, neck, and trunk, proximal limb movements, and control of respiration (Lemon 2008). The second group, the dorsolateral brainstem pathways, includes the rubrospinal tract from the red nucleus and the pontospinal tract from the ventrolateral pontine tegmentum. The dorsolateral brainstem tracts terminate in the dorsal and lateral regions of the intermediate zone in the spinal cord, which gives rise to propriospinal neurons with local projections. This suggests that these tracts may play a role in the movement of the distal limb segments such as the elbow and the wrist. However, the divisions between the two categories are not absolute. For instance, some tectospinal and medullary reticulospinal fibers belonging to the ventromedial brainstem tract terminate in the lateral intermediate zone rather than the ventromedial intermediate zone (Alstermark et al 1987).

The two pathways in the pyramidal tract, the corticospinal and corticobulbar pathways are present in all mammals but to very different extents (Lemon 2008). In more primitive mammals such as edentates, marsupials, and lagomorphs, the

corticospinal pathways project primarily to the dorsolateral intermediate zone and the motor nuclei of the spinal cord. Thus, in these mammals, the majority of the projections overlap with those of the dorsolateral brainstem tracts but not the ventromedial tracts. In contrast, in mammals such as rodents, carnivores, and primates, the corticospinal pathways have much more extensive projections whose targets overlap with those of ventromedial and dorsomedial brainstem tracts.

In invertebrates, very little was known about the descending pathways at the time at which I began this study. Several studies had determined that there were 17 clusters of DNs in crickets and 22 clusters of DN pathways in cockroaches (Staudacher 1998, Okada, Sakura et al. 2003). However, because of the lack of genetic tools available, knowledge of the function of these DNs and their inputs and projections was limited to individual characterization of randomly filled neurons or individual DNs with a distinctive enough size and location to be identified repeatedly across individuals (Strausfeld and Gronenberg 1990, Ye and Comer 1996, Fotowat, Harrison et al. 2011, Gonzalez-Bellido, Peng et al. 2013).

1.3 Models of descending control

1.3.1 Command neuron model of descending control

A common framework for characterizing descending control is the command neuron model, in which the brain specifies the desired motor output and when to initiate it, and relies on downstream processes (namely the central pattern generators) to

successfully execute the output and monitor the ongoing feedback. Under this model, the central pattern generators provide a template of the existing possible motor programs, and rely on modulating commands from the descending pathway to dictate the appropriate motor output (Dietz 2003, Drew, Prentice et al. 2004, Grillner, Wallen et al. 2008). The role of command neurons has been identified in a wide variety of behaviors from diverse model systems such as reaching in cats (Alstermark and Ekerot 2015) and primates (Isa, Ohki et al. 2007), locomotion in the lamprey (McClellan 1988) and the leech, as well as courtship singing (von Philipsborn, Liu et al. 2011), involuntary escape (von Reyn, Breads et al. 2014), and backwards walking in *Drosophila* (Bidaye, Machacek et al. 2014).

While the command neuron framework is useful for elucidating critical components of a particular behavior, it primarily emphasizes whether or not a particular neuron is sufficient and necessary for a specific behavior, rather than how these neurons may participate in other behaviors. Conversely, a framework of how more general motor components (either upstream or downstream of these command neurons) is also difficult to attain through this approach. As a result, determining if a particular behavior or features of such behavior is the consequence of descending commands or recurring feedback from sensory inputs is difficult.

1.3.2 Dynamical decision making and motor control

Dynamical decision making suggests that neurons which might in some circumstances appear to behave as command neurons may participate in several other distinct behaviors by exhibiting different patterns of activity (Kristan 2008). In the leech, optical imaging of neuronal populations has demonstrated that this mechanism mediates the switch between swimming and crawling (Briggman, Abarbanel et al. 2005). A small number of individual neurons within a mid-body segmental ganglion were found to be early predictors of whether swimming or crawling patterns of motor neuron activity would be observed. However, stimulation of these neurons did not influence the probability of swimming or crawling. Instead, a linear discrimination analysis found that the co-varying activity of a subpopulation of neurons was able to discriminate between swimming and crawling at an earlier timepoint (an average of 290 ms earlier than any single individually discriminating neuron). Neurons which individually appeared to be early discriminators made a very small contribution to this population analysis. At least one of the seventeen neurons which contributed strongly to the linear discriminant between swimming and crawling was found to, when stimulated, bias the decision of which motor pattern to evoke.

In the studies of the motor cortex, the dynamical systems perspective describes cortical activity as a time-varying vector of neuronal activity which changes with can be transformed into another time-varying vector to describe muscle activity (Shenoy,

Sahani et al. 2013). Although the second vector represents muscle activity, its dimensionality is set to be roughly equal to the number of independent muscle synergies and is thus much lower than the number of neurons (the dimensionality of the vector used to represent cortical activity). This model is used to characterize how the activity of individual neurons in the motor cortex changes during the time from movement preparation to movement onset during reaching behaviors.

While the dynamic systems approach has made extensive insights with regards to the function of the motor cortex, this approach has not been extensively studied in the context of other descending tracts. This is the result of a combination of factors, including the complexity of the DN population and the role of many brainstem tracts in a diversity of behaviors.

1.4 Role of central pattern generators (CPGs) in movement

Central pattern generators in the body ganglia play an important role in the successful execution of motor behavior, although their precise relationship to most DN tracts is not yet fully characterized.

Central pattern generators are neuronal networks intrinsically capable of producing rhythmic motor output. This rhythm can be produced via two general mechanisms: they can either be driven by inherently rhythmic or tonically active pacemaker neurons, or they can emerge as a result of the synaptic connections among neurons which by themselves are not rhythmic (Marder and Bucher 2001). While the

role of pacemaker neurons have been well characterized in several circuits, such as the crab stomatogastric ganglion and the Botzinger complex that controls breathing in the mammalian brainstem, emergent rhythms are often attributed to locomotion, as in the case of tadpoles and the lamprey (Marder and Bucher 2001).

Half-center oscillators, in which two sets of neurons reciprocally inhibit one another, are among the simplest examples of emergent rhythms. They are particularly important in locomotion because they govern the stretch reflex, which typically prevents antagonistic pairs of muscles (such as flexors and extensors) from being active at the same time. In insects, a combination of spiking and non-spiking local interneurons modulate this reflex to engage different motor programs (Clarac, Cattaert et al. 2000).

However, effective locomotion requires coordination to occur at multiple levels of control, specifically within the different joints of a limb, and across different segments or across the midline of the animal's body axis. In particular, gaits that exhibit alternations between left and right are the most commonly employed strategy for locomotion in terrestrial animals, although they are capable of synchronizing ipsilateral limbs under conditions that require a more rapid gait (Pearson, Acharya et al. 2005, Grillner 2006, Kiehn 2011, Bellardita and Kiehn 2015, Satoh, Pudenz et al. 2016).

Many experiments have demonstrated that circuits in the spinal cord (or thoracic ganglia in invertebrates) are still capable of producing rhythmic activity in motor neurons even in a deafferented system that lacks sensory inputs; this rhythmicity has

often been cited as the source of alternating patterns of limb movements in a wide range of species such as cat (Grillner 1973), rodent, crayfish (Chrachri and Clarac 1990), stick insect (BÄSSLER and WEGNER 1983). However, studies of this intrinsic rhythmicity, which is often termed “fictive locomotion”, are limited in several ways. First, they are performed in deafferented preparations, where the neurons providing sensory feedback are no longer intact. As a result, the rhythm measured across preparations is 10-30 times slower than is observed in normal walking (Cruse 2002, Gosgnach, Lanuza et al. 2006). In addition, because locomotor circuits do not oscillate on their own, the rhythm must be chemically induced, which often results in unnatural patterns of neuronal activity.

1.5 The insect as a model system

Because insects demonstrate highly differentiated motor repertoires through controlling their multi-jointed limbs and relatively few neurons, they are an excellent system for unraveling the general principles of motor control.

1.5.1 The insect brain consists of two major structures

The insect brain is divided into two major regions, the cerebral and the gnathal ganglia, both of which contain DNs. These two regions are believed to be functionally analogous, if not evolutionarily homologous, to regions of the brain observed in vertebrates. Both the vertebrate brainstem and the gnathal ganglia DNs contain tonically firing neurons which are strongly activated during locomotion (Kien and Altman 1992, Tschida and Bhandawat 2015). Similarly, functions subserved by DNs in the cerebral

ganglia parallel functions carried out by DNs which originate from the cortex. Many previously characterized sensory specific DNs in insects also have cell bodies located in the cerebral ganglia, such as the descending neurons of the ocellar and vertical system (DNOVs) (Wertz, Gaub et al. 2009), the descending contralateral motion detector (DCMD)(Fotowat, Harrison et al. 2011), and the target selective descending neurons (TSDNs)(Gonzalez-Bellido, Peng et al. 2013).

1.5.2 Anatomy of insect legs

Insect limbs consist of the four major segments: the coxa, the femur (to which the trochanter is fused), the tibia, and the tarsus (Figure 1). In each of these joints, movement occurs around a single axis of rotation. Specifically, the thoraco-coxal (TC-) joint enables protraction (forward movement) and retraction (backward movement), the coxa-trochanteral (CTr-) joint enables levation (upward movement) and depression (downward movement), and the femur-tibia (FTi-joint) enables flexion and extension (Buschges 2005). Movement of the tibial-tarsal joint is controlled three muscles, the tarsus levator muscle (Talm), the tarsus depressor muscle (Tadm), and the tarsus redactor muscle (Tarm), which allow the tarsus to be raised, lowered, or moved laterally (Bässler 1983, Baek and Mann 2009). The tarsus itself is subdivided into five segments and at its distalmost end contains a sixth segment, the pretarsus. These segments do not contain musculature, but the pretarsus can be moved via the *retractor unguis* muscle, which originates in the femur and inserts a long cuticular tendon through the tarsal

segments. The *retractor unguis* flexes the pretarsal-tarsal joints when activated by the campaniform sensillum in the tarsus. This enables the tarsus to grip the substrate (Zill, Keller et al. 2010, Cordoba and Estella 2014).

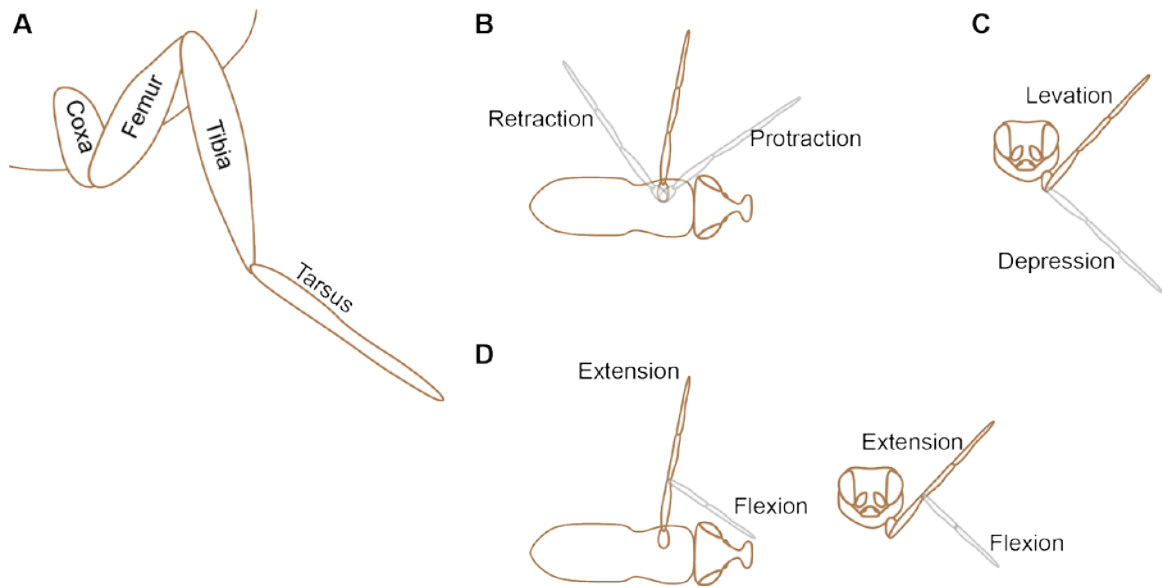


Figure 1: Segments, joints, and their respective degrees of freedom in an insect leg.

(A) The four major limb segments in *Drosophila* and other insects. (B) Retraction (backwards motion) and protraction (forwards motion) occurs around the Thorax-Coxa joint, where the coxa attaches to the thorax. (C) Levation (upwards motion) and depression (downwards motion) occurs around the Coxa-Trochanter joint, located between the coxa and the femur. (D) Extension and flexion occurs around the femur-tibia joint.

1.5.3 Stance and swing phases are driven by coordination among multiple joints in a single leg

Coordination among joints within a leg during walking has been well characterized in the stick insect model (Buschges 2005). When transitioning from swing to stance, activity in the depressor muscles holds the leg down, resulting in an increase in load that is detected by the trochanteral and femoral campaniform sensilla. This

increased load has two effects: it induces the TC-joint to transition from protraction to retraction, moving the fly forward, and induces flexion in the FTi-joint, which in turn induces increased activity in the levation muscles. Increased activity in the levation muscles terminates activity in the depressor muscles and allows the leg to lift, entering the swing phase of the next step.

1.5.4 Coordination among legs

1.5.4.1 Straight line forward locomotion

Generally, locomotion in insects such as *Drosophila* is categorized as exhibiting one of two possible gaits, the tripod gait or the tetrapod gait. The tripod gait is described as “the alternating movement of two distinct groups of legs”, specifically the ipsilateral front and hindleg and the contralateral middle leg (Wosnitza, Bockemuhl et al. 2013). While this gait can be most strictly defined as the “simultaneous lift-off and touchdown of all legs in one tripod group, while the legs associated with the other tripod group are on the ground”, there are very few instances in which this level of precision actually occurs, given the inherent variability in the phase relationships of the legs (Bender, Simpson et al. 2011, Wosnitza, Bockemuhl et al. 2013). The tetrapod gait, as its name suggests, is described as a gait during which four legs are in stance phase and two are in swing phase; the legs that are in swing phase are typically contralateral and one segment apart from each other (prothoracic and mesothoracic or mesothoracic and metathoracic) (Mendes, Bartos et al. 2013).

There is significant evidence that the tripod and tetrapod gaits are not discrete but instead represent two different idealized scenarios, with actual locomotion falling on a continuum between these two states. In addition, both Mendes et al and Wosnitza et al have described the existence of “non-canonical gaits” that are neither tripod nor tetrapod. For instance, pentapod gaits, during which only one leg is in swing phase, make up 30.15% of the leg combinations observed during slow locomotion (<19.9 mm/s) and 13.33% of the leg combinations observed during fast locomotion (>34 mm/s) (Mendes, Bartos et al. 2013).

1.5.4.2 Perturbations of feedback

Although the alternation between stance and swing is typically attributed to feedback from the load sensors and cuticular strain, several experiments show that insects are still able to maintain a patterned gait even in the absence of normal feedback (GRAHAM and CRUSE 1981, Mendes, Bartos et al. 2013). For instance, Mendes et al found that when sensory neurons in the leg were genetically inactivated in *Drosophila*, flies were still capable of exhibiting a patterned tripod gait, though they walked more slowly and the placement of their footprints was more variable.

Another perturbation to feedback described previously in the literature was to remove the load on an animal’s limbs by suspending it in the air (Hooper, Guschlbauer et al. 2009). Insect leg segments maintain a specific posture, regardless of how the body is oriented relative to the gravitational vector. In both the stick insect and the cockroach,

changing the orientation of the insect such that it was perpendicular to the ground had no effect on the positions of the legs at the ThC or the FTi-joints, regardless of whether the head was pointed away from or towards the ground. Gravity-independent postures persisted even after deafferentation and de-efferentation (achieved by severing nerves from the thoracic ganglia to the legs). This is most likely due to passive muscle forces, as experiments on the isolated flexor and extensor muscles in the stick insect showed that they exerted equivalent forces when the FTi joint was held between 70° and 90°. In addition, the forces generated by these muscles are 30 to 200 times that of gravity. Thus, an important consideration in investigating motor control is the relative contribution of passive versus active muscle forces, which by themselves are capable of biasing the positions of the legs.

1.5.4.3 Independent control

Legs can also be controlled independently. This is particularly relevant when an animal is moving over uneven terrain, and may encounter situations where one of its feet fails to find a foothold. (Durr 2001, Blaesing and Cruse 2004). Depolarization of one particular non-spiking interneuron, found in each hemi-segment of the thoracic ganglia, was sufficient to induce searching in the absence of substrate (Berg, Hooper et al. 2015).

The ability to control legs independently also raises the question of how much cross-talk there is between the different hemi-segments of the thoracic ganglia. When stepping was induced in the single foreleg of an insect whose other five legs have been

amputated, the motoneuron pools in the ipsilateral mesothoracic hemiganglion also became rhythmically active, although the degree of coupling was variable (Ludwar, Goritz et al. 2005). In particular, the coupling was strongest between the prothoracic and mesothoracic TC-joint (responsible for protraction and retraction) and weakest between the prothoracic and mesothoracic CTr-joint (responsible for depression and levation). Subsequent studies in which at least three legs were present found that the metathoracic CTr-joint would only become active in response to the stepping motions of either the prothoracic or the metathoracic leg on the ipsilateral side if both these legs were present, although only one needed to be actively stepping (Borgmann, Hooper et al. 2009). The authors proposed that this indicated that both rhythmic sensory input from the stepping leg and tonically activated sensory input from the unmoving leg were necessary for the metathoracic TC joint to be activated.

While these studies show that there is a significant amount of motor behavior that can be generated by the motor circuits within the individual leg neuromeres, the context under which these motor circuits are activated and these behaviors are elicited in response to descending inputs is still unknown.

1.6 Characterizing the logic of descending control

Here, I present the results of several key studies that lay the groundwork for using *Drosophila* as a model system for studying descending control. These studies can be summarized with three aims:

First, I characterized the anatomy of the DNs, establishing the number of neurons through which information from the brain can reach the thoracic ganglia (Chapter 2). In addition, I characterized the distribution of cell bodies and the neurotransmitter identity of these DNs. Understanding the anatomical organization of these DNs informs subsequent approaches to characterizing the diversity of possible roles they play in achieving motor flexibility.

Second, I present a load free preparation, which allows the study of descending control on limb movements in a context where sensory feedback (namely mechanosensory load) is reduced while still leaving the nervous system, musculature, and cuticle of the animal relatively intact (Chapter 3). By removing the interaction between an animal and a physical substrate, we are able to identify the different combinations of motor primitives that are elicited by circuits in the thoracic ganglia versus those whose expression are highly biased by descending control.

Third, I investigate the variation in both anatomy and function of a specific subset of DNs, the AOTU DNs. The long term goal of this project is to be able to understand how these DNs interact with other DNs, descending inputs from processing in the brain, and feedback from the thoracic ganglia in order to produce flexible and adaptive behaviors.

2. Anatomical organization of DNs

2.1 Overview and rationale

A conserved feature of motor control across the animal kingdom is the anatomical separation between circuits that control rhythm generation, which are found in spinal cord/ventral nerve cord/segmental ganglia (collectively called body ganglia), and the circuits that integrate sensory information and initiate movement, which are found in the brain. These two circuits are connected by descending neurons (DNs), which have their cell bodies in the brain and carry sensory processing and motor-related information to the body ganglia, and ascending neurons (ANs), which have their cell bodies in the body ganglia and carry motor-related and sensory feedback information to the brain.

Insects can control multiple jointed limbs to produce highly differentiated motor repertoires using relatively few neurons. Thus, they are an excellent system for unraveling the general principles of motor control. However, to effectively take advantage of the numerical simplicity of insects, we must first be able to quantify the number of neurons and the variability in their anatomy and neurotransmitter expression. Two studies have taken such a comprehensive approach: One study in cricket (Staudacher 1998) and another in cockroach (Okada, Sakura et al. 2003) both used retrograde labeling from the cervical connective to quantify the number and distribution of DNs in cricket (Staudacher 1998). These studies showed that the DN

population is similar in these two insect species and provided an anatomical framework for understanding information flow in the insect brain (Okada, Sakura et al. 2003).

Although the anatomical studies in cricket (Staudacher 1998) and cockroach (Okada, Sakura et al. 2003) have identified how DNs are organized, the lack of molecular and genetic tools in these insects have limited our progress in understanding descending motor control (Buschges, Scholz et al. 2011). In contrast, these tools are readily available in *Drosophila melanogaster*. The availability of genetic tools as well as recent technical developments have made it possible to assess or manipulate the activities of identified neurons.

As a first step towards a comprehensive understanding of DNs in *Drosophila*, here we present an anatomical survey of DNs. We performed retrograde labeling of axons via the fly's cervical connective to estimate the number and distribution of DNs. We also describe the projections of DNs, and the distribution of DNs according to expression of specific neurotransmitters. We find that the number and distribution of DNs is similar to that observed in other insect species, suggesting evolutionary conservation in the number and organization of DNs amongst insect species. Our study is the first (to our knowledge) to present the distribution of DNs in both the supraesophageal and subesophageal zones, as well as the first study to present the organization of DNs according to the neurotransmitter they employ. The results in this chapter have been previously published in *Scientific Reports* (Hsu and Bhandawat 2016).

2.2 *Drosophila* have ~1,100 DNs distributed in six major clusters

Backfilling of the axons through the cervical connective labels a small number of somata in the brain in a distinctive pattern. These are the DN cell bodies (by definition). Backfilling also labels the neuropil in a characteristic pattern. Neuropil labeling reflects DN dendrites and axon collaterals, as well as the axons of ascending neurons (ANs). Here, I present our estimate of DN cell bodies and their distribution in the brain. Next, I describe our strategy for assessing the efficiency of labeling. Third, I describe the six different clusters in which these cell bodies are distributed.

2.2.1 *Drosophila* have ~1,100 DNs

The total number of cell bodies labeled in the brain varied between 837 and 907, with a mean of 878.5 DNs (± 29.8 STD, $n=5$) (Table 1). This variation likely reflects differences in the efficacy of the labeling procedure rather than an individual-to-individual variation in the number of DNs. Thus, higher numbers are likely to be closer to the actual number of DNs. Following the method of Okada and colleagues (Okada, Sakura et al. 2003), we also estimated the total number of DNs as a sum of the largest number of DNs observed for each cluster (see below) yielding an upper estimate of 1,113 DNs. Our method of backfilling will also label neck motor neurons that have their cell body in the brain as well as neurons that project through the cardiac recurrent nerve, resulting in a small overestimate for the number of DNs. In blowflies, it has been estimated that there are ~20 neck motor neurons (Strausfeld and Seyan 1985, Shiga,

Toyoda et al. 2000) and 16 neurons that project through the cardiac recurrent nerve²⁵. Thus, these other populations make only a small contribution towards the overall cell count.

2.2.2 DNs are organized in 6 clusters

In this section, we describe the distribution of DNs. Because the distribution of *Drosophila* DNs resembles the distribution of DNs in cricket (Staudacher 1998) and cockroach (Okada, Sakura et al. 2003), we will relate the distribution of *Drosophila* DNs to their descriptions in cricket (Staudacher 1998) and cockroach (Okada, Sakura et al. 2003). DNs have cell bodies distributed across 6 clusters (Fig. 2b-d). In the following section, we describe these clusters in order from their *b*-anterior to *b*-posterior positions in the brain, where the prefix “*b*-” denotes the body axis rather than the embryonic neuroaxis (see methods and (Ito, Shinomiya et al. 2014) for more details). The number of neurons in each cluster, and the corresponding number of neurons in cricket and cockroach is reported in Table 1.

Table 1: Number of DNs per cluster in *Drosophila* versus other insects

Cluster Name	This Study			Corresponding Cluster in Cricket, Cockroach	Cricket ¹		Cockroach ²	
	Mean ± SD	Median	Max		Median	Max	Median	Max
AOTU (n=10) ³	17 ± 17.1	19	38	i5,i5n	10	22	23	35
AVLP (n=10) ⁴	23.5 ± 23.7	18	29	NA	NA	NA	NA	NA
PENP (n=5)	34.4 ± 23.7	18	80	i7a,i7b,c7	6	17	11	18
PI (n=5)	34.3 ± 12.5	26	48	PI	5	19	2	6
SMP(n=5)	277.5 ± 48.4	280	325	i1-i4,c1-c4	111	154	116	169
GNG(n=5)	483.2 ± 38.3	462	526	NA	NA	NA	NA	NA

¹ Counts represent pairs of neurons, since only one of the two cervical connectives of the cricket were labeled in these experiments (Staudacher 1998)

² Counts represent pairs of neurons, since only one of the two cervical connectives of the cockroach were labeled in these experiments (Okada, Sakura et al. 2003)

³ n refers to the number of hemispheres rather than the number of flies.

⁴ n refers to the number of hemispheres rather than the number of flies.

2.2.2.1 b-Anterior clusters

There are three anterior clusters: the anterior optic tubercle (AOTU) cluster, the anterior ventrolateral protocerebrum (AVLP) cluster, and the periesophageal (PENP) cluster (Fig. 2b-c). All three clusters contain relatively few DNs. The AOTU clusters and the AVLP clusters are paired (one in each hemisphere).

The AOTU cluster (Fig. 2b, olive green) is located lateral to the vertical lobe of the mushroom body and medial to the anterior optic tubercle. Neurons in this cluster send projections through the medial antennal lobe tract (mALT) toward the ventromedial neuropils. Based on both the soma location and the projection of the primary neurites, this cluster corresponds to the cluster i5 described in cricket (Staudacher 1998) and cockroach (Okada, Sakura et al. 2003). In the cricket, an additional cluster was identified, i5n, which was medial to cluster i5 and whose neurites projected along a distinct but parallel tract. Although we could not distinguish two distinct clusters of soma in our study, two sets of neurites projecting from this cluster are labeled, suggesting that the AOTU cluster in *Drosophila* may also be subdivided into two separate clusters.

The AVLP cluster (Fig. 2b, dark blue) is located between the anterior ventrolateral protocerebrum and the antennal lobe. The AVLP cluster does not have an obvious equivalent in cockroach (Okada, Sakura et al. 2003), but may be analogous to cluster i6 in the cricket (Staudacher 1998).

The PENP cluster (Fig. 2b, golden yellow) is located between the prow of the periesophageal neuropil and the antennal lobe. The location of this cluster corresponds to cluster i7 previously reported in the cockroach and cricket (Staudacher 1998, Okada, Sakura et al. 2003).

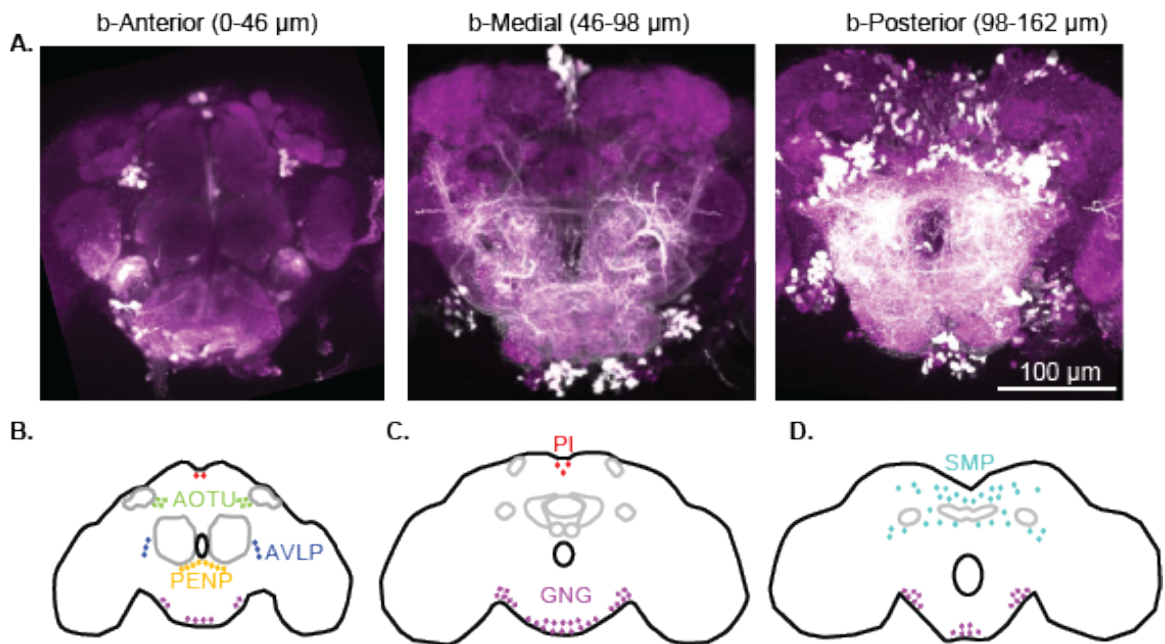


Figure 2: *Drosophila* have ~1100 DNs distributed in 6 clusters. (A) Representative confocal image stacks showing the distribution of DN clusters. Maximum projection of dextran label (white) over the range specified, superimposed on a section of neuropil containing the representative anatomical markers (anti-nc82, purple). (B) Schematic illustrating the mean distribution of DNs in the 6 clusters. Each cluster is represented with a different color. Each dot represents approximately 10 DNs.

2.2.2.2 *Pars Intercerebralis* cluster

The PI cluster (Figure 2C, red) is located between the hemispheres of the superior medial protocerebrum. Neurons in this cluster send projections into the median bundle (Rajashekhar and Singh 1994). Of these neurons, 14 have been characterized in *Drosophila* as insulin producing cells (IPCs) that project through the cardiac recurrent

nerve to the corpora cardiac and the associated aorta, proventriculus, and crop, rather than through the ventral nerve cord to the thoracic ganglia (Rajashankar and Singh 1994, Nassel, Kubrak et al. 2013). However, a previous study in the locust has identified at least one DN from the PI cluster which innervates the thoracic ganglia (Trager and Homberg 2011). In addition, studies in the cockroach have also identified DNs with soma located in the PI (Mizunami 1995).

2.2.2.3 Gnathal ganglia cluster

The GNG cluster is the largest DN cluster, containing an average of 483.2 neurons (± 61 STD, $n=5$) (Figure 2B-D, lavender). This cluster is further subdivided into a medial cluster and two lateral clusters. The medial cluster is found near the *b*-ventral (*n*-posterior) surface of the gnathal ganglia, while the lateral clusters are found lateral to the gnathal ganglia and *b*-ventral (*n*-posterior) to the saddle. There were 187.8 neurons (± 62.9 STD, $n=5$) in the medial GNG cluster and 110.5 neurons (± 33.5 STD, $n=10$) in each of the lateral GNG clusters. Because of ambiguity in assigning neurons to medial versus lateral clusters, in Table 1 we report these clusters as a single cluster. The number of GNG-DNs we report here is similar to a previous study in the locust (Kien, Fletcher et al. 1990), which reported a total of 153 neurons labeled through introduction of cobalt chloride into one of the two cervical connectives.

2.2.2.4 Superior Medial Protocerebrum (SMP) cluster

The SMP cluster consists of cell bodies distributed in the posterior superior medial protocerebrum, the superior intermediate protocerebrum, the posterior lateral protocerebrum, the inferior bridge, and the inferior and superior clamp (Figure 2D, cyan). In the cricket and cockroach studies, the fact that the authors only labeled one connective allowed the authors to divide this cluster into four clusters – i1 (or c1) through i4 (or c4), where “i” vs “c” refer to whether the neurons project to the ipsilateral or contralateral side of the brain (Staudacher 1998, Okada, Sakura et al. 2003). The cricket and cockroach studies also described a large soma projecting into the ocellar tract that separated clusters i3 and c3 from i4 and c4 clusters. However, in *Drosophila*, unlike in the cockroach, the ocellar nerve is found in the midline of the brain (Mizunami 1995, Garcia-Alonso, Fetter et al. 1996, Lee, Blackband et al. 2015); thus the ocellar nerve was not a feasible landmark. Because of the lack of clear landmarks and thus a lack of obvious boundaries between the four clusters, in this study we report the number of neurons in the four clusters as a single number.

2.2.3 Assessing efficiency of backfilling technique for labeling DNs

The narrow range of the numbers of labeled DNs across individuals and their stereotyped distribution suggests a high labeling efficiency. To estimate labeling efficiency, we backfilled the cervical connective in flies in which a small number of DNs are genetically labeled. We chose *e49-Gal4/tsh-Gal80; UAS-mCD8-GFP/+* flies because

e49-Gal4 labels a small number of DNs in several DN clusters (Figure 3). Because the genetically labeled DNs are isolated from other genetically labeled neurons in this line, we were able to unequivocally conclude that there are exactly 18 genetically labeled DNs in this line. We found that in the fly in which we labeled the largest fraction of DNs (out of 5 flies of this genotype that we bulk-labeled), we labeled 15 of the 18 genetically labeled DNs implying a labeling efficiency of 83%. In this same fly, a total of 883 DNs were labeled suggesting 1,060 DNs. This number is comparable to the number of DNs that we estimated by summing the maximum number per cluster.

The above experiment suggested a second method for measuring labeling efficiency: If the labeling efficiency were 100%, the number of genetically labeled axons in the cervical connective should be equal to the number of double-labeled cell bodies in the brain and thoracic ganglia. To facilitate axon counting, we employed *tsh-Gal80* which represses Gal4 in most ANs, thus reducing the number of labeled axons in the cervical connective. The maximum number of axons in the neck connective out of the 5 we measured is 18. The maximum number of GFP+ cell bodies we labeled was 29, 18 of which were in the brain and 11 in the thoracic ganglia. We interpret this result to reflect the fact that the number of axons counted in the neck connective is an underestimate. Although this experiment did not allow us to quantitatively estimate the labeling efficiency, the simplest interpretation is that the labeling efficiency is high.

The number of DNs reported in this study is remarkably similar to the numbers of DNs reported in previous studies performed in cockroach (Okada, Sakura et al. 2003) and cricket (Staudacher 1998). After accounting for the fact that the gnathal (formerly subesophageal) ganglia are not fused to the cerebral (formerly supraesophageal) ganglia in the cockroach and cricket as they are in *Drosophila*, the 235 pairs of DNs in cockroach and approximately 200 pairs of DNs in cricket match the 412 neurons (206 pairs) we found in the cerebral ganglia.

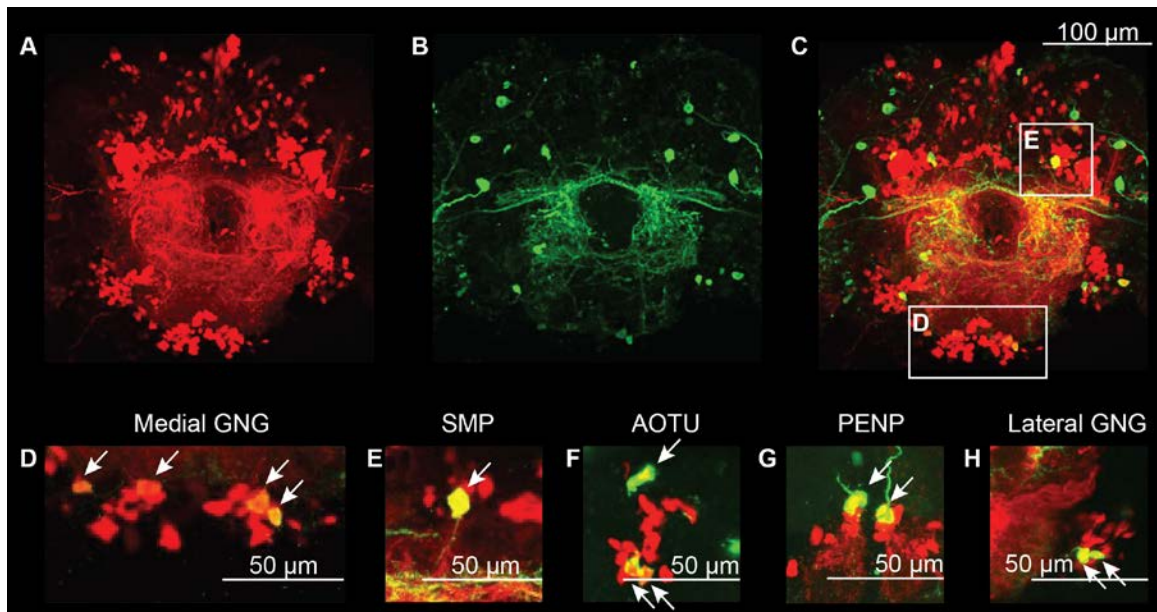


Figure 3 : Using a sparse genetic label to estimate the efficiency of labeling. E49-Gal4/tsh-Gal80;UAS-CD8GFP labels a small number of DNs which are distributed across five of the six clusters. **(A)** Retrograde labeling to identify the DNs in the brain. **(B)** GFP+ neurons labeled by the E49-Gal4 driver. **(C)** Merge showing colabeling **(D)** Inset showing the GNG cluster. Arrows indicate colabeling (GFP+ DNs). **(E)** Inset showing the colabeled DNs in the SMP cluster. **(F)**, **(G)**, and **(H)** are from a different brain.

2.3 Neuropil labeled by backfill from cervical connective

In addition to the cell bodies, backfill through the neck also labels the axons and dendrites of DNs and axons of ANs. The pattern of neuropil labeling was distinct and consistent from brain to brain. We could not distinguish between DN and AN processes and therefore report the overall neuropil labeling. The density of labeling for different neuropil regions (averaged over 5 brains) is shown in Figure 4A.

The labeling was densest in the posterior slope, located in the *b*-posterior region of the brain. In contrast, known associative areas of the brain - the mushroom body and the central complex - had no detectable labeling, suggesting that these regions neither send direct outputs to nor receive direct inputs from the thoracic ganglia.

Some sensory neuropils were sparsely labeled: these include the lobula (Figure 4C), the optic tubercle (Figure 4D), and the lateral horn (Figure 4E). This sparse labeling of sensory neuropil suggests that these regions are innervated by very few DNs (or ANs), and that most sensory information represented in these brain regions is further processed before being relayed to the DNs. In contrast, the ventrolateral protocerebrum, the majority of whose volume is composed of optic glomeruli that receive output from optic lobes, is densely labeled (Otsuna and Ito 2006, Strausfeld and Okamura 2007) (Figure 4F). Previous studies in both *Drosophila* (Mu, Bacon et al. 2014) and *Calliphora* (Strausfeld and Gronenberg 1990) have also identified individual DNs whose dendrites innervate the optic glomeruli. AMMC (antennae mechanosensory and motor center,

Figure 4G), which processes mechanosensory information, is also densely labeled. This is in agreement with previous studies which have identified descending neurons that carry information from the AMMC to the thoracic ganglia (Kamikouchi, Inagaki et al. 2009, Mu, Bacon et al. 2014).

The distribution of neuropil labeling is consistent with that observed in the cockroach (Okada, Sakura et al. 2003) and suggests that, as in the cockroach, both direct and indirect pathways connect cephalic sensory processing to behavior (Okada, Sakura et al. 2003) in *Drosophila*. Thus, information from AMMC and optic glomeruli can be directly communicated to DNs. At the same time, a lack of labeling in mushroom body and central complex implies that processing in these centers affect behavior indirectly; in this case the effect of sensory input on DNs is separated by at least two synapses.

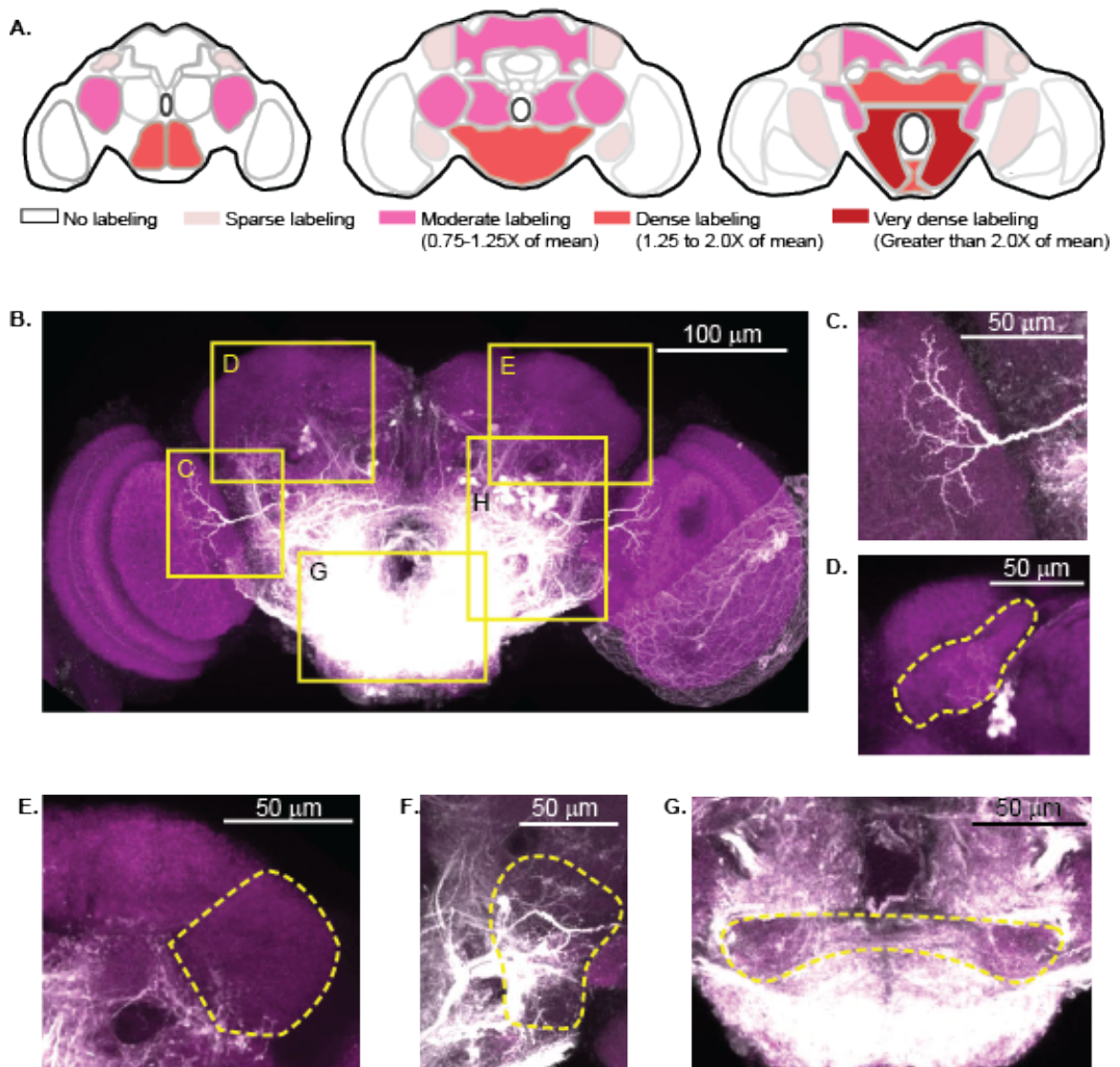


Figure 4 : Pattern of neuropil labeling suggest distinct regions for sensory, associative, and motor processing. (A) Density of labeling for different neuropil regions. (B) Projections of a confocal stack show dextran labeling (white) and neuropil labeling (magenta). Regions marked in yellow are expanded in panels (C-G). (C) Sparse innervation of the lobula. (D) Sparse innervation of the anterior optic tubercle. (E) Sparse innervation of the lateral horn. (F) Dense innervation of the posterior ventrolateral protocerebrum, where optic glomeruli are found. (G) Dense innervation of AMMC and surrounding neuropil. For clarity, only a single representative 1 μm slice is shown. The extent of the image stack is different for the images in (B-G).

2.4 Distribution of DNs by neurotransmitter

Because the neurotransmitter used by a given neuron is an important determinant of its function, we wanted to estimate the distribution of DNs by neurotransmitter. To label all DNs that utilize a given neurotransmitter, we perform labeling in flies in which the neurons utilizing a given neurotransmitter is also labeled (Fig. 5a). For instance, Figure 5b-d shows projections of the anterior, medial, and posterior portions of the brain in a *Cha-Gal4, UAS-GFP* fly. Multiple studies have shown that *Cha-Gal4* labels most cholinergic neurons (Salvaterra and Kitamoto 2001, Kolodziejczyk, Sun et al. 2008). When this is combined with red dextran dye (Fig. 5e-g), the neurons that are labeled with both GFP and red dextran dye appear yellow (Fig. 5h-j, m). These neurons are the DNs that express the neurotransmitter in question (in this case cholinergic DNs).

We performed experiments analogous to the ones described in Figure 5 for acetylcholine (n=4), GABA (n=4), glutamate (n=4), octopamine (n=4), and serotonin and dopamine (n=4). We found that DNs as a population use all the neurotransmitters we tested (Table 2). As in the counts for total number of neurons, we assumed that variability in the number of DNs reflected variability in labeling efficiency; therefore, we report the maximum number of DNs per

cluster rather than the mean. We first describe the distribution of DNs that belong to the major excitatory and inhibitory neurotransmitter types followed by DNs which do not use these major neurotransmitters (Fig. 6, Table 2 and Appendix A).

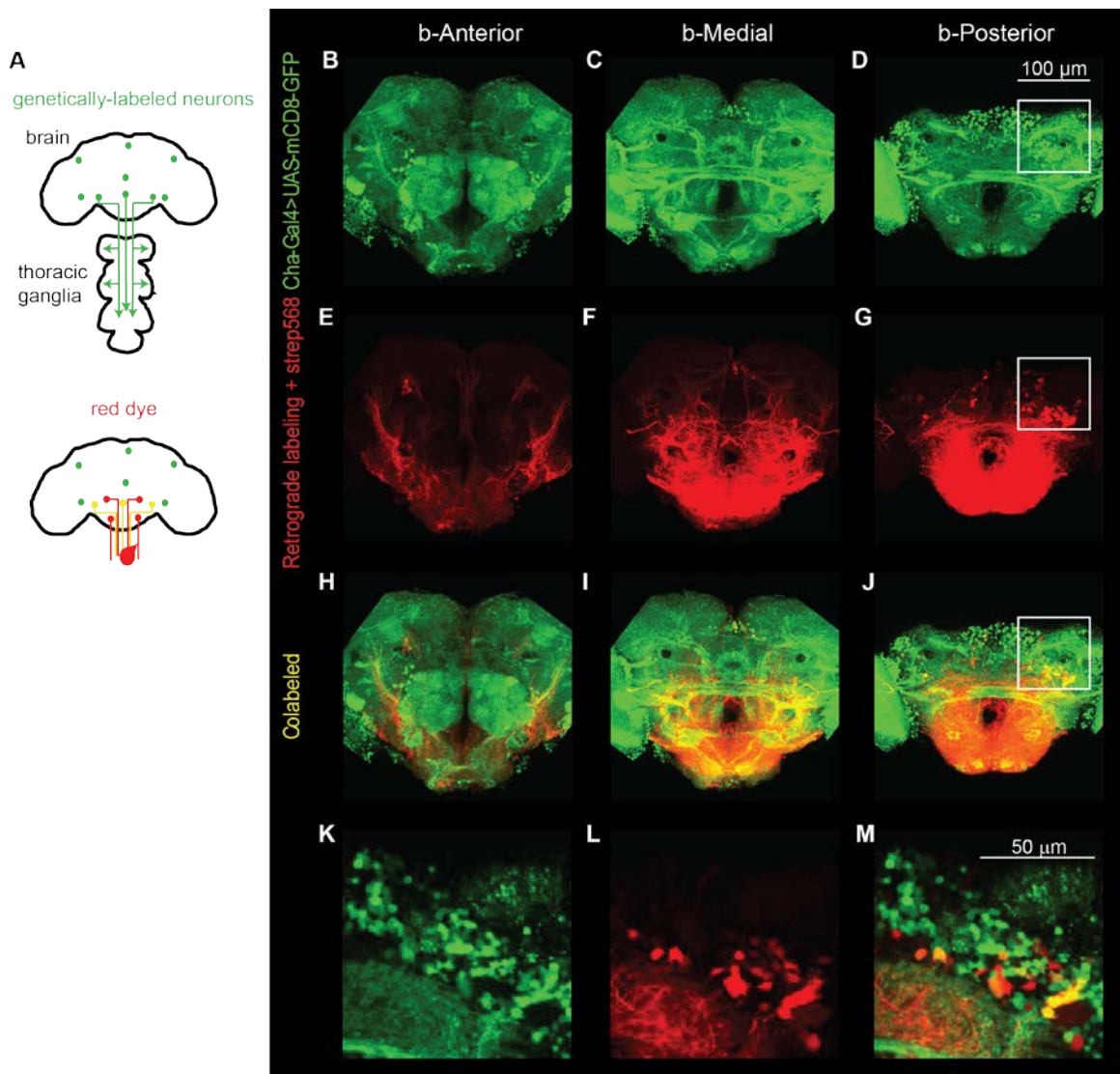


Figure 5 : Strategy for labeling DNs with a given neurotransmitter. (A) Schematic illustrating that the subset of GFP+ neurons labeled by a Gal4 driver can be identified as

DNs if they are also colabeled by retrograde labeling (yellow). Schematic illustrating that the subset of GFP+ neurons labeled by a Gal4 driver can be identified as DNs if they are also colabeled by retrograde labeling (yellow). **(B-J)** Projection of a confocal stack of a retrogradely labeled brain in which all cholinergic neurons are labeled using *Cha-Gal4,UAS-GFP* (green). Retrograde label is in red. Cholinergic DNs are colabeled and appear yellow. **(K-M)** Close-up of the region in white square in **(D)**, **(G)**, and **(J)** show the co-labeled neurons

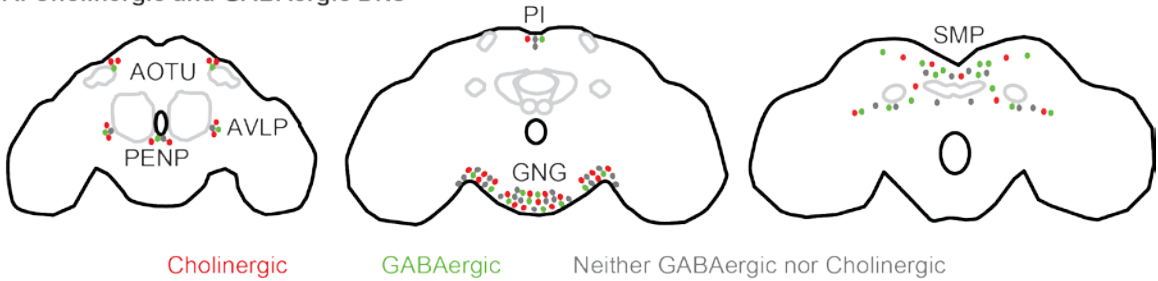
2.4.1 Major excitatory (cholinergic) and inhibitory (GABAergic) neurotransmitters in the DN populations

The major excitatory neurotransmitter in the *Drosophila* brain is acetylcholine (Yasuyama and Salvaterra 1999, Kolodziejczyk, Sun et al. 2008). To label cholinergic neurons, we performed bulk-labeling in *Cha-Gal4, UAS-GFP* flies (Figure 5B-M and Figure 6A). To label DNs which express the major inhibitory neurotransmitter, GABA (Sattelle, Lummis et al. 1991, Hosie, Aronstein et al. 1997, Enell, Hamasaka et al. 2007), we employed two methods: First, we performed experiments in *Gad1-Gal4;UAS-mCD8-GFP* flies. Second, we performed labeling in a standard lab strain (w^{1118}) and used an anti-GABA antibody to label GABAergic neurons. We found that for all clusters except the GNG cluster, more neurons were labeled by the antibody method than by *Gad1-Gal4*. This is consistent with previous reports which show that *Gad1-Gal4* does not label all GABAergic neurons (Liu, Mazor et al. 2015). Therefore, we report our results with the GABA antibody (Figure 6A, Table 2, and Appendix A).

We found that all clusters contain both cholinergic and GABAergic DNs (Figure 6A, Table 2, and Appendix A). However, the majority of the DNs in two of the anterior clusters (AOTU and PENP) were cholinergic. A greater fraction of the SMP DNs was

GABAergic, while a greater fraction of the GNG DNs was cholinergic (especially in the lateral GNG). Overall roughly 40% of the DNs are cholinergic and 40% are GABAergic.

A. Cholinergic and GABAergic DNs



B. DNs using minor neurotransmitters

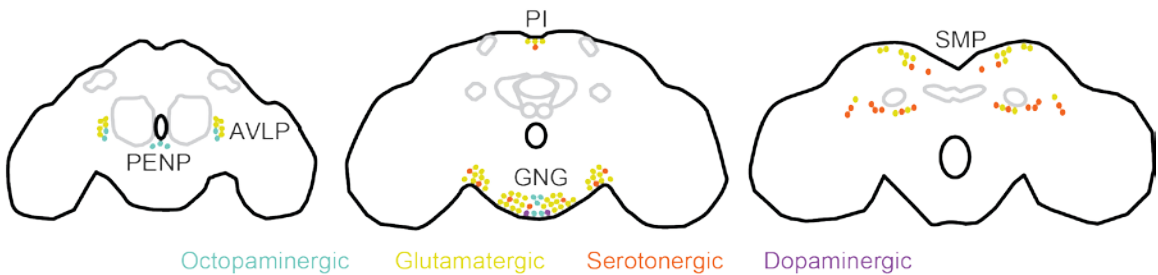


Figure 6 : Schematics showing distribution of DNs by neurotransmitter. (A) Distribution of cholinergic (red) and GABAergic DNs (green). Dots are in proportion to the fraction of DN of a given type. **(B)** Distribution of DNs which employ other (minor) neurotransmitters. Each dot represents a single DN.

2.4.2 Minor neurotransmitters

There are 56 glutamatergic DNs (Figure 6B and Appendix A). Glutamatergic neurons are labeled in *Vglut-Gal4;UAS-CD8GFP* flies, in which Gal4 is driven under the control of the vesicular glutamate transporter (Vglut). These are distributed in all clusters except for the AOTU and the PENP cluster, but most are found in the SMP and the GNG clusters (9 and 18 DNs, respectively, per hemisphere). Of these, at least 3 pairs of DNs in the SMP cluster and 5 pairs of DNs in the GNG cluster may be neck motor neurons, assuming homology between the blowfly *Calliphora* and *Drosophila* (Strausfeld

and Seyan 1985). Consistent with this study, a previous study in the honeybee also found 5 DNs with glutamatergic-like reactivity located in the ocellar tract (the midline of the SMP cluster) and 16 additional DNs elsewhere in the SMP (Bicker, Schafer et al. 1988).

The next most common neurotransmitter used is serotonergic (Figure 6B and Appendix A). Serotonergic DNs were labeled using *Ddc-Gal4* which labels both dopaminergic and serotonergic neurons and labels up to 30 DNs (summed over all clusters). Out of these, 2 DNs located in the GNG have been confirmed to be dopaminergic by performing labeling in TH-Gal4 flies in which only dopaminergic neurons are labeled (Tschida and Bhandawat 2015). Eighteen of the serotonergic DNs are in the SMP cluster and occur in a location similar to serotonergic DNs reported in locust (Nassel 1988). The other 10 are present in the GNG cluster. Two of the lateral GNG serotonergic DNs have been previously reported in the moth (*Manduca sexta*) and described as also innervating the labial neuromere of the GNG (Homberg and Hildebrand 1989). There are also reports of a pair of medial GNG serotonergic DNs in the blowfly (*Calliphora*) (Nassel 1988).

Tdc2-Gal4 which labels octopaminergic neurons, labels 12 DNs (Figure 6B and Appendix A). Octopaminergic DNs are distributed across three clusters (PENP, AVLPL, and GNG). Ten of these DNs have been described previously (Busch, Selcho et al. 2009).

Table 2 : Percent of DNs by neurotransmitter

Neurotransmitter	Labeled using:	Percent ¹
Acetylcholine	Cha-Gal4>GFP (neurons expressing choline acetyltransferase)	38
GABA	GABA antibody	37
Glutamate	VGlut-Gal4>UAS-mCD8-GFP (neurons expressing vesicular glutamate transporter)	6
Serotonin	Ddc-Gal4>UAS-mCD8-GFP (neurons expressing dopamine decarboxylase)	3
Octopamine	Tdc2-Gal4>UAS-mCD8-GFP (neurons expressing tyramine decarboxylase)	1
Dopamine	TH antibody	0.2
Total		85

2.4.3 Neurotransmitters not accounted for and other caveats

Assuming that most DNs only employ a single neurotransmitter, 85% of the DNs can be attributed to utilizing one of the five neurotransmitters we characterized. Some of the remaining 15% of DNs represent small diameter DNs which use minor neurotransmitter and are not labeled. We think that this is unlikely because we have shown in a previous study that small diameter dopaminergic neurons are reliably labeled (Tschida and Bhandawat 2015). Moreover, all the octopaminergic DNs that have been labeled genetically (Busch, Selcho et al. 2009) were also identified in our study.

¹ For acetylcholine and GABA, the percentage was computed by summing the largest number of colabeled neurons in each cluster, then dividing by the total number of bulk labeled neurons found in those clusters. Percent for neurotransmitters other than acetylcholine and GABA reported as the result of dividing the sum of the maximum number of colabeled neurons per cluster by 900, the average number of neurons labeled by our bulk labeling technique.

Therefore, it is more likely that the remaining 15% of DNs use neurotransmitters not characterized in this study: histamine, tyramine or peptidergic neurotransmitters. For instance, previous studies in the moth *Manduca sexta* have found DNs that express FMRFamide in the midline of the GNG (Homberg, Kingan et al. 1990). Our strategy for labeling DNs also labels neurosecretory cells, such as those found in the PI and in the pars lateralis, whose location coincides with the SMP cluster. These neurosecretory cells secrete neuropeptides such as *Drosophila* insulin-like peptide and FMRF, and thus they may not express any of the neurotransmitters examined in this study (de Velasco, Erlik et al. 2007, Nassel, Kubrak et al. 2013).

2.5 Discussion

We present here, what is to our knowledge, the first comprehensive description of the number and distribution of DNs in *Drosophila*. Our results suggest that *Drosophila* have ~1,100 DNs that are distributed across 6 clusters. Using a genetic strain in which a small number of DNs were labeled (Figure 3), we were able to show that the labeling efficiency is high. Similarly, the number and distribution of octopaminergic DNs in our study matches the description of octopaminergic DNs (Busch, Selcho et al. 2009) in a study that used a different approach (characterizing individual octopaminergic neurons). Thus, our estimate of ~1,100 DNs is likely to be close to the actual number of DNs. We also find that in *Drosophila*, DNs employ multiple neurotransmitters and no DN cluster exclusively expresses any single neurotransmitter type.

A comparison of our study to previous studies suggests a high degree of conservation in the number and organization of DNs across arthropods. The number of DNs in the cerebral ganglia of flies is similar to the number reported in cricket (Staudacher 1998) and cockroach (Okada, Sakura et al. 2003), while the number of DN cell bodies we found in the gnathal ganglia is similar to the number previously described in locusts (Kien, Fletcher et al. 1990). The similarity between cricket (Staudacher 1998), cockroach (Okada, Sakura et al. 2003) and fly (this study) is also supported by a study in another holometabolous insect, the moth *Bombyx mori*, which found three different groups of DNs in the cerebral ganglia (Namiki, Iwabuchi et al. 2014), corresponding to the AOTU, SMP, and PENP clusters described in this study.

Cricket (order: Orthoptera) and cockroach (order: Blattodea) are both hemimetabolous insects, while *Drosophila* is a holometabolous insect (Ito, Shinomiya et al. 2014). Since hemi- and holo- metabolous insects diverged at least 280 million years ago (Labandeira and Phillips 1996, Wiegmann, Trautwein et al. 2009, Ito, Shinomiya et al. 2014), the similarities in the number and distribution of DNs among these insects implies a high level of conservation. In addition to the conservation in DN numbers across the insect class, the number of supraesophageal DNs in lobster have been estimated to be around 600-700 (Notvest and Page 1981), suggesting that DN numbers are conserved across arthropods.

The organization of DN processes is also evolutionarily conserved among insects. Although we were not able to distinguish between axonal and dendritic processes, the overall organization of the labeled neural processes is strikingly similar to the cockroach study (Okada, Sakura et al. 2003). Both our study and the cockroach study suggest that DNs receive input from regions of the brain that are innervated by outputs from mushroom body and central complex. Equally importantly, neither DNs nor ANs innervate the central complex or mushroom body, implying that these neuropils do not directly affect motor output. Thus, one important pathway in the insect brain for information flow from sensory circuits to motor circuits is through the mushroom body and central complex to the DNs. There is also direct sensory input into descending neurons (DNs): The labeling presented in this study is consistent with visual inputs into DNs from optic glomeruli and mechanosensory input from AMMC. Similarly, the large number of DNs and dense labeling in the GNG is consistent with the prominent role of GNG in motor control.

3. Characterization of load free leg movements

3.1 Overview and rationale

The ability to execute precise, well-timed and coordinated movements that can be flexibly adapted to changes in the environment is a complex procedure that requires integration of both feedforward control (from the brain to circuits in the body) and feedback control (from the environment). Both feedforward and feedback control can alter the pattern of muscle activity by acting on local motor circuits, or central pattern generators (CPGs), which are neuronal networks characterized with intrinsic rhythmic activity.

Because the interactions between feedforward influences and feedback circuits are inextricably linked during many motor outputs (including but not limited to walking), the contribution of central, feedforward inputs to the generation of movements is difficult to study. Here, we approach this limitation by using a load free preparation, which enables the study of descending control on limb movements in a context where sensory feedback can be reduced while leaving the nervous system, musculature, and cuticle of the animal relatively intact. We propose that the patterns of leg movement observed in this preparation are more natural than the patterns observed in studies of fictive locomotion: first, because they do not need to be induced by drugs, second, because their frequency is comparable to that observed in a freely walking preparation, and third, all feedforward circuit elements are fully intact and thus able to engage in

locomotor control as they would in an intact preparation. The load free preparation enabled us to identify the different combinations of motor primitives that are elicited by circuits in the thoracic ganglia versus those that are likely to be elicited by descending control.

3.2 Methodology

Female flies (1-3 days post eclosion for *nsyb-Gal4/UAS-P2X2*, 1-4 days post eclosion for *UAS-ort/+*; *nsyb-Gal4/nsyb-Gal4* and *UAS-mCD8-GFP/+*; *VT50660/UAS-P2X2*) were anesthetized briefly on ice, then immobilized between two glass microscope slides at room temperature. To enable tracking of leg movements, insect pins were used to apply UV-curable glue and colored polyethylene spheres (212-250 μm in diameter) to the tarsus (the most distal leg segment). The flies were then anesthetized briefly on ice again, then transferred to a custom made chamber. The chamber was painted red for maximum contrast (Figure 7A). The gaps between the head and the foil and the thorax and the foil were sealed in place with candle wax. Wings were removed.

A camera (Marlin F131C IRF, Allied Vision Technologies) with a 94mm/0.5X lens (Infinistix Proximity Series, Infinity Photo-Optical Company) was placed below the fly to capture video of leg movements. The data in this chapter was collected under two different lighting conditions, in an effort to optimize the automatic tracking. In both conditions, two lights of different wavelengths were used. Under the first lighting condition, one light had a wavelength of 465 nm (LED Supply) and the other light had a

wavelength of 385 (SmartVision) (Figure 7B). Under the second lighting condition, one light had a wavelength of 420 nm (LED Supply) and the other with a wavelength of 385 nm (Thor Labs). In the second condition, excess light was filtered out with a 425 nm high pass filter (Edmund Optics), and light from the 385 nm light was collimated using an adjustable collimation adaptor (SM1P25-A, Thor Labs). The x and y positions of each ball were determined using custom built Matlab software and then manually checked and corrected as necessary.

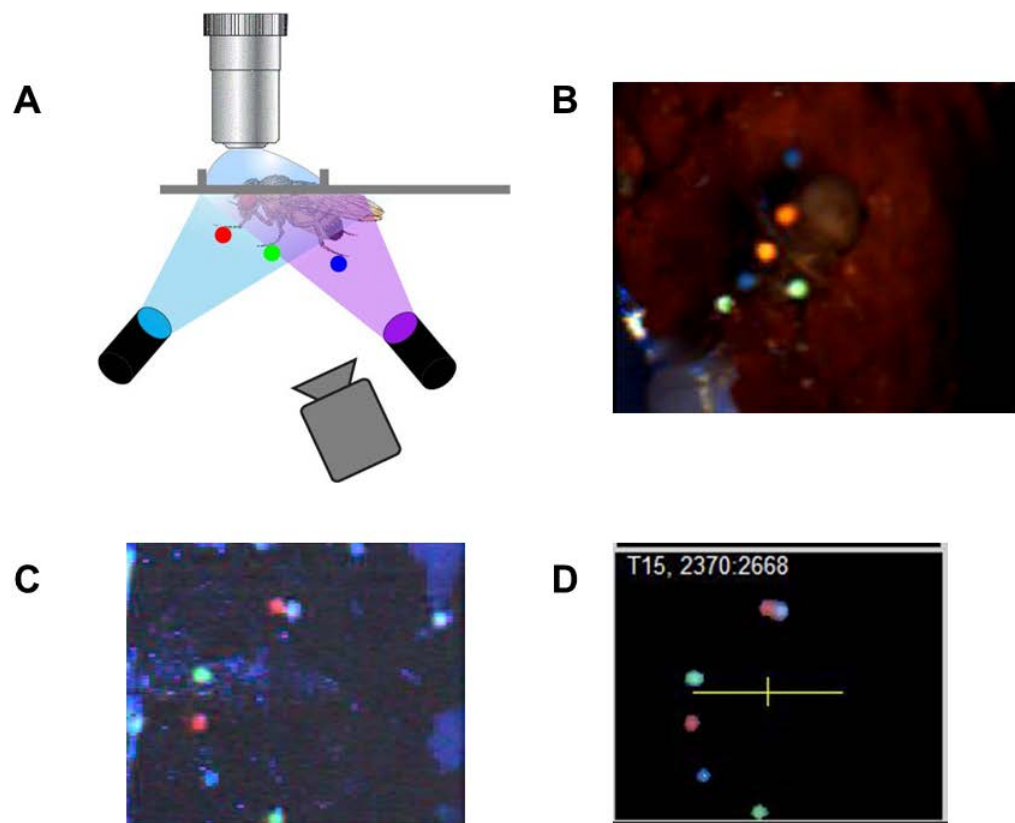


Figure 7 : Autotracking in a load free preparation. (A) Diagram showing the preparation, in which the fly has fluorescent polyethelene spheres glued to its legs, is fixed to a foil, then illuminated and filmed from below. (B) Image of a fly with natural

light, a 365 nm light, and a 420 nm light. (C) Image of the fly with a 365 nm and a 465 nm light conditions. (D) Background subtraction removes everything except the balls, which marks the tips of the legs.

Spontaneous (without drug, or intact/before neck severing) data presented here is accumulated from 27 flies. Figures 8, 9, and 10 currently only represent data collected from flies of the genotypes *nsyb-Gal4/UAS-P2X2* (n=9) and *UAS-ort/+; nsyb-Gal4/nsyb-Gal4* (n=7). Figures 13, 14, and 15 refer to data collected from all 27 flies, the remaining eleven of which are of the genotype *UAS-mCD8-GFP/+; VT50660/UAS-P2X2*.

With the exception of data presented in Figures 12 and 16, data presented here represents the Spontaneous (without drug, or intact/before neck severing) data from several different experiments. In the case of all flies represented in Figures 8, 9, and 10 and 21 of the 27 flies represented in Figures 13, 14, and 15, spontaneous without drug trials were interleaved with trials in which neurons were activated and inactivated through application of either ATP or His, respectively (Section 3.7, 3.8, Appendix B). For the remaining six flies represented in Figures 13, 14, and 15, data was collected from intact flies prior to when the neck was severed (Section 3.6).

3.3 Kinematics of load-free leg movements can be categorized into stop, initiation, and burst phases

The kinematics of the movements of individual legs in load free flies can be categorized into three major classes, primarily on the basis of speed. We refer to these as stop, initiation, and burst phases. A fourth phase, the transition phase, is also observed,

although they were ignored in this study because they comprised only a small fraction of the observed behavior.

The probability that a leg moves spontaneously is 64.2%. Movement can be separated into discrete bouts. We observed that most bouts initiated with a slow movement which transitioned into a burst like movement (Figure 8A-B).

Time periods in which there was no movement were first identified as periods when speed was below a “high threshold” for 100 ms (solid gray line, Figure 8A). To distinguish slow but directed movements from noise in the “stop” bout, we also computed how far the leg had moved from the initial stopping position (Figure 8A, lower panel) and identified additional movement periods within the putative stop as periods when this movement threshold was crossed. Within these movement bouts, the onset of the “burst” phase was identified as the first time point when speed exceeded an empirically set burst speed threshold (dashed red line, Figure 8A). A fourth phase, the transition phase, is observed when burst movements exhibit a speed below the burst speed threshold for at least 200 ms. By definition, movements in the transition phase have a comparable speed to movements in the initiation phase, but in this study we have focused our analysis on the initiation bouts because they make up the majority of the bouts within this speed range (82.7% initiation bouts, $n_{\text{initiation}} = 11084$ and $n_{\text{transition}} = 1913$).

Of the bursts with a duration of at least 100 ms ($n_{\text{bouts}} = 1739$), 86.7% were preceded by an initiation period that lasted at least 50 ms and only 2.4% lacked any

discernible initiation period. However, 84.3% ($n_{\text{bouts}} = 11084$) of the initiation bouts were followed by a stop rather than a burst.

Although the movement of the legs may initially appear random and chaotic, this is primarily the result of independent movements of legs. Movement of individual legs is strikingly structured and resembles features observed in legs during walking. We will characterize this in the following section, but first, we will describe two features that are observed in Figure 8C.

First, legs tend to stop at stereotypical positions. To quantify this, we found the mean of the X and Y position of each leg for each fly during the first frame of each stop bout that was at least 100 ms long. We then computed the distribution of the distance from this mean initial stopping position for each fly. This distribution of distance from mean stopping position is shown in Figure 8C.

Second, a significant fraction of burst bouts showed patterned oscillatory movements ($n_b = 840$). The amplitude and frequency observed during these oscillatory movements are within the range typically observed in walking (Mendes, Bartos et al. 2013, Wosnitza, Bockemuhl et al. 2013).

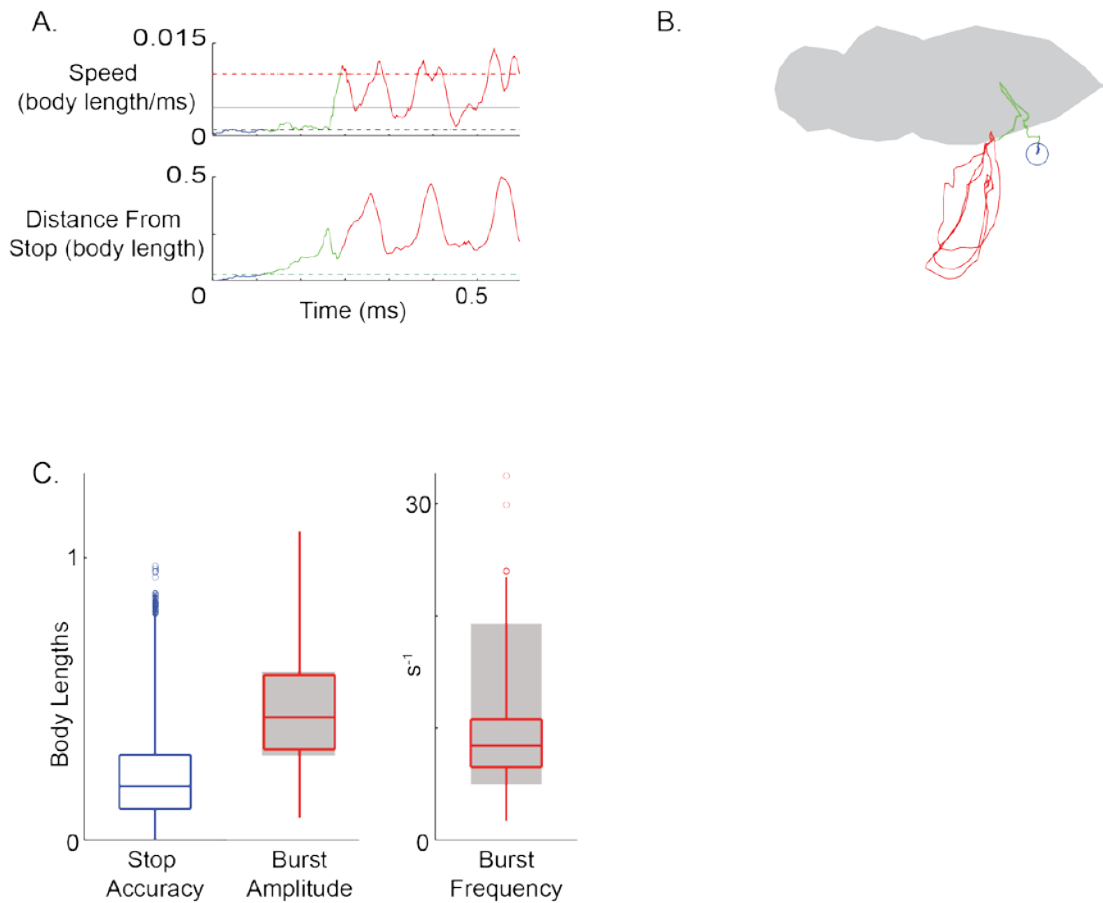


Figure 8 : Movement can be separated into discrete phases on the basis of speed. (A) Bursting type movements (red) were time when speed exceeded an empirically set threshold (red dashed line). Slow initiation type movements were separated from burst movements on the basis of speed, if they occurred between a stop and a burst; initiation movements that followed a burst were identified as such if the below threshold speed was observed for at least 200 ms. **(B)** Representative example of a stop, initiation, and burst bout shown in blue, green, and red, respectively. The blue circle identifies the first timepoint during which the leg was stopped. **(C)** The distribution of stop accuracy, burst amplitude, and frequency. Amplitude and frequency of bursts overlaps with that which is typically seen in freely walking flies, as indicated by the grey boxes (Wosnitza, Bockemuhl et al. 2013). Boxes represent quartiles; outliers represent points outside the whiskers (more than three times the interquartile range).

3.4.1 Stops return to a small region with high probability, suggesting the stop position is mostly determined by passive muscle control

Previous work in the stick insect and cockroach has shown that insects can maintain their limbs in a position independent of the gravitational vector, even if the efferents and afferents to and from the limb have been severed (Hooper, Guschlbauer et al. 2009). This is largely due to passive forces generated by the muscles, which are of a magnitude sufficient for holding the limbs in place. We theorized that because the limbs of *Drosophila* are, like other insects, relatively small, they will behave similarly.

For each leg, we determined the region in space that it occupied during all observed stop bouts. From these regions, we determined which pixels represented the top 80% most frequently occupied positions. We found that within an animal, the top 80% of positions occupied during the stop bouts covered a fairly precise (small area) within the possible range across space (Figure 9). However, there was a large degree of variability in the stop positions across individual flies, as well as across the full range of stop positions observed within a single leg of an individual fly. This variability may be attributed to either variation in passive muscle forces, which have previously been reported to be variable across individuals in both stick insect (Hooper, Guschlbauer et al. 2006) and lobster (Thuma, Morris et al. 2003), or active control via the motor neurons, play a role in holding the legs stationary either in preparation of or following a movement bout.

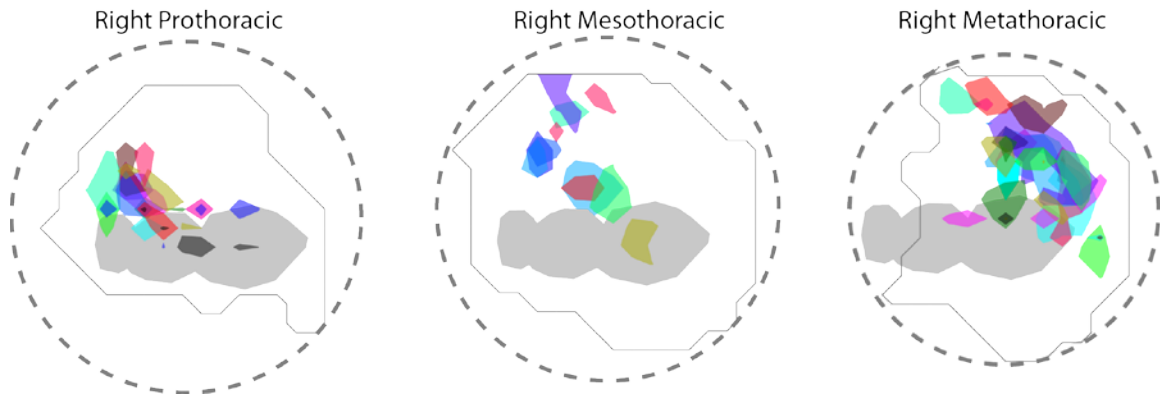


Figure 9 : Stops return to a small region with high probability. Each color represents the 80% most likely stop positions for an individual fly (different flies represent different individuals). The irregular polygon outlined in gray represents the distribution of all XY positions observed in all flies for the leg in question. The dashed grey circle represents the theoretical region a leg might occupy, computed using the maximum distance between the leg and its associated CTr joint as the radius.

3.4.2 Movement initiation is driven primarily along the protraction/retraction axis

Movement initiation typically occurred along a similar trajectory both within flies (Figure 10A-B) as well as across flies (Figure 10C), as shown by representative movement bouts in Figure 10A. To quantify this, we first computed the distribution of movement trajectories throughout the duration of all initiation periods, and plotted the distribution for individual flies (representative example for one fly shown in Figure 10B). For all legs and all flies, this distribution was found to be non-uniform ($p < 0.001$) by the Rayleigh test for circular uniformity (Berens 2009).

To compare the distributions across flies, we determined the axis of movement (rather than the trajectory) by rotating the trajectory vectors so that they fell between $-\pi/2$ and $+\pi/2$. We then computed the resultant vector (which sums the trajectories across

all available time points and computes the average vector). This resultant vector is shown superimposed for all flies (Figure 10C).

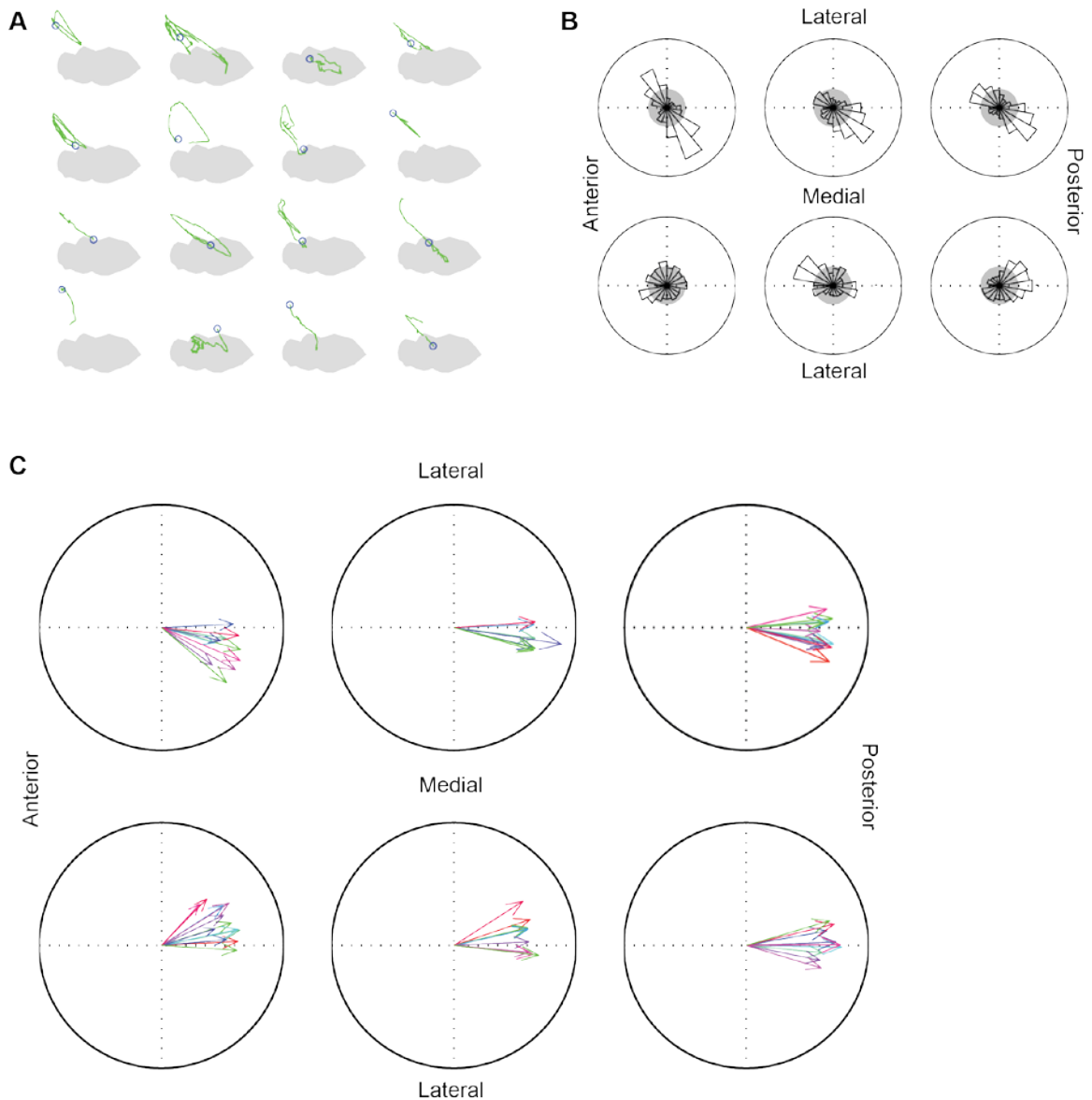


Figure 10 : Movement initiates along a stereotyped direction. (A) Representative examples of different movement initiation bouts observed in the right prothoracic leg. **(B)** Distribution of probability of movement in a particular trajectory during initiation represented in an angle wedge histogram. Each wedge represents 20° . The radius of the circle represents 0.2. The solid gray circle represents the distribution that would be

expected if all directions of motion were equally probable. (C) Resultant vector computed from the axis of the movement trajectories of individual flies. Each individual fly is represented by a different arrow. The magnitude of the arrow represents the relative magnitude of the vector. As in (B), the radius of the circle represents 0.2.

3.4.3 Bursting movement in different legs is controlled independently

Unlike the freely walking preparation, during which all six legs are moving in a patterned tripod or tetrapod gait, the load free preparation allows individual legs to move independently. In flies in which all six legs were tracked ($n=7$), there was bursting in at least one leg 21.1% (573.56 seconds out of 2714.97 seconds) of the time. Of the time periods during which at least one leg was bursting, two or more legs were bursting only 33.4% of the time (191.42 seconds) (Figure 11A-B).

We next wanted to determine how well coordinated the legs are in instances where more than one leg is bursting. To determine if the movements between two legs are correlated, we converted the XY coordinates of each leg's trajectory into the angle of the foot's position relative to the "flyaxis" (the line parallel to the length of the fly through the CTr-joint) (Figure 12B). We considered the legs to be coordinated if the peak of the normalized cross covariance was at least 0.5 and the offset was less than 100 ms. To account for cases where the cross covariance was oscillatory, we also ran a Fast Fourier Transform on the output of the cross covariance and determined the amplitude of the highest peak. If this was above what would be expected in cases where the cross covariance was at least 0.5, we also considered this to be an instance when the two legs were coordinated.

Of the time periods in which at least two legs were bursting, legs were coordinated only 37.0% of the time. Thus, unlike in the load-bearing (freely walking preparations), flies in this preparation are capable of moving their legs independently and at different frequencies.

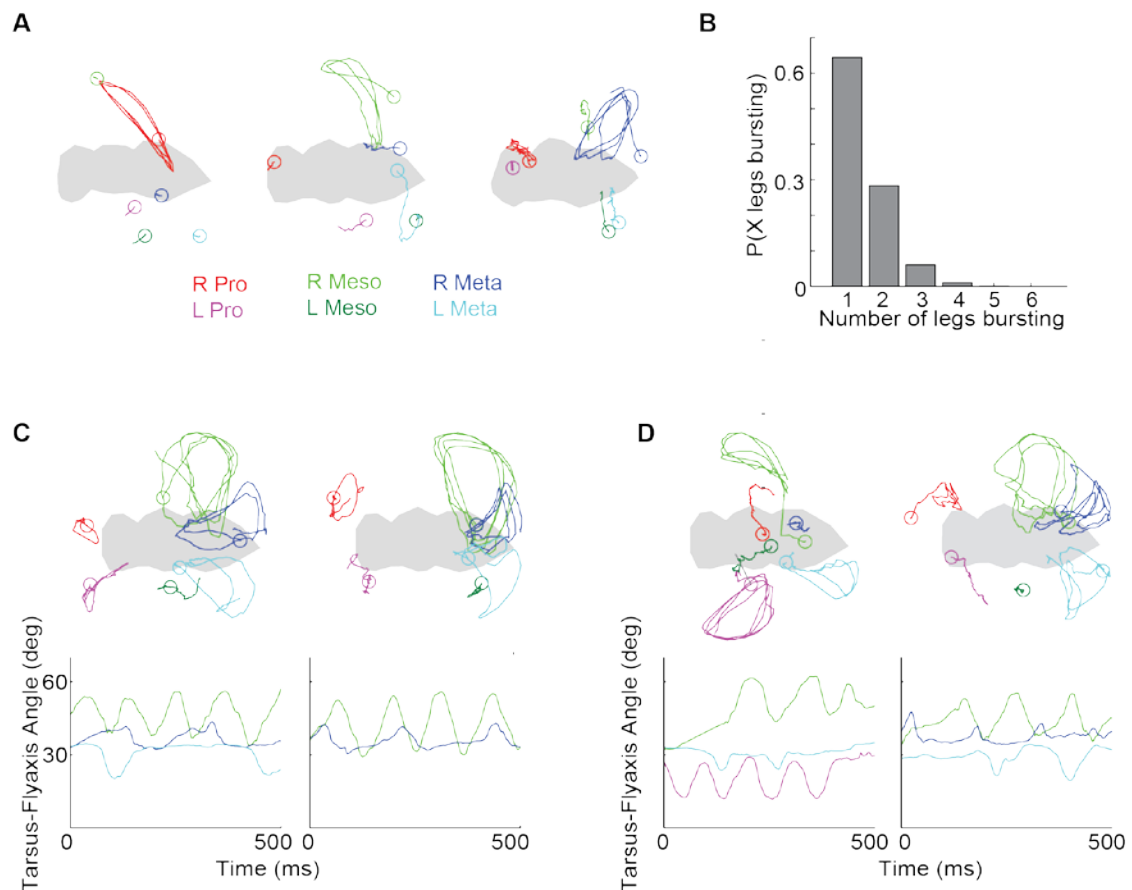


Figure 11 : Legs are under independent control. (A) Examples of time periods during which only one leg was bursting. For the first (left) two examples, 200 ms are plotted for each leg. For the third example, 417 ms are plotted. Each leg is drawn in a different color. Open circles represent the first timepoint plotted. **(B)** Number of legs bursting during times when at least one leg is bursting. **(C)** Examples periods of bursting in which individual legs do not maintain a constant phase relationship with each other. Symbols are the same as in **(A)**. **(D)** Examples of legs in which bursts do maintain a constant phase relationship with each other. Symbols are the same as in **(A)**.

3.5 Characterization of burst types

3.5.1 Discrete types of bursts are achieved via different combinations of joint movements

In insects, walking is achieved primarily through movement in three joints, each of which can rotate about a single axis. These are the thoraco-coxal (ThC-) joint, which enables protraction (forward movement) and retraction (backward movement), the coxa-trochanteral (CTr-) joint, which enables levation (upward movement) and depression (downward movement), and the femur-tibia (FTi-joint), which enables flexion and extension (Buschges 2005) (see Section 1.6 and Figure 1).

To characterize how combinations of movements within these joints result in different types of bursts, we fixed different colored balls to the femur, tibia, and tarsus segment of the leg and tracked them in a spontaneously behaving fly. We then computed the angle of each ball to the flyaxis (Figure 12A). We also computed the radius from the tarsal ball to the CTr-joint (Figure 12B), and approximated the flexion angle as the angle between the coxa, the femur ball, and the tibia ball (Figure 12C).

As is the case during walking, movement in the load free preparation during burst bouts could be described in terms of protraction and retraction about the ThC-joint (Figure 12D-G) and flexion and extension about the FTi-joint (Figure 12H-6K). For instance, for the burst trajectory shown in Figure 6E, the tibia-flyaxis angle maintains a constant linear relationship with the femur-flyaxis angle (Figure 12E). The flexion angle and the tarsus-coxa radius are also constant during the course of this movement motif

(Figure 12G-H). Thus, motion in this case, which is represented as changes in the angle of all three leg segments with respect to the fly, is primarily along the protraction-retraction direction, which is mediated by the ThC-joint.

In some cases, as in Figure 12H, movement is driven primarily by extension and flexion. In this case, there is relatively little movement of the femur, in contrast to that of the tibia and the tarsus (Figure 12I). This represents extension and flexion about the FTi-joint, which results in a large change in the distance of the tarsus from the coxa (the tarsus-coxa radius) (Figure 12K).

A third possibility is that there is movement around both the ThC joint (protraction-retraction) and the FTi joint (Figure 12L-O). In this scenario, the tibia-flyaxis angle generally maintains a linear relationship with the femur-flyaxis angle. However, the tibia-flyaxis angle can have more than one value for a given femur-flyaxis angle, because extension/flexion provides it with an additional degree of freedom (Figure 12M).

In all three of these scenarios, the tarsus-flyaxis angle and the tibia-flyaxis angle had a similar relationship to the femur-flyaxis angle. Thus, for subsequent experiments, in which one ball is glued to the tarsus of each leg rather than a different ball glued to the leg segment, we use the tarsus-flyaxis angle to approximate the amount of flexion (rather than the angle between the CTr-, FTi-, and TTi joints, which was unavailable in those experiments).

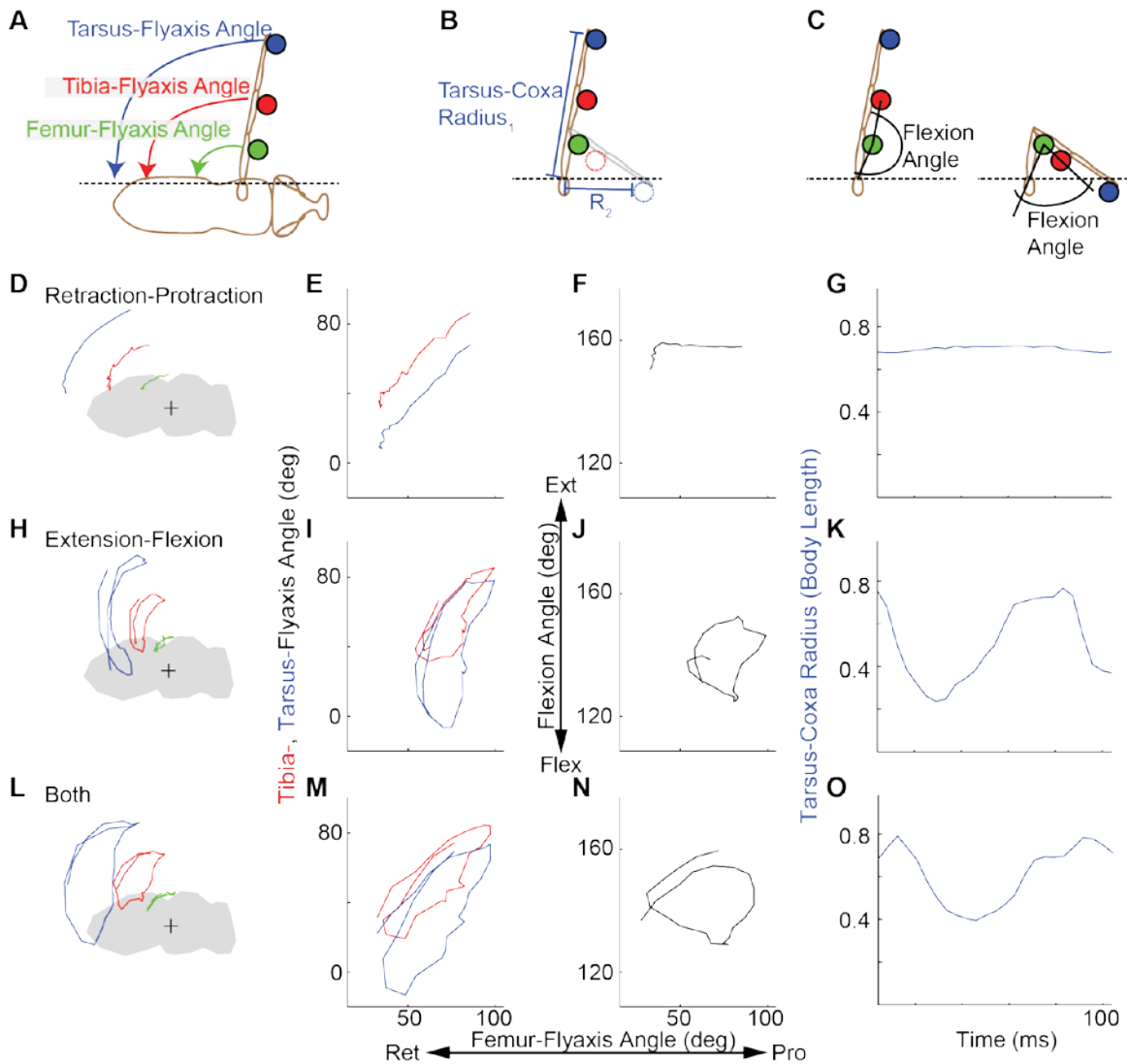


Figure 12 : Characterizing different degrees of freedom displayed by the different limb segments of the fly's legs. (A) Diagram demonstrating how fixing different colored balls to different limb segments changes in the orientation of these limb segments with respect to the line parallel to the length of the fly (the tibia-flyaxis and the tarsus-flyaxis angles) could be computed. **(B)** Diagram demonstrating how the tarsus-coxa radius is computed and how it varies as a result of extension (filled circles, brown leg) or flexion (open circles, grey leg). **(C)** Diagram demonstrating how the tarsus-coxa radius is computed and how it varies as a result of extension (filled circles, brown leg) or flexion (open circles, grey leg). **(D)** Representative example of movement of the femur but not the tibia. **(E)** The tarsus-flyaxis angle and the tibia-flyaxis angle maintain a constant linear relationship with the femur-flyaxis angle, suggesting that any changes in the orientation of the tarsus and tibia relative to the flyaxis are the result of

changes in the orientation of the femur. **(F)** The flexion angle remains constant because there is no movement of the tibia independent of the movement in the femur. **(G)** The tarsus-coxa radius remains constant, indicating no movement around the FTi axis. **(H)** Representative example of movement driven primarily by extension and flexion around the FTi joint. **(I)** The tibia-flyaxis angle changes even during periods when there is little change in the femur-flyaxis angle, indicating flexion and extension. The tarsus-flyaxis angle also has a similar relationship to the femur-flyaxis angle. **(J)** As predicted by **(I)**, the angle of flexion is changing throughout the trajectory of the movement shown in **(H)**. **(K)** Extension and flexion of the FTi-joint results in a large decrease in the distance of the tarsus from the coxa. **(L)** Representative example of movement with both protraction-retraction and flexion/extension. **(M)**, **(N)**, and **(O)** similar to **(I)**, **(J)**, and **(K)**.

These combinations represent different possible states which can exist, of which there are eight in total (Retraction Flexion, Retraction Only, Retraction Extension, Flexion Only, Extension only, Protraction Flexion, Protraction Only, and Protraction Extension). All eight states were observed in all each of the three pairs of legs, but the most commonly observed states for each of the three pairs was Retraction Only and Protraction Only (Figure 13A). Retraction Flexion (RetFlex) and Protraction Extension (ProExt) states, which are states observed in the stance and swing phase respectively during normal forward locomotion in insects, were also observed. In contrast, states not typically observed in normal forward locomotion, such as Retraction-Extension and Protraction-Flexion were also observed, although they were less likely than the Ret-Flex and Pro-Ext states. This indicates that in the absence of load feedback, there is increased variability in the states observed, although certain combinations of joint movements are still coupled and thus observed with a higher probability (RetFlex as opposed to RetExt, ProExt as opposed to ProFlex).

We also computed the transition probability from state to state. All legs had similar distribution of transition probabilities, with transitions between Retraction Only and Protraction Only being observed most often (Figure 13B). Retraction Only and Protraction Only were also the most commonly observed “first” state (immediately following burst initiation). Thus, much of the motion in the load free preparation is generated in the retraction-protraction direction, or changes about the ThC-joint.

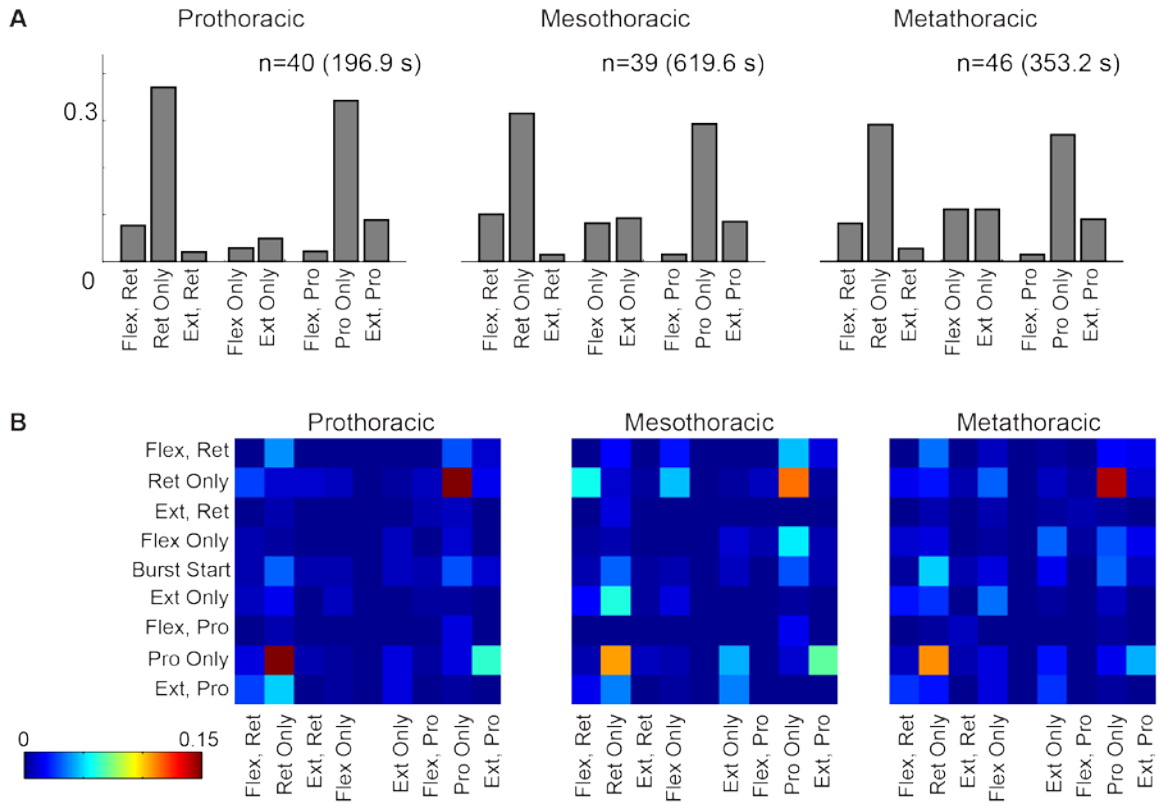


Figure 13 : Probability of states and state transitions. (A) Fraction of bursting time the fly spends in each of the eight states. n=number of legs for which data was obtained. Total time bursting in parentheses. **(B)** Probability of transitioning from State A (row) to State B (column). Number of legs same as in A.

3.5.2 Bursts can be defined as repeating sequences of different states

Because burst type movements are characterized by patterned, oscillatory movements, we wanted to categorize them based on the sequence of states through which they cycle. This enabled us to distinguish between several different types of bursts (Figure 14-15). For instance, one type of burst commonly observed in the mesothoracic legs was primarily characterized by changes in the angle of the tarsus-flyaxis angle but not the tarsus-coxa radius. Thus, these bursts were defined as bursts containing Retraction Only-Protraction Only cycles (Figure 14A). However, in some cases the Retraction Only state was followed by a state during which there was a reduction in the tarsus-coxa radius (Figure 14B). Thus, these bursts were defined as containing cycles of Retraction Only, Flexion Only, Protraction Only (Ret-Flex-Pro).

There were also many bursts in which we found more than one type of cycle (Figure 14C-D). In many cases, the presence of multiple cycle types within a burst bout was the result of variability throughout the bout on a cycle by cycle basis (Figure 14C). Instances of bursts when a single burst bout contained several sequential repetitions of one cycle type, followed by several repetitions of a different cycle type (Figure 14D), were rare. The trajectory of the different cycle types within a burst also typically covered similarly overlapping regions in space. Because of the large fraction of burst bouts in which more than one cycle type was observed, we chose to quantify types of bursts in terms of the number of cycles observed, rather than discrete burst bouts.

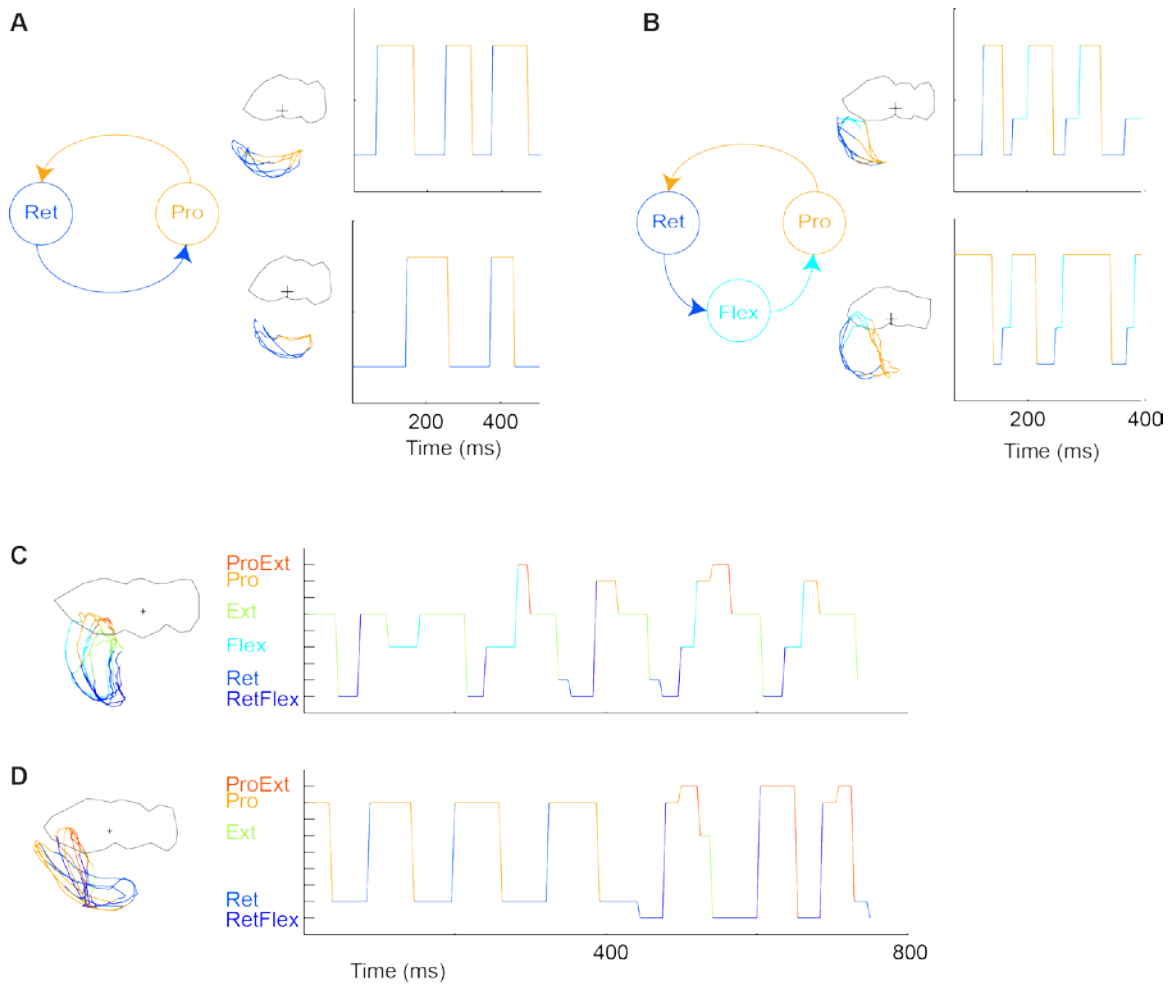
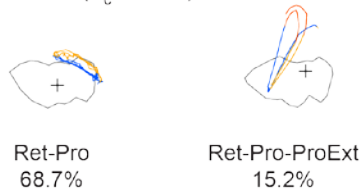


Figure 14 : Bursts can be defined as repeating sequences of different states. (A) Two representative examples of the most common type of burst cycle, Ret-Pro-Ret, for the mesothoracic leg. The trajectories through x and y are shown as well as the change in state over time. **(B)** Two representative examples of another type of burst cycle, Ret-Flex-Pro, commonly observed in the mesothoracic leg. As in **(A)**, the trajectories through x and y are shown as well as the change in state over time. **(C)** Example of a burst bout observed in the metathoracic leg where multiple cycle types were observed within a single bout, as a consequence of variability throughout the bout on a cycle by cycle basis. **(D)** Example of a burst bout observed in the metathoracic leg where there were several sequential repetitions of one cycle type (Ret-Pro), followed by several repetitions of a different cycle type (RetFlex-Pro-ProExt).

We found that 80% of the cycles observed in the prothoracic, mesothoracic, and metathoracic legs could be described using two, four, and five types of cycles,

respectively (Figure 15). Thus, the prothoracic legs exhibit less diversity in the burst type than the mesothoracic and metathoracic legs. In all three sets of legs, the most common cycle type observed was Retraction-Protraction.

Prothoracic ($n_c=1033$)



Mesothoracic ($n_c=2241$)



Metathoracic ($n_c=1992$)

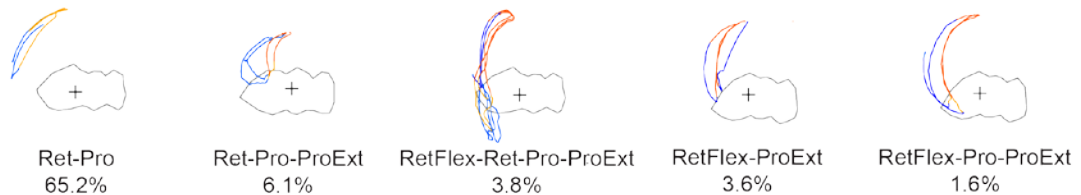


Figure 15 : The burst cycle types that make up 80% of the cycles observed in each leg. Each color represents a different state. n_c refers to the total number of cycles observed.

3.6 Descending inputs are necessary for generating cycle to cycle variability

To determine whether the motor output observed in the load free preparation was generated from descending inputs from the brain or from the motor circuitry within the thoracic ganglia, we tested the effect of severing the neck (thus removing all

descending input) on limb movements. In these experiments, only the mesothoracic and metathoracic legs were tracked. This decision was made to expedite the tracking process; prothoracic legs were not chosen because of their limited variability in cycle types relative to the other two pairs of legs.

Probability of bursting in all flies was greatly reduced after severing the neck (Figure 16A). In two of the five flies tested, no bursting activity in the legs was detected following the neck lesion. For the 1617.67 s of data recorded from five flies after severing the neck, there were only 5.68 seconds during which bursting was observed in any leg. Once the neck was severed, there were no instances where bursting occurred in more than one leg at the same time, although bursting leg movements were observed in three out of four legs in one fly and two out of four legs in another fly.

In addition to burst probability, the region covered by the trajectory of the legs during bursting was greatly reduced, as shown by the distribution of XY positions in the representative individual in Figure 16B. The diversity in the types of bursts was also reduced following neck lesion, although different flies exhibited different states (and subsequently different burst cycles). For instance, most burst cycles observed in the metathoracic leg shown in Figure 16C were composed of Flex, ProExt, or RetFlex states. In the metathoracic leg shown in Figure 16D, bursts were exclusively composed of the RetExt, Flex, ProRet, and Pro states. We found that across all burst bouts observed in all legs and flies, there was an increase in the fraction of bursting time spent in the RetExt

state in both the mesothoracic and the metathoracic legs and an increase in time spent in the ProFlex state in the metathoracic leg. Thus, in the absence of descending inputs, the legs exhibit combinations of joint movements that are rarely observed in normal forward locomotion. The increased representation of unusual states such as ProFlex and RetExt is shown in Figure 16E.

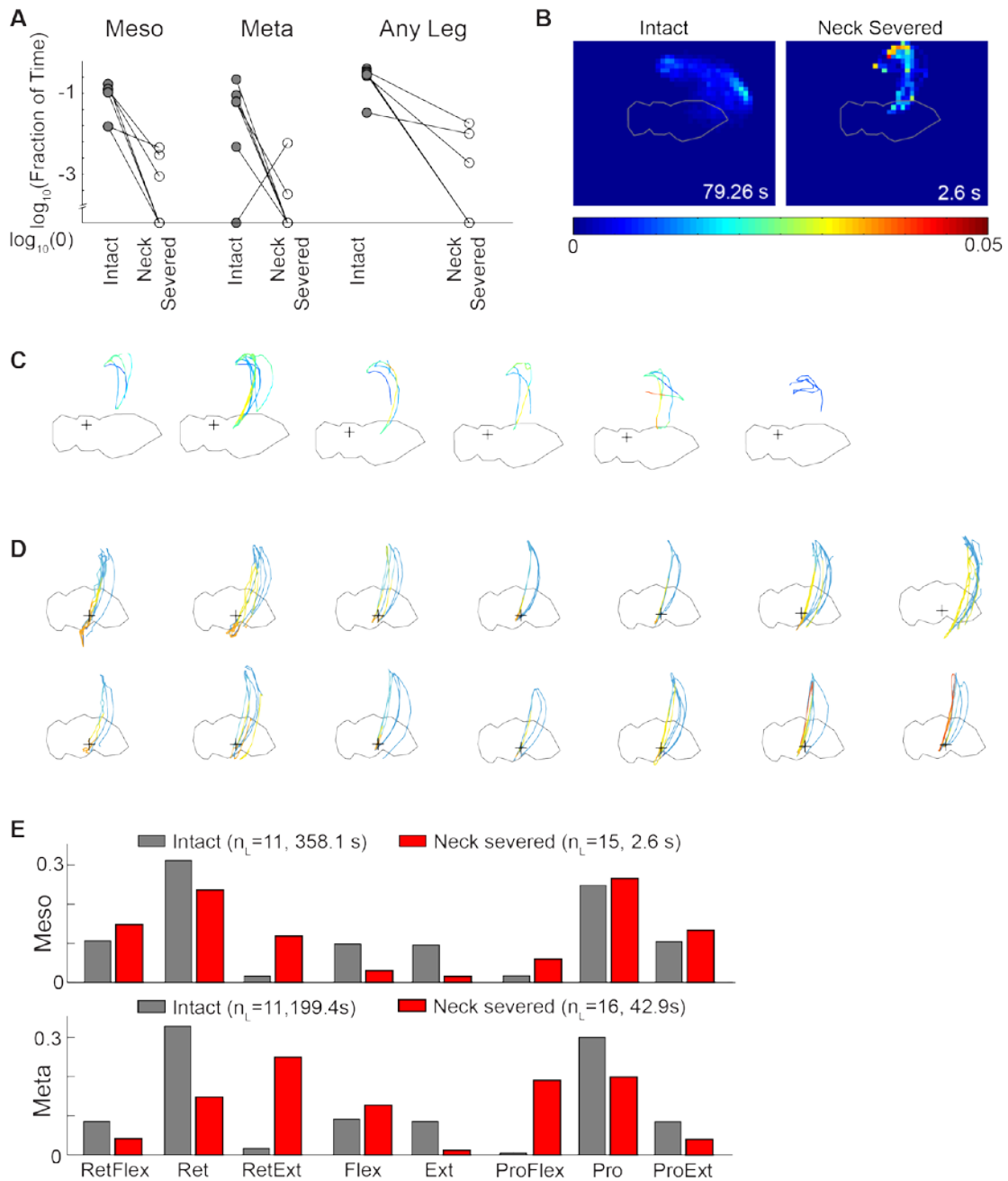


Figure 16 : Headless flies show a reduction in burst probability and burst diversity, but an increased probability of exhibiting atypical states. (A) For individual flies, probability of bursting was greatly reduced after severing the neck. This was true for both the meso and the meta legs. Probability of bursting in any of the four legs that were tracked was also reduced. **(B)** Representative example of the distribution of burst trajectories in one metathoracic leg in an individual fly, showing the reduction in the

range of motion after the neck has been severed. (C) All of the burst bouts observed in the fly/leg shown in (B) after severing the neck. Colors represent different states. (D) Representative example of the burst bouts observed in a different fly after severing the neck. (E) Fraction of total bursting time spent in each state.

3.7 Structured movement in load free preparations is affected by activity in the brain

Having demonstrated that descending inputs are necessary for generating cycle to cycle variability, we next wanted to test if transiently activating or inactivating specific regions of the brain known to contain DN cell bodies would change the distribution in cycle types in any way.

To activate the neurons, we used a pan-neuronal Gal4 driver, *nsyb-Gal4*, to drive expression of a non-endogenous of an ionotropic purinoreceptor P2X₂, which is gated by the binding of an ATP ligand (Lima and Miesenbock 2005). We activated the neurons in four different regions of the brain known to contain DN cell bodies: the central GNG, the middle SMP cluster, the left SMP cluster, and the right SMP cluster. The SMP and GNG clusters were chosen because they contain the largest number of DNs (Hsu and Bhandawat 2016). The spatial range and the magnitude of activation was confirmed using whole cell patch-clamp electrophysiology (Appendix B).

To inactivate the neurons, we used the same pan-neuronal Gal4 driver, *nsyb-Gal4*, to drive expression of the histamine gated chloride channel, ort channel (Liu and Wilson 2013). Histamine was delivered to silence neurons in the same four regions in the activation study: the central GNG, the middle SMP cluster, the left SMP cluster, and the

right SMP cluster. As with the P2X₂ receptor, the spatial range and the magnitude of inactivation was confirmed using whole cell patch-clamp electrophysiology (Appendix B).

In the experiments where the head position of the fly was oriented to enable targeting of the GNG cluster, the prothoracic and mesothoracic legs showed almost no variability in the cycle types even in the absence of pharmacological stimulation. Over 80% of the cycles observed in the prothoracic and mesothoracic legs for the No Drug trials were of the Ret-Pro type. For the metathoracic legs, activation of the middle of the gnathal ganglia appeared to increase the probability of observing the most common type of bursts (Ret-Pro) (Table 3). Conversely, inactivating these neurons appeared to decrease the probability of observing Ret-Pro cycles, although there were very few bursts observed during inactivation.

Table 3 : Activation and inactivation of the midline gnathal ganglion (where the GNG cluster is located)

	Cycle Types	No drug, P2X ₂		ATP, P2X ₂		No drug, ort		His, ort	
		# of cycles	%	# of cycles	%	# of cycles	%	# of cycles	%
Prothoracic		(n _c =268)		(n _c =51)		(n _c =6)		(n _c =1)	
Top 80% of observed cycles	Ret-Pro	243	90.7	41	80.4	5	83.3	1	1
Mesothoracic		(n _c =556)		(n _c =203)		(n _c =65)		(n _c =23)	
Top 80% of observed cycles	Ret-Pro	532	95.6	181	89.2	57	87.7	21	91.3
Metathoracic		(n _c =200)		(n _c =34)		(n _c =31)		(n _c =11)	

Top 80% of observed cycles in:									
P2X2 controls	Ret-Pro	75	37.5	19	55.9	10	32.3	2	18.2
	Flex-Ext	29	14.5	3	8.8	1	3.2	0	0
	Ret-Pro-ProExt	21	10.5	2	5.9	4	12.9	3	27.3
	RetFlex-ProExt	18	9.0	0	0	6	19.4	0	0
	Ret-Flex-Pro-ProExt	12	6.0	0	0	0	0	0	0
	RetFlex-Pro-ProExt	5	2.5	2	5.9	3	9.7	0	0
ort controls (but not P2X2 controls)	RetFlex-Ret-ProExt	3	1.5	1	2.9	2	6.5	0	0
ort with His (but not controls)	Pro-ProExt	2	1	0	0	0	0	4	36.4

In the experiments where the head position of the fly was oriented to enable activation and inactivation of the SMP clusters, the prothoracic legs showed no change in the distribution of cycles (Table 5). For the mesothoracic and metathoracic legs, activation of the right side of the brain had a more dramatic effect than activation of the left side of the brain, which may suggest some asymmetry in drug delivery

, Appendix C). In particular, delivering ATP to the right side of the brain reduced the fraction of time the right mesothoracic and metathoracic leg spent in the retraction-protraction state (from 79% to 6.7% for mesothoracic and from 44.6 to 12.5% for

metathoracic). There was also an increased fraction of atypical cycles, although there were not enough to discount that they may be the result of spurious events.

During inactivation of each of the three regions of the brain containing the SMP clusters, the number of burst cycles was not sufficient for determining whether or not there was any effect.

Table 4 : Number of cycles observed during inactivation of the SMP cluster with histamine

	No Drug Ctrl	Left His	Right His	Middle His
Prothoracic	14	3	0	3
Mesothoracic	43	2	0	8
Metathoracic	10	0	2	3

Table 5 : Prothoracic cycle types in response to activation of SMP

Top 80% of cycles in		Control (n _c = 98)		ATP, right				ATP, middle (n _c = 12)		ATP, left			
				Right Leg (n _c = 0)		Left Leg (n _c = 2)		Right Leg (n _c = 1)		Left Leg (n _c = 38)			
		#	%	#	%	#	%	#	%	#	%	#	%
Ctrl	Ret-Pro	74	75.5	-	-	1	0.5	10	83.3	0	0	38	100
	Ret-ProExt	6	6.1	-	-	0	0	0	0	0	0	0	0
Right	Ret-ProFlex	0	0	-	-	1	0.5	0	0	0	0	0	0
	Ret-Flex-Pro			-	-	0	0	0	0	1	1	0	0

Table 6 : Mesothoracic cycle types in response to activation of SMP

Top 80% of cycles in		Control (n _c = 101)		ATP, right				ATP, middle (n _c = 5)		ATP, left			
				Right Leg (n _c = 15)		Left Leg (n _c = 2)		Right Leg (n _c = 29)		Left Leg (n _c = 1)			
		#	%	#	%	#	%	#	%	#	%	#	%
Ctrl	Ret-Pro	51	79	1	6.7	0	0	0	0	19	65.5	0	0
	Ret-ProFlex	9	8.9	0	0	0	0	1	20	0	0	0	0
	RetFlex-ProExt	7	6.9	10	66.7	0	0	1	20	1	3.4	1	1
	Ret-RetExt	7	6.9	0	0	0	0	0	0	2	6.9	0	0
	Ret-Pro-ProExt	4	4.0	1	6.7	0	0	0	0	0	0	0	0
	RetFlex-Ret-Pro	3	3.0	0	0	0	0	0	0	0	0	0	0
	RetFlex-Pro	3	3.0	0	0	0	0	0	0	0	0	0	0
	RetFlex-Pro-ProExt	3	3.0	0	0	1	0.5	0	0	0	0	0	0
	Pro-ProExt	3	3.0	0	0	0	0	0	0	0	0	0	0
Flex-Ext	3		0	0	0	0	1	20	0	0	0	0	
ATP right	RetFlex-Ret-ProExt	0	0	2	13.3	0	0	0	0	0	0	0	0
	Pro-ProExt	1	1.0	0	0	1	0.5	0	0	0	0	0	0
ATP middle	RetFlex-Ret	0	0	1	6.7	0	0	1	20	0	0	0	0
	Ret-Ext	0	0	0	0	0	0	1	20	0	0	0	0
ATP left	Ret-ProFlex-Pro	0	0	0	0	0	0	0	0	3	10.3	0	0
	Ret-RetExt	0	0	0	0	0	0	0	0	2	6.9	0	0

Table 7 : Mesothoracic cycle types in response to activation of SMP

Top 80% of cycles in		Control (n _c = 83)		ATP, right				ATP, middle (n _c = 11)		ATP, left			
				Right Leg (n _c = 8)		Left Leg (n _c = 4)		Right Leg (n _c = 19)		Left Leg (n _c = 31)			
		#	%	#	%	#	%	#	%	#	%	#	%
Ctrl	Ret-Pro	37	44.6	1	12.5	4	1	5	45.5	0	0	24	77.4
	RetExt-ProFlex	23	27.7	0	0	0	0	2	18.2	0	0	3	9.7
	Ret-ProExt	3	3.6	0	0	0	0	0	0	0	0	0	0
	RetExt-ProFlex-Pro	3	3.6	0	0	0	0	0	0	0	0	0	0
	RetFlex-Ret-Pro-ProExt	2	2.4	0	0	0	0	0	0	0	0	0	0
	RetFlex-ProExt	2	2.4	0	0	0	0	0	0	0	0	0	0
ATP right	RetFlex-Ret-ProExt	1	1.2	2	25	0	0	2	18.2	0	0	0	0
	RetExt-ProFlex-Pro	1	1.2	2	35	0	0	0	0	2	10.5	0	0
	RetExt-Flex-Pro	0	0	1	12.5	0	0	0	0	0	0	0	0
	RetExt-ProFlex	1	1.2	1	12.5	0	0	1	9.9	15	78.9	0	0
	RetExt-ProFlex-ProExt	0	0	1	12.5	0	0	0	0	0	0	0	0

3.8 Activation of specific DNs changes the probability distribution of bursts observed in a subset of legs

We next chose to determine how activating DNs with known effects on behavior would perturb the types of bursts observed. For this purpose, we used a Gal4 driver which labels neurons that result in backwards walking when activated in the freely behaving fly (Bidaye, Machacek et al. 2014). Neurons labeled by this Gal4 driver, VT50660, include at least two DNs per hemisphere of the SMP cluster. We transiently activated neurons located in the SMP cluster by using the VT50660 Gal4 driver to drive expression of mCD8-GFP and P2X2 and delivering 250 μ M ATP through a 2 μ M glass pipette ($R_{input}=5-6$ M Ω) 10 μ m above the surface of the posterior dorsal surface of the brain (see Appendix B).

For the prothoracic and metathoracic legs, we found that the identities and probability distributions of the top 80% of cycles when the moonwalking DNs were activated with ATP was similar to those observed under the no drug control conditions (Table S1). For the metathoracic legs, the same top two cycles were observed in both ATP and control conditions. However, these cycles only represented approximately 60% of the cycle types observed in either condition. When the moonwalking DNs were activated, there was an increased probability of observing four types of cycles that were atypical under control conditions: Ret-Pro-ProExt, Ret-Flex-Ext, Ret-Flex-ProExt, and Ret-Pro-Ext (Figure 11A). Together, these four cycle types represented 17.8% of the total cycles observed during neuronal activation.

Prothoracic	Cycle Types	No drug (n _c =782)		ATP (n _c =220)	
		# of cycles	%	# of cycles	%
Top 80% of observed cycles	Ret-Pro	543	69.4	170	77.3
	Ret-Pro-ProExt	102	13.0	9	4.1
Mesothoracic		No drug (n _c =499)		ATP (n _c =154)	
Top 80% in no drug controls ¹	Ret-Pro	282	56.5	94	61.0
	RetFlex-ProExt	30	6.0	5	3.2
	Ret-Flex-Pro	28	5.6	9	5.8
	Ret-Pro-ProExt	23	4.6	3	1.9
	RetFlex-Pro-ProExt	16	3.2	7	4.5
	Flex-Ext	14	2.8	1	0.6
	RetFlex-Ret-Pro-ProExt	8	1.6	1	0.6
Metathoracic		No drug (n _c =427)		ATP (n _c =174)	
Top 80% in no drug controls	Ret-Pro	187	43.8	75	43.1
	Flex-Ext	76	17.8	34	19.5
	RetFlex-ProExt	20	4.7	6	3.4
	Ret-Ext	18	4.2	1	0.6
	Flex-ProExt	17	3.9	2	1.2
	Ret-Pro-ProExt	9	2.1	13	7.5
	Ret-ProExt	9	2.1	4	2.3
	RetFlex-Ret-ProExt	8	1.9	1	0.6
Top 80% during activation	Ret-Flex-Ext	5	1.2	10	5.7
	Ret-Flex-ProExt	4	0.9	4	2.3

Because transition from stance to swing in forward locomotion typically is initiated with retraction of the leg, we hypothesized that the opposite would happen in backwards walking. Thus, we next asked if activation of the moonwalking DNs

¹ The remaining cycle types that comprised the top 80% during ATP activation were RetFlex-Flex-Ext, RetFlex-Flex-Pro-ProExt, Ret-Flex, Ret-Flex-Pro-ProExt, and Ret-ProFlex-Pro, each of which occurred 3 times (thus representing less than 2% of the cycles).

increased the probability of a protraction-like state (ProFlex, ProExt, or Protraction Only) appearing earlier in a burst bout than a retraction-like state (RetFlex, RetExt, or Retraction Only). Activating these DNs had no consistent effect across flies on the probability with which bursts exhibit a retraction like state prior to exhibiting a protraction like state. However, the variability in whether protraction or retraction was exhibited first within a burst bout was reduced following activation (Figure 11B).

Despite the lack of consistent effects in the order of protraction versus retraction across individuals, the atypical cycle types observed when the moonwalking DNs are activated have some features that are consistent with the hypothesis that activating moonwalking DNs in a load free preparation biases the legs towards motions that are analogous to those that may be observed in backwards walking. Specifically, because we define retraction as a reduction in the tarsus-flyaxis angle, the force vector generated by retraction in these atypical cycles is directed more towards the midline of the fly than the posterior portion of the fly. Thus, a future analysis would be to quantify the direction of motion of the metathoracic legs with respect to the anterior posterior axis.

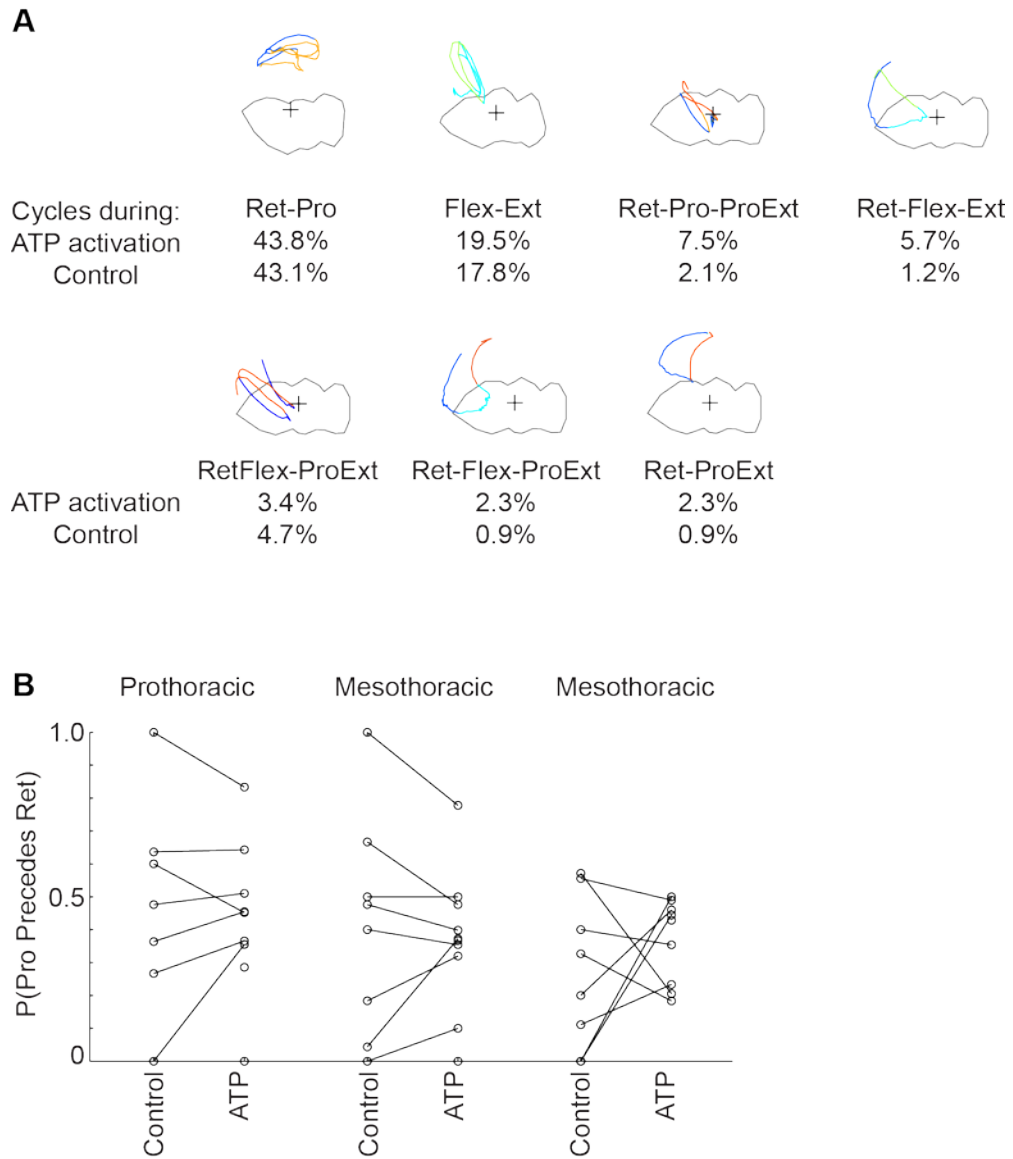


Figure 17 : Activation of moonwalking DNs. (A) Although activating the moonwalking DNs did not greatly perturb the probability of observing common cycles such as Ret-Pro and Flex-Ext, there was an increased probability of observing atypical cycles such as Ret-Pro-ProExt, Ret-Flex-Ext, Ret-Flex-ProExt, and Ret-Pro-Ext. The control data in this figure only includes the no drug trials recorded from the same individual flies. (B) There was no consistent change in the probability of protraction preceding retraction across individual flies.

3.9 Conclusions

In this chapter, we have characterized how legs move in a load-free preparation. We find that by removing both the mechanosensory load as well as the physical obstruction caused by a substrate, we can perturb the fly and reduce the feedback it receives without causing significant physical damage. This allows us to gain some unique insights into the differences between descending (feedforward) control from the brain versus feedback control from circuits in the thoracic ganglia.

We find that even in the absence of physical feedback from the ground, leg movements are highly structured, and we can define this structure as a series of a repeating sequence of states, where each state represents motion in a specific direction and axis. These cycles are often repeated many times within a burst bout. We find that individual legs are capable of exhibiting this structured movement independent of each other and even in the absence of descending input (from the head). This cyclical repetition of a specific sequence of states suggests that the thoracic ganglia are capable of producing not only rhythmic but coordinated joint movements between different joints of a single limb. However, the states observed in the absence of descending inputs are atypical from those observed in the intact fly, and represent joint movements that would not be observed in the freely walking fly during normal forward locomotion.

We also find that perturbing large regions of the brain in which DNs are known to exist or subsets of DNs with known ethological functions will perturb the probability of observing certain types of burst cycles.

4. The role of the AOTU DN cluster in descending control

4.1 Overview and rationale

In our previous two chapters, we established first, the number of DNs through which information from the brain can reach the thoracic ganglia (Chapter 2), and second, particular types of bursts whose distribution changes depending on which sets of DNs are activated or inactivated (Chapter 3). Taken together, these two strategies provide a framework for understanding the different components of the DN population and how they interact to produce flexible and adaptive descending control. To this end, we wanted to investigate individual DNs and characterize the sensory stimuli to which they respond and the motor primitives (states) which they control, to determine if particular subset of neurons mediates there is a particular subset of behavioral responses a particular .

We selected the AOTU DNs for several reasons. First, their small number (~40 per hemisphere) suggested that a comprehensive characterization of these DNs was tractable. Second, their distinct location in the dorsal and anterior portion of the brain suggested that they may serve a special function relative to the other DNs, since the majority of DNs are located in large clusters on the posterior or ventral to the surface of the brain. In addition, these DNs were found in close proximity to the anterior optic tubercle and sent projections through the medial antennae lobe tract (mALT), which suggested that they may have some interactions with sensory processing regions.

The mALT is also one of the few processes labeled by our retrograde labeling procedure that passes in close proximity to the LAL, suggesting that DNs that send projections through this tract were putative candidates for LAL innervating DNs. This is significant because the LAL is one of the major outputs of the central complex, a group of four midline neuropil regions previously implicated in coordinated walking, gap crossing, and visual and spatial memory (Strauss, Hanesch et al. 1992, Strauss and Heisenberg 1993, Liu, Seiler et al. 2006, Neuser, Triphan et al. 2008, Poeck, Triphan et al. 2008, Ofstad, Zuker et al. 2011, Seelig and Jayaraman 2013, Seelig and Jayaraman 2015, Weir and Dickinson 2015). Based on the functionality and the expression of particular genes, the central complex is believed by some to be homologous to the basal ganglia in vertebrates (Strausfeld and Hirth 2013).

4.2 Methodology

We used *in-vivo* whole cell patch clamp electrophysiology to record from individual AOTU DNs while simultaneously recording the leg movements and the responses to sensory stimuli of different modalities. Data was collected from both genetically identifiable DNs as well as DNs that did not express a genetic label (but were found in physical proximity to a genetically identifiable DN). The recording electrode contained internal saline with 1% neurobiotin, which was diffused into the cell over the course of the electrophysiological recording. This enabled us to confirm whether or not the neuron we recorded from was in fact a DN.

To reliably characterize individual DNs, we first needed to use a Gal4 driver to genetically label AOTU DNs. We selected candidate Gal4 drivers as those which had expression in the neck and the lateral accessory lobes and cell bodies in the region between the anterior optic tubercle and the mushroom body peduncle (where AOTU DN cell bodies are located, as described in Section 2.2.2.1). We then used the backfill strategy (described in Section 2.2 and 2.4) to confirm whether these cell bodies sent processes through the neck.

We found several Gal4 drivers that labeled AOTU DNs (R15E12, R10A07). However, with the exception of instances where we recorded from a non-genetically tagged DN, most of our data was collected from AOTU DNs expressing the e49-Gal4 driver (of which there were four).

4.3 AOTU DNs subdivide into two clusters

AOTU DNs subdivide into two clusters, one of which is *b*-dorsal to the anterior optic tubercle and the other which is *b*-ventral (Figure 18). As described in Section 2.2.1, we assume that variations in the number of DNs per in each subcluster is the result of variations in the efficacy of the retrograde labeling rather than in the number of DNs. Thus, we report the maximum number of DNs per subcluster, which is 19 for the dorsal subcluster (n=4, mean \pm SD = 9.75 ± 6.40 , median = 7.5) and 21 for the ventral subcluster (n=8, mean \pm SD = 15.5 ± 2.82 , median = 15). We found one GABAergic DN and three

cholinergic DNs in the dorsal subcluster, and four GABAergic DNs and 14 cholinergic DNs in the ventral subcluster (using the methods and data described in section 2.4.1).

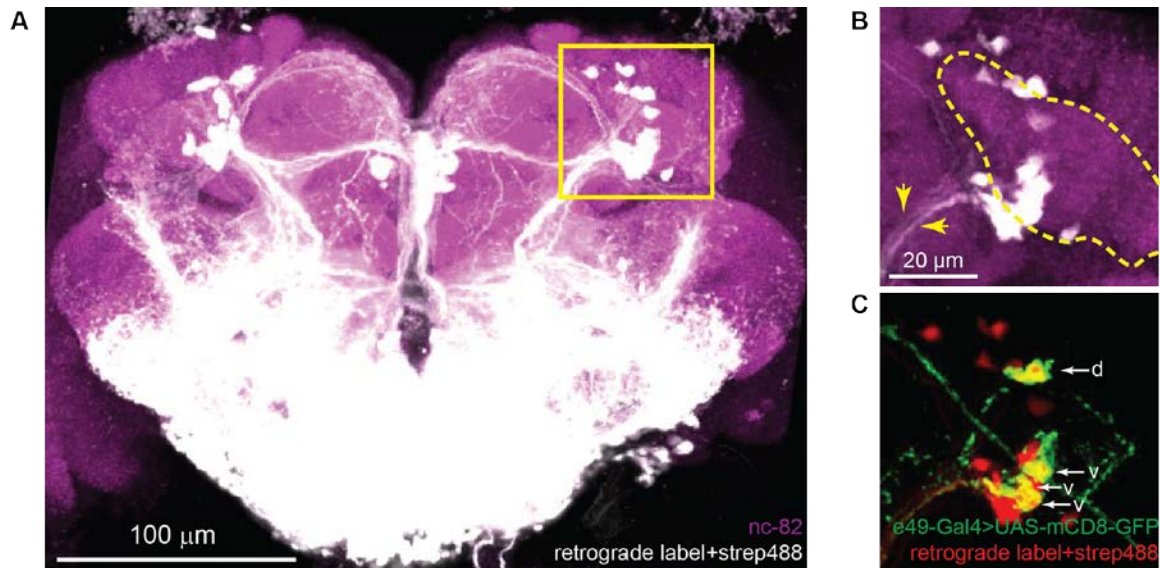


Figure 18 : AOTU DNs can be further subdivided into two clusters. (A) Representative Z-projection of the anterior half of a brain in which the retrograde label has been applied to the neck. The yellow square indicates the region shown in (B) and (C). (B) Zoomed in image of the AOTU cluster, illustrating the presence of two distinct clusters. The anterior optic tubercle outlined in yellow. Yellow arrowheads indicate the presence of two different tracts leading away from the AOTU cluster (suggesting a separate tract for the dorsal and the ventral subcluster). (C) Identical confocal stack as shown in (A) and (B), but recolored to show the colabeling between the Gal4 driver specific to AOTU DNs (e49-Gal4, shown in green) and the retrograde label identifying DNs (shown in red). Arrows represent dorsal (d) and ventral (v) cells labeled by the e49-Gal4 driver.

4.3.1 Most if not all AOTU DNs in the ventral cluster are leg innervating

We labeled twelve AOTU DNs in the ventral cluster. Three were labeled with e49-Gal4, one was labeled with R10A07-Gal4, and were eight non-genetically labeled. All twelve innervated the ipsilateral LAL, and the ipsilateral inferior slope (Figure 19). There were some neurons that innervated the contralateral inferior slope; however,

bilateral innervation of the LAL was only observed in one case where a neuron (e49-v1, see below for nomenclatures) was gap junction coupled to another neuron (that was not labeled by the same Gal4 driver). Thus, although these DNs had common features, they also showed heterogeneous innervation patterns in the brain.

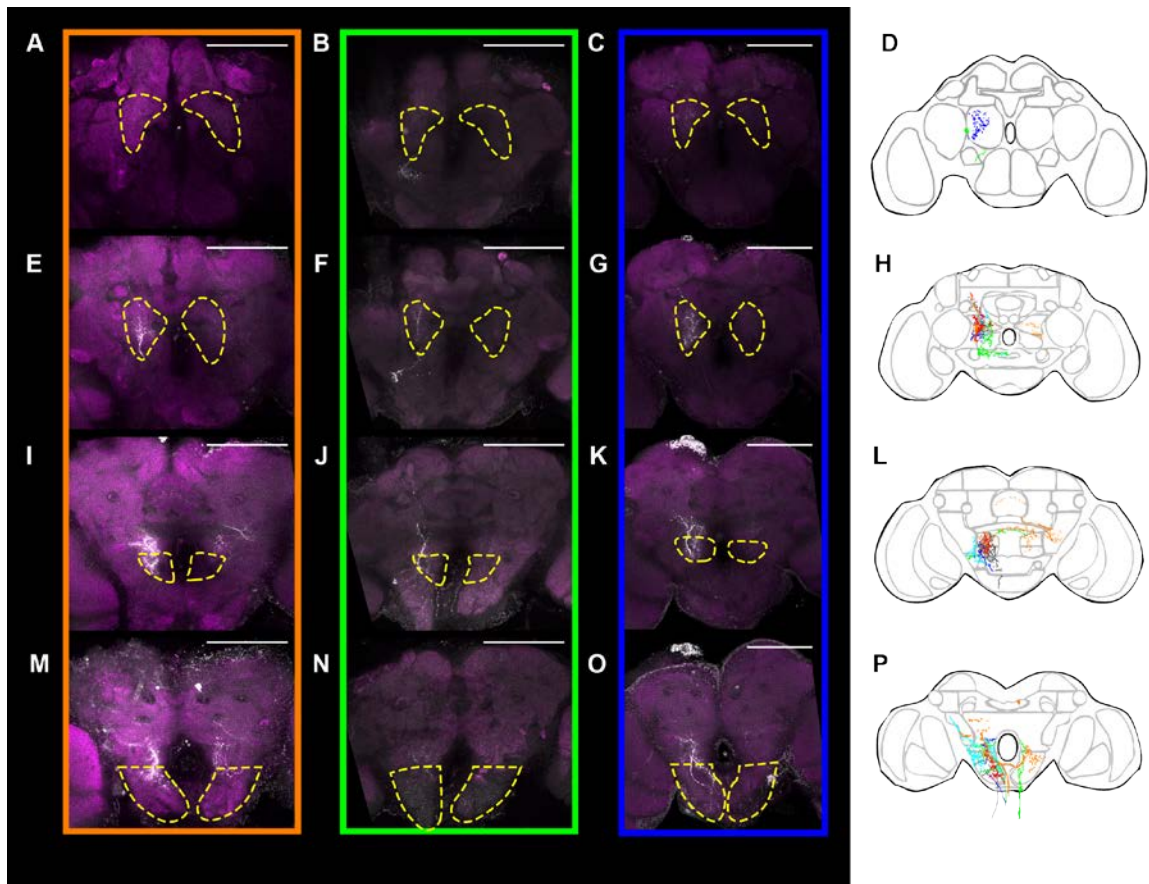


Figure 19 : Representative examples of DNs in the ventral AOTU subcluster, showing that while the projections of DNs in this subcluster are heterogeneous, all innervate the LAL and the inferior slope. (A-C). Single cell fills of ventral AOTU DNs obtained through diffusion of neurobiotin into the cell during whole cell patch clamp recording. White represents the Z projection of the neurobiotin in the anterior portion of the brain. Purple represents a representative section of the neuropil (stained with nc-82) containing the reference markers shown in (D). (A), (B), and (C) represent different example neurons. The color with which their respective columns has been outlined corresponds to the color drawn in the schematics in (D), (H), (L), and (P). (D). Six

representative cell fills for different ventral AOTU DNs are manually traced and shown superimposed on neuropil markers in a reference brain. Each color represents a different DN. **(E-P)**. Same as **(A-D)**, but for successively more posterior sections of the brain with corresponding reference neuropil markers as drawn in **(H)**, **(L)**, and **(P)**. Scalebars in all panels represent 100 μm . In **(A-C)** and **(E-G)**, the dotted outline indicates the LAL. In **(I-K)** and **(M-O)**, the dotted yellow line indicates the inferior slope.

Projections into the thoracic ganglia and leg neuromeres fell into at least two distinct patterns. The first type, which we will refer to as ventral 1 (v1), consisted of many short branches that did not penetrate very deeply into the leg neuromeres (Figure 20A-D). This type appears to be the predominant innervation pattern of DNs in the ventral subcluster. It appeared in six of the seven non-genetically labeled AOTU DNs we were able to obtain complete fills for and in two of the four AOTU DNs labeled by e49-Gal4. The second type, which we will refer to as ventral 2 (v2), consisted of several long branches that penetrated more deeply (both towards the lateral and ventral direction) into the leg neuromeres than the v1 type (Figure 20E-I). We found three examples of this type of DN: one was genetically labeled by e49-Gal4, one was genetically labeled by R10A07, and the third was a non genetically labeled DN.

The difference between v1 and v2 type innervation is significant because there exists some evidence of a “myotopic map” in the leg neuromeres. Specifically, motor neurons controlling the muscles in the tibia typically have dendrites that are more densely distributed in the dorsal half of the leg neuromeres, while those that control the muscles in the femur, coxa, and trochanter typically have denser dendritic arborization in the ventral half of the leg. This suggests that the v1 type of neurons may primarily

control movements related to flexion and extension, while v2 type of neurons may be more involved in protraction, retraction, depression, and levation. However, more detailed anatomical and functional analyses of individual neurons will be necessary to determine if this is true.

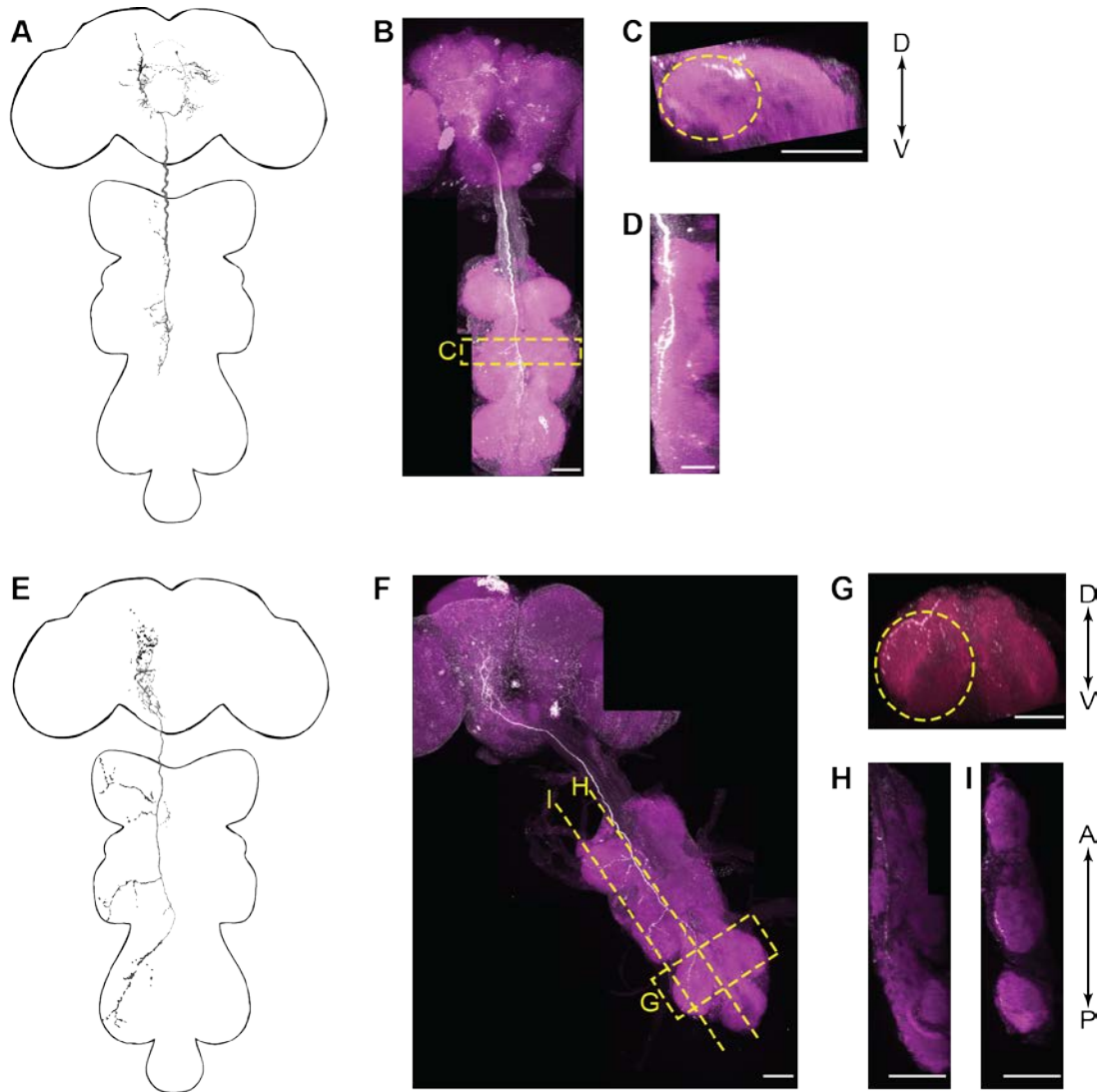


Figure 20 : The pattern of leg neuromere innervation of DNs in the ventral AOTU subcluster could be subdivided into two types. (A) Schematic representation of a single cell fill of type v1. The darker the trace, the more anterior the projection in the brain and the more ventral projection in the thoracic ganglia. (B) Z projection of the confocal stack

from which the schematic in (A) was obtained. The square with the dotted yellow outline represents the region used in (C). (C) The projection along the anterior to posterior axis of the mesothoracic ganglia, as outlined by the square with a dotted yellow line in (B). (D) Projection from the lateral view of the thoracic ganglia shown in (A). (E) Schematic representation of a single cell fill of type v2. Intensity of the trace represents the same as in (A). (F) Z projection of the confocal stack from which the schematic in (E) was obtained. The square with the dotted yellow outline represents the metathoracic ganglia, the region used in (G). (G) The projection along the anterior to posterior axis of the metathoracic ganglia, as outlined by the square with a dotted yellow line in (E). (H) Representative slice through the axonal tract of the neuron shown in (F). (I) Representative slice showing the innervation of the leg neuromeres by the neuron shown in (F). In all panels, the scale bar represents 50 μm .

To determine whether the innervation of these neurons represents dendritic or synaptic arbors, we used the *e49-Gal4* driver, which labeled two type v1 DNs and one type v2 DN, to drive the expression of the presynaptic marker synaptotagmin (Zhang, Rodesch et al. 2002) and the dendritic marker Denmark (Nicolai, Ramaekers et al. 2010). There was expression of Denmark but no expression of synaptotagmin, indicating that the neurites innervating the LAL of *e49-Gal4* DNs of type v1 and v2 are primarily dendrites (Figure 21). The *e49-Gal4* driver drove expression of both Denmark and synaptotagmin in the inferior slope. Because *e49-Gal4* is not exclusively expressed in AOTU DNs, we could not use this tool to conclusively determine whether this mixture of expression indicates that AOTU DNs have both dendritic and synaptic arbors in the inferior slope, or if the presence of both types of neurites is the result of neurons other than AOTU DNs also innervating the inferior slope.

To overcome this limitation in the genetic tool, we also performed single-cell fills of AOTU DNs in flies of the genotype *e49-Gal4>UAS-Denmark*. In the single-cell fill of

one of the two e49-Gal4 labeled neurons of type v1, the inferior slope contained no colabeling between the genetically expressed dendritic marker and the neurobiotin fill of the single cell. This suggests that the innervation of the e49-v1 DN in the inferior slope is an axon collateral, and that the primary input into these neurons is the LAL. We have not yet obtained a single cell fill of the e49-Gal4 labeled neuron of type v2.

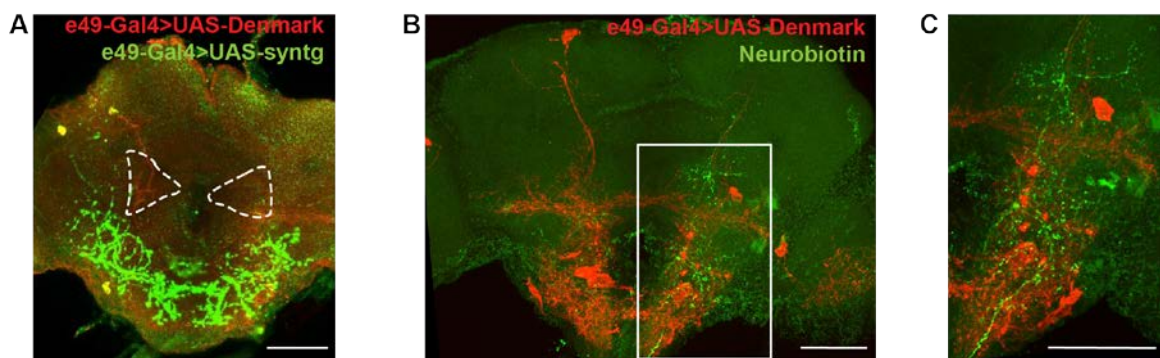


Figure 21 : Denmark and synaptotagmin labeling for ventral clusters. (A) e49-Gal4>UAS-Denmark, synaptotagmin. The e49-Gal4 driver labeled three AOTU ventral DNs and one AOTU dorsal DN. White dashed lines outline the LAL. **(B)** Neurobiotin single cell fill of one of the two e49-v1 DNs, shown in green. Denmark shown in red. White rectangle represents the region magnified in panel **(C)**. **(C)** Magnification of the region outlined by the white rectangle in panel **(B)**, showing that the innervation of the e49-v1 DN in the inferior slope is probably axonal rather than dendritic. Colors are the same as in panel **(B)**. In all three panels, the scale bar represents 50 μ m.

4.4.2 Wing innervating AOTU DN in dorsal cluster

We were able to fill one dorsal AOTU DN, which was labeled by the e49-Gal4 driver. This DN did not innervate the LAL but did innervate the anterior optic tubercle, the AMMC, and the inferior slope. In the thorax, projections from this DN innervated the accessory mesothoracic neuromeres, where the circuitry for controlling wing movements is located, but none of the leg neuromeres (Figure 22).

To determine whether these projections were dendritic or axonal, we used e49-Gal4 to drive expression of the dendritic marker Denmark (Nicolai, Ramaekers et al. 2010). We found that dendritic arbors for this DN were located in the anterior optic tubercle, the AMMC, the inferior bridge, and posterior ventrolateral protocerebrum.

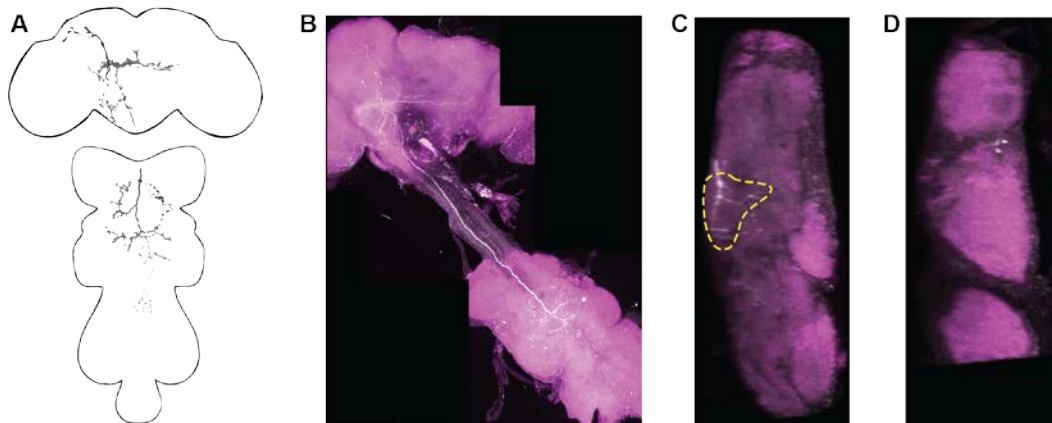


Figure 22 : Neurons in the dorsal AOTU subcluster innervate the accessory mesothoracic neuromere but not the legs. (A) Schematic representation of a single cell fill of type v1. The darker the trace, the more anterior the projection in the in the brain and the more ventral projection in the thoracic ganglia. **(B)** Z projection of the confocal stack from which the schematic in **(A)** was obtained. **(C)** Representative slice through the approximate midline of the fly, showing the innervation of the wing neuromere (outlined in dashed yellow). **(D)** Representative slice showing the lack of innervation in the leg neuromeres.

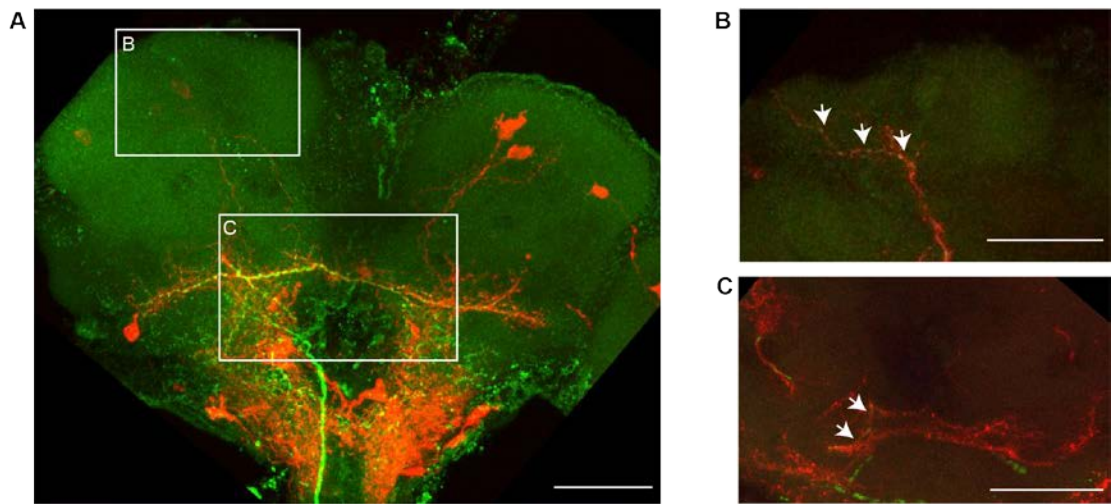


Figure 23 : Denmark labeling for e49-dorsal. (A) Single cell fill (green) of e49-Gal4>UAS-Denmark (Denmark shown in red). Z projection over the entire brain shows the colabeling (yellow) between the Denmark and the neurobiotin fill of the inferior slope on the posterior surface of the brain. The regions for which a subset of the stack were magnified in panels (B) and (C) are shown outlined in white. (B) Colabeling in the anterior optic tubercle of neurobiotin (green) and Denmark (red). Colabeling appears yellow and is indicated by the white arrows. (C) Colabeling in the anterior optic tubercle of neurobiotin (green) and Denmark (red). Colabeling appears yellow and is indicated by the white arrows. In all three panels, the scale bar represents 50 μm .

4.5 AOTU DNs are broadly tuned to sensory information

Our initial approach for determining whether or not AOTU DNs responded to any and if so, how many, stimuli of different sensory modalities. Thus, we first recorded from these DNs while determining their response to strong stimuli. To test olfaction, we used pure apple cider vinegar, which is a complex food odor and thus activates multiple ORN classes and is attractive to the fly (Semmelhack and Wang 2009, Jung, Hueston et al. 2015). To test visual responsiveness, we presented the fly with a 1 s pulse of full field

light, as well as a light that flickered at 10 Hz. To test the responsiveness of the DN to wind, we used a 2L/min stimulus.

We found that DNs in the AOTU cluster are all tuned to sensory information but have heterogeneous responses to the same stimuli (Figure 24). For instance, e49-v1 (Figure 24A) and e49-v2 (Figure 24B) both had a strong depolarization to full field light with very little decay, while e49-dorsal had a large decay following a strong but transient depolarization, and another depolarization at the offset of the light stimulus. Both e49-v1 and e49-v2 hyperpolarized slightly in response to apple cider vinegar, but in the case of e49-v1, this hyperpolarization was more pronounced when the legs were moving, while in e49-v2 this hyperpolarization is less pronounced when the legs were moving. In contrast, e49-dorsal showed a large depolarization response to presentation of apple cider vinegar odor, especially in instances when the fly's legs did not move.

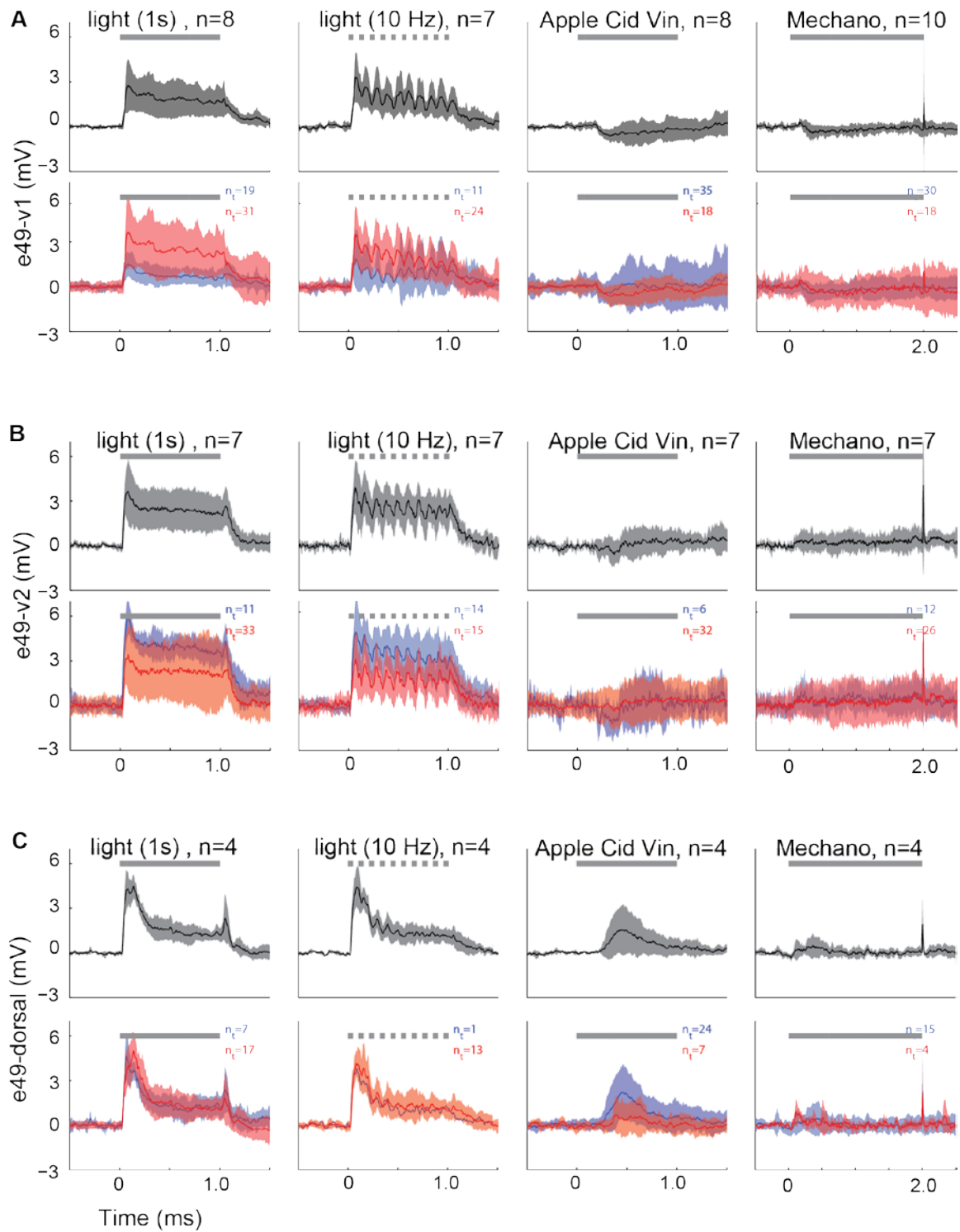


Figure 24 : Comparison of how DNs in the AOTU cluster are tuned to sensory information but have heterogeneous responses to the same stimuli. (A) Responses of

e49-dorsal. Gray trace in top panels are shown as the mean and STD of cells, where the data collected from each cell is averaged over all trials. Bottom panels contain the mean and STD of all moving (red) and non-moving (blue) trials. **(B)** e49-v1. Colors are the same as in **(A)**. **(C)** e49-v2. Colors are the same as in **(A)**. Stray capacitance current from noise in the electrophysiology rig was observed at the offset of the mechanosensory stimulus. Movement of the legs was computed as a change in pixel intensity in the recorded video.

After determining that AOTU DNs were highly responsive to light, we next wanted to ask if there were specific visual stimuli that they responded to. We tested the response of these DNs to the following stimuli: gratings moving in one of the eight cardinal directions, progressive and regressive optic flow gratings, a rotating grating, a small horizontal bar, a tall vertical bar, and visually looming (expanding) squares approaching from one of three directions (Appendix C).

We found that all DNs responded to broad field motion, such as a moving grating, but none of them responded to small visual stimuli such as a rapidly expanding square (Figure 25).

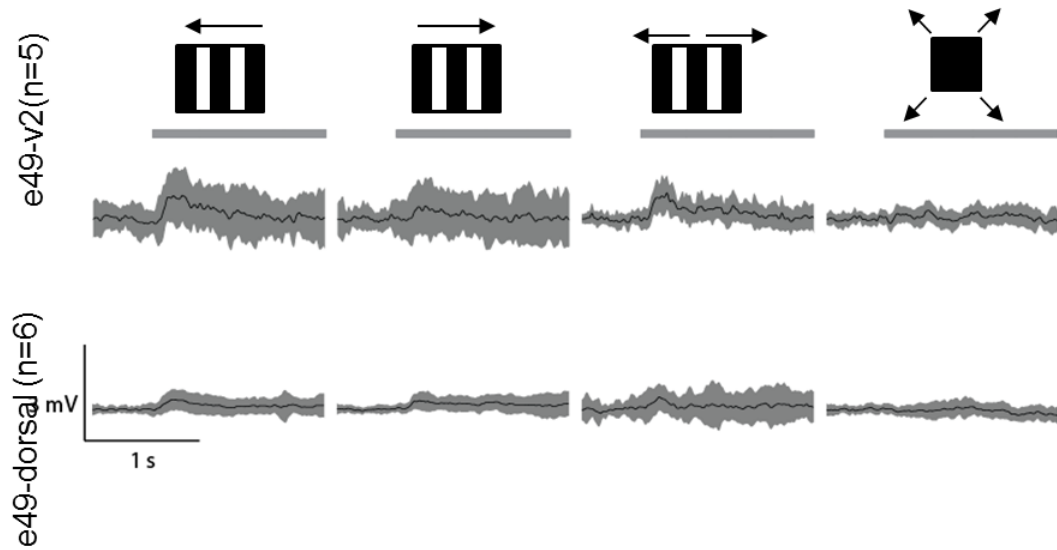


Figure 25 : DNs in the AOTU cluster respond to broad field stimuli (moving gratings) but not small field stimuli (such as an expanding square). However, these responses vary in magnitude.

4.6 Activity in the ventral cluster corresponds to movement initiation in the legs

Because activity in AOTU DNs was primarily triggered by the presentation of specific stimuli, depolarization was more correlated with sensory information than with movement initiation. However, comparing trials in which leg movements were observed to those where there was no leg movement (Figure 24) showed that neuronal responses to stimuli changed depending on whether or not leg movements occurred. In particular, e49-v2 neurons depolarized more in trials when leg movements were observed. They also had a more pronounced response to apple cider vinegar trials in those cases, exhibiting a transient hyperpolarization followed by depolarization, although this depolarization had a high standard deviation.

We next asked if “movement initiation” (defined as the timepoint at which a change in pixel intensity passed the noise threshold) was typically preceded by depolarization. We found this to be the case for e49-v2 (Figure 26) but not e49-dorsal. The depolarization prior to movement onset was present even when movement occurred spontaneously in the absence of sensory stimulation.

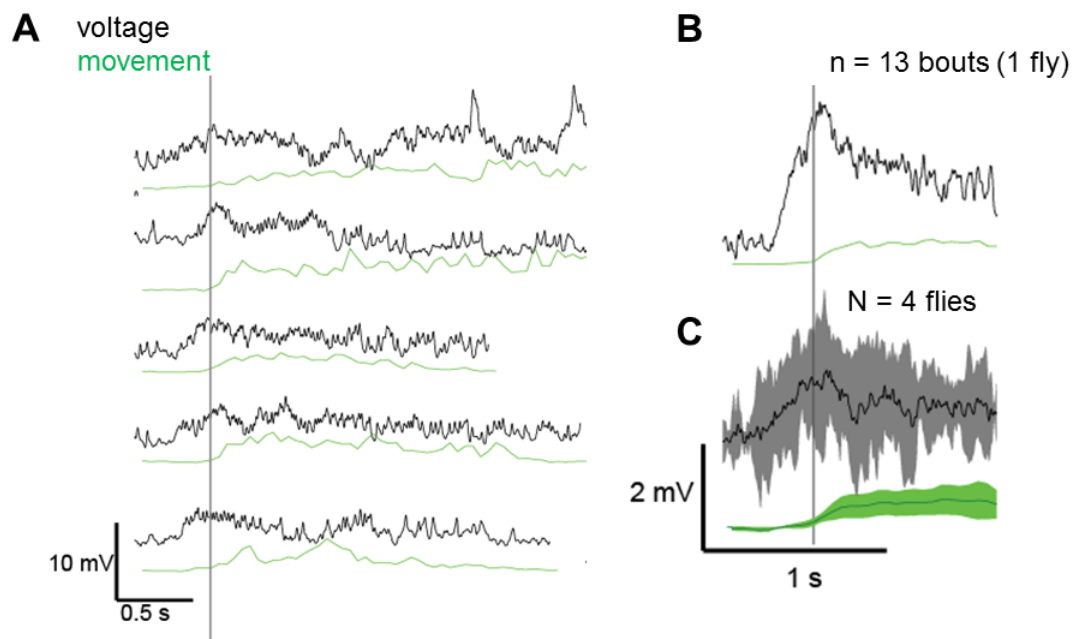


Figure 26 : Depolarization precedes movement initiation in e49-v2. (A) Individual representative movement bouts, lined up according to movement onset. **(B)** Average voltage and movement for one fly. **(C)** Mean and standard deviation in response for 4 flies.

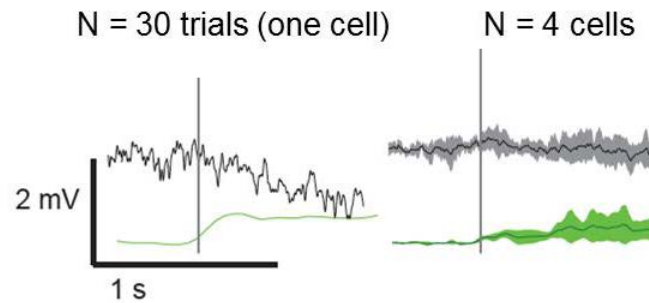


Figure 27 : There is no relationship between activity in e49-dorsal and movement initiation. Left: average voltage and movement for one fly. Right: mean and standard deviation in response for 4 flies.

4.7 Conclusions

We have found that the AOTU cluster of DNs subdivides into two clusters, a dorsal and a ventral cluster. DNs from the ventral cluster typically innervated the leg neuromeres, although their innervation patterns fell into two different types.

All DNs in the AOTU cluster appeared to be broadly tuned to sensory stimuli, but their responses were heterogeneous. Moreover, they were all responsive to light, and some, but not all, were responsive to apple cider vinegar.

5. Discussion

5.1 *Drosophila* have ~1100 DNs in at least six discrete clusters

We present here, what is to our knowledge, the first comprehensive description of the number and distribution of DNs in *Drosophila*. Our results suggest that *Drosophila* have ~1,100 DNs that are distributed across 6 clusters.

5.1.1 Clusters of DNs express multiple neurotransmitter types

Drosophila DNs employ multiple neurotransmitters and no DN cluster exclusively expresses any single neurotransmitter type. A hallmark of descending motor control is that, irrespective of size and complexity of the movements being controlled, descending control systems employ DNs of multiple neurotransmitter type (Marder 2012); the use of multiple neurotransmitter type is considered important for flexible control of behavior. Thus, it is not surprising that the fly's DN population also consists of multiple neurotransmitter types.

However, this does contrast with the fact that the DN population in mammals is comprised of largely excitatory neurons. The corticospinal tract, rubrospinal tract and the vestibulospinal tract are all glutamatergic and thus presumably excitatory (Du Beau, Shrestha et al. 2012). Only the reticulospinal tract has a significant fraction of GABAergic neurons; although, even in this case the 59% glutamatergic neurons dominate the 20% GABAergic axons (Du Beau, Shrestha et al. 2012). In contrast, the two major clusters of DNs in flies, SMP and GNG, contain comparable numbers of excitatory cholinergic

neurons and inhibitory GABAergic neurons, although the SMP has more GABAergic DNs and the GNG has more cholinergic DNs.

5.1.2 Number and organization of DNs across arthropods appears conserved

A comparison of our study to previous studies suggests a high degree of conservation in the number and organization of DNs across arthropods. The number of DNs in the cerebral ganglia of flies is similar to the number reported in cricket (Staudacher 1998) and cockroach (Okada, Sakura et al. 2003), while the number of DN cell bodies we found in the gnathal ganglia is similar to the number previously described in locusts (Kien, Fletcher et al. 1990). The similarity between cricket (Staudacher 1998), cockroach (Okada, Sakura et al. 2003) and fly (this study) is also supported by a study in another holometabolous insect, the moth *Bombyx mori*, which found three different groups of DNs in the cerebral ganglia (Namiki, Iwabuchi et al. 2014), corresponding to the AOTU, SMP, and PENP clusters described in this study.

Given the overall conservation of the structure and function in the arthropod brain (Ito, Shinomiya et al. 2014) and the reports of many homologous neurons such as the giant fiber neurons and the neck motor neurons (Strausfeld 2012), the conservation in the distribution of DN clusters across insect orders is not surprising. But the remarkable conservation in the number of DNs is surprising given that the number of neurons in other structures such as antennal lobe (Chittka and Niven 2009), optic lobe (Chittka and Niven 2009) and mushroom body (Schürmann 1987) varies by several-

orders of magnitude across different insect species. This conservation might reflect the fact that the number of muscles is similar across insects. Since most insect muscles are innervated by 1 to 3 motor neurons (no more than 13 motor neurons) (Belanger 2005), insect motor systems likely have similar level of complexity. A similar result was also observed in comparing analogous brain regions in bumblebees to honeybees (Mares, Ash et al. 2005). The authors found that sensory areas of the brain and mushroom body scaled with the size of the insect, but the central body (also referred to as central complex), which is associated with movement control, was smaller relative to brain size in the larger insects.

Cricket (order: Orthoptera) and cockroach (order: Blattodea) are both hemimetabolous insects, while *Drosophila* is a holometabolous insect (Ito, Shinomiya et al. 2014). Since hemi- and holo- metabolous insects diverged at least 280 million years ago (Labandeira and Phillips 1996, Wiegmann, Trautwein et al. 2009, Ito, Shinomiya et al. 2014), the similarities in the number and distribution of DNs among these insects implies a high level of conservation. In addition to the conservation in DN numbers across the insect class, the number of supraesophageal DNs in lobster have been estimated to be around 600-700 (Notvest and Page 1981), suggesting that DN numbers are conserved across arthropods.

The organization of DN processes is also evolutionarily conserved among insects. Although we were not able to distinguish between axonal and dendritic

processes, the overall organization of the labeled neural processes is strikingly similar to the cockroach study (Okada, Sakura et al. 2003). Both our study and the cockroach study suggest that DNs receive input from regions of the brain that are innervated by outputs from mushroom body and central complex. Equally importantly, there is also direct sensory input into descending neurons (DNs): The labeling presented in this study is consistent with visual inputs into DNs from optic glomeruli and mechanosensory input from AMMC.

5.2 Descending control of limb movements is multi-layered

5.2.1 Some coordination between joints within a leg is generated at the level of the thoracic ganglia

Using our load free preparation, we find that the movements of individual legs are highly structured even in the absence of feedback from the ground. We define this structure as a series of a repeating sequence of states, where each state represents a specific combination of joint movements.

We find that individual legs are capable of exhibiting this structured movement independently of each other and even in the absence of descending input from the brain. The persistence of this cyclical repetition of a specific sequence of states suggests that the thoracic ganglia are capable of producing not only rhythmic but coordinated joint movements between different joints of a single limb. However, the states observed in the absence of descending inputs are atypical from those observed in the intact fly, and represent joint movements that would not be observed in the freely walking fly during

normal forward locomotion. Moreover, in the absence of both descending inputs from the head and feedback from the load sensors (campaniform sensillae) in the legs, we found no instances in which more than one leg was showing structured, oscillatory motions at any given time.

One question that remains is what the mechanism or source for this structured movement is. In the absence of both descending inputs and load sensors, there are still two sources of sensory inputs that may play a role in organizing the movement: the chordotonal organs, which detect the stretching of the muscles, and the hair plates, whose responses signal the relative positions of the joints to each other (Clarac, Cattaert et al. 2000, Zill, Schmitz et al. 2004). It is unclear whether the patterned movement observed in the decapitated fly depends on these inputs, or whether the intrinsic rhythmicity of CPGs in the leg neuromeres is sufficient to generate these structures.

5.2.2 Coordination across legs requires some form of feedback

Although the movements of individual legs are highly structured, we found that in a load free preparation there is little coordination across legs. This agrees with previous work by Ludwar et al (Ludwar, Goritz et al. 2005), which showed that stimulating the prothoracic femoral chordotonal organ, which occurs during femur-tibia flexion, increases the activity of retractor muscles in the mesothoracic coxa. Moreover, studies in which at least three legs were present found that the metathoracic CTr-joint would only become active in response to the stepping motions of an ipsilateral leg if

both prothoracic and mesothoracic legs were present, even if only one was actively stepping (Borgmann, Hooper et al. 2009). This again suggests that tonically activated sensory input (such as from a chordotonal organ) from an ipsilateral leg plays a significant role in driving the coupling of activity between the metathoracic leg and either of the other two ipsilateral legs.

Given the lack of multi-leg coordination described in this study as well as previously reported studies in the stick insect studies, one question that remains is why previous work in *Drosophila* found that *Drosophila* were still able to maintain a tripod gait even when all sensory neurons in the legs were inactivated (Mendes, Bartos et al. 2013). One possibility may be that sensory neurons near the body wall of the thorax may still be able to detect load. For instance, *Drosophila* possess a tergotrochanteral muscle (TTM) that controls the depression and levation of their mesothoracic legs and extracoxal depressor muscles that perform homologous functions on their prothoracic and metathoracic legs (Koenig and Ikeda 2005). While the TTM has primarily been implicated in jump used by flies for flight initiation, it may play a role in load detection, particularly once feedback from most of the sensors in the legs is removed.

5.2.2 DNs in the GNG

Both the vertebrate brainstem and the gnathal ganglia DNs contain tonically firing neurons which are strongly activated during locomotion (Kien and Altman 1992, Tschida and Bhandawat 2015). They also both play a crucial role in regulating indirect

aspects of motor control such as respiration and posture and interact with other tracts in the brain in a parallel, hierarchical, but recurrent fashion (Kien and Altman 1992).

We presented anatomical data indicating a large number of DN cell bodies in the GNG cluster and dense DN arborization in the subesophageal zone, consistent with the prominent role of subesophageal zone in motor control (Kien, Fletcher et al. 1990, Gal and Libersat 2006). Activating or inactivating the neurons in this region of the brain appeared to increase or decrease, respectively, the probability of observing bursts of the Retraction-Protraction type in the metathoracic legs. This agrees with previous studies showed that lesions of the gnathal ganglion appear to reduce leg movements (Gal and Libersat 2006).

5.2.3 A subset of DNs tuned to sensory stimuli may be involved in movement initiation

We present in this study evidence that AOTU DNs are broadly tuned to sensory stimuli, and that those located in the ventral cluster typically innervate both the LAL and the leg neuromeres. Thus, these DNs are ideal candidates for relaying some sensory information, which may include the output from the central complex, to the circuits in the thoracic ganglia.

There are several remaining questions related to the inputs to the AOTU DNs, especially those in the ventral subcluster. The AOTU DNs have strong responses to visual stimuli, especially broad field stimuli such as translating gratings or progressive and regressive optic flow. However, it is unclear whether the ventral AOTU DNs receive

their visual information from the central complex, as opposed to other parts of the brain. For instance, the optic tubercle has significant projections into the LAL in *Drosophila* as well as other insects (Yang, Awasaki et al. 2013, Namiki, Iwabuchi et al. 2014). Previous studies in the moth have also heavily implicated the role of flip-flopping LAL-DNs, which appear anatomically very similar to the AOTU DNs, in turning in response to pheromones (Mishima and Kanzaki 1999, Namiki, Iwabuchi et al. 2014).

Because our preliminary anatomical results using dendritic and presynaptic markers show that at least some of these DNs appear to send axons to innervate the inferior posterior slope, we suspect that DNs in the GNG cluster may either directly or indirectly receive inputs from these DNs. Thus, we propose a model in which movement initiation is provided by the AOTU DNs, while the ongoing cycle to cycle bursting may be mediated by the GNG DNs.

The two different patterns of innervation in the leg neuromeres may also indicate control of different joints and consequently different burst states. The axonal projection of type 2 ventral AOTU DNs overlaps with the region of the leg neuromeres that also contains the dendritic arbors of many motor neurons controlling the coxa and the femur (Baek and Mann 2009). Thus, we speculate that depolarization of type 2 ventral AOTU DNs may be responsible for movement of the coxa. This includes Retraction-Protraction type movements, which are not only the most commonly observed burst type but also the axis of motion that is observed during movement initiation. In contrast, type 1

ventral AOTU DNs innervate the dorsal half of the leg neuromeres, overlapping with the dendritic arbors of motor neurons that control the tibia. Thus, we predict that depolarization in these DNs may correspond to states that involve extension or flexion of the ipsilateral legs.

5.2.4 Putative roles of DNs in other clusters

Unlike the DNs presented here, many previously characterized DNs in insects are tuned to very specific sensory stimuli. Many of these DNs are found in the SMP cluster and include the descending neurons of the ocellar and vertical system (DNOVs) (Wertz, Gaub et al. 2009), the descending contralateral motion detector (DCMD) (Fotowat, Harrison et al. 2011), and the target selective descending neurons (TSDNs) (Gonzalez-Bellido, Peng et al. 2013). The TSDNs are a particularly interesting example of a sensory specific DN, as they process behaviorally relevant sensory information (visual stimuli resembling prey) and relay information directly to the wing motor centers using a population vector representation. They may function similarly to similar to the DNs responsible for reaching behavior in the vertebrate corticospinal tract.

Here we present experiments in which we activated the right, middle, and left portion of the part of the brain over which the SMP cluster is distributed. Activating the dorsal right side of the brain (where the right half of the SMP cluster was located) reduced the fraction of cycles that were of the retraction protraction type in both the right mesothoracic and the left metathoracic legs. Though not conclusive, this suggests

that activation of the SMP DNs may have an effect on leg movements than what is observed when the GNG is activated. In other words, activating SMP DNs reduces the probability that the legs engage in their typical motor behavior. When taken in conjunction with the fact that these DNs have been previously implicated in many flight related behaviors, the data presented here suggests that the large number of inhibitory GABAergic DNs in this cluster may play a role in suppressing leg movements in favor of wing movements. However, more careful anatomical and functional characterization is necessary before making this conclusion.

Appendix A: Neurotransmitter Specific DNs by Cluster

The following tables present the numbers of DNs found of each neurotransmitter type using the strategy described in Section 2.4.

Table 8 : Octopaminergic DNs labeled using Tdc2-Gal4

Cluster Name	Mean \pm SD	Median	Max
AOTU (n=8) ²	0	0	0
AVLP (n=8)	0.86 \pm 1.1	0	2 (per hemisphere)
PENP (n=4)	1.5 \pm 1.7	1.5	3
PI (n=4)	0	0	0
SMP (n=4)	0	0	0
Medial GNG (n=4)	4 \pm 1.4	4.5	5
Lateral GNG (n = 8)	0	0	0
Total (n=4)	6.5 \pm 1.3	7.5	9

Table 9 : Serotonergic and Dopaminergic DNs labeled using Ddc-Gal4

Cluster Name	Mean \pm SD	Median	Max
AOTU (n=8)	0	0	0
AVLP (n=8)	0	0	0
PENP (n=8)	0	0	0
PI (n=4)	0.5 \pm 0.6	0.5	1
SMP (n=8) ³	4.5 \pm 2.4	4	9 (per hemisphere)
Medial GNG (n=4)	3.25 \pm 1.5	3	5
Lateral GNG (n=8)	2 \pm 1.3	2	4
Total	16.8 \pm 2.4	16.5	20

² For AOTU and avPB clusters, the n is listed as the number of hemispheres, rather than brains.

³ In the case of minor neurotransmitters where there were relatively few DNs labeled, divisions between genetically labeled DNs located on the left versus the right hemisphere were easily distinguished. Thus, the n is listed as the number of hemispheres, rather than brains (n=10 instead of n=5).

Table 10 : Glutamatergic DNs labeled using VGlut-Gal4

Cluster Name	Mean \pm SD	Median	Max
AOTU (n=6)	0	0	0
AVLP (n=6)	2.2 \pm 2.0	2	5 (per hemisphere)
PENP (n=6)	0	0	0
PI (n=3)	2 \pm 1	2	3
SMP (n=6)	4.7 \pm 2.3	4	9 (per hemisphere)
Medial GNG (n=3)	14 \pm 5.6	13	20
Lateral GNG (n=6)	4 \pm 2.1	3.5	8 (per hemisphere)

Table 11 : GABAergic DNs labeled using a GABA antibody

Cluster Name	Mean \pm SD Fraction Colabeled	Median Fraction Colabeled	Max Cell Bodies Colabeled/Total Bulk Labeled for that Cluster (in an individual fly)	Cell bodies colabeled/Max bulk labeled (in an individual fly)
AOTU (n=6)	0.144 \pm 0.078	0.133	4/17	2/20
AVLP (n=6)	0.150 \pm 0.168	0.183	$\frac{3}{4}$	2/8
PENP (n=3)	0.182 \pm 0.257	0.182	4/11	4/11
PI (n=3)	0.242 \pm 0.094	0.231	14/41	14/41
SMP (n=4)	0.468 \pm 0.149	0.469	107/165	107/165
Medial GNG (n=3) ⁴	0.309 \pm 0.047	0.315	35/99	26/100
Lateral GNG (n=6)	0.132 \pm 0.156	0.136	14/95	14/95

Table 12 : Cholinergic DNs labeled by Cha-Gal4 driver

Cluster Name	Mean \pm SD Fraction Colabeled	Median Fraction Colabeled	Max Cell Bodies Colabeled/Total Bulk Labeled for that Cluster (in an individual fly)	Cell bodies colabeled/Max bulk labeled (in an individual fly)
AOTU (n=8)	0.577 \pm 0.167	0.577	12/15	12/18

⁴ Because the division between the medial and lateral GNG is not clear, the distinction between GABAergic and cholinergic DNs in the medial and lateral GNG are approximate.

AVLP (n=6)	0.350 ± 0.136	0.303	3/5	3/11
PENP (n=3)	0.645 ± 0.233	0.529	11/12	10/20
PI (n=3)	0.286 ± 0.094	0.313	5/16	4/22
SMP (n=3)	0.246 ± 0.142	0.327	76/231	76/231
Medial GNG (n=3)	0.404 ± 0.108	0.436	51/180	51/180
Lateral GNG (n=6)	0.412 ± 0.132	0.400	44/108	38/108

Appendix B: Neuronal activation and inactivation by P2X2 and ort

Flies were anesthetized briefly on ice and transferred to a custom made chamber. Gaps between the head and the foil and the thorax and the foil were sealed in place with candle wax. Wings were removed. The posterior surface of the head and body was immersed in external saline (103 mM NaCl, 5 mM KCl, 5 mM Tris, 10 mM glucose, 26 mM NaHCO₃, 1 mM NaH₂P0₄, 1.5 mM CaCl₂, 4 mM MgCl₂, osmolarity adjusted to 270-285 mOsm, bubbled with 95% O₂/5% CO₂ to pH 7.1-7.4).

For activation and inactivation of neurons located in the SMP cluster, the head was tilted such that the b-posterior surface of the head, b-dorsal to the neck, was almost parallel with the plane of the foil. Forceps were used to remove the cuticle covering the b-posterior surface of the brain. For activation and inactivation of neurons located in the GNG cluster, the head position was positioned as described in Tschida and Bhandawat (Tschida and Bhandawat 2015). Trials in which the drug was delivered were interleaved with no drug trials.

To confirm the magnitude and the duration of the response elicited by drug delivery, whole cell patch clamp recording was performed in flies which did not have balls glued their legs. Glass electrodes were filled with internal solution (140 mM K-aspartate, 1 mM KCl, 10 mM HEPES, 1 mM EGTA, 0.5 mM Na₃GTP, 4 mM MgATP, 265-

270 mOsm, pH 7.1-7.4, 1% neurobiotin). Voltage was recorded at 10 kHz using a model 2400 patch-clamp amplifier (A-M systems) and low-pass filtered at 5 kHz.

Different drug concentrations, pipette diameters, and delivery durations were varied until a diameter roughly equivalent to one third of the brain, which was ~300 μm wide when fixed, was reached. This diameter was chosen so that the left, right, and middle SMP cluster could be activated or inactivated separately from other regions in the SMP, and so that the neuron would be activated or inactivated for roughly 3 seconds (Figure 27 and Figure 28). For activating and inactivating the GNG clusters, the same drug delivery conditions were used.

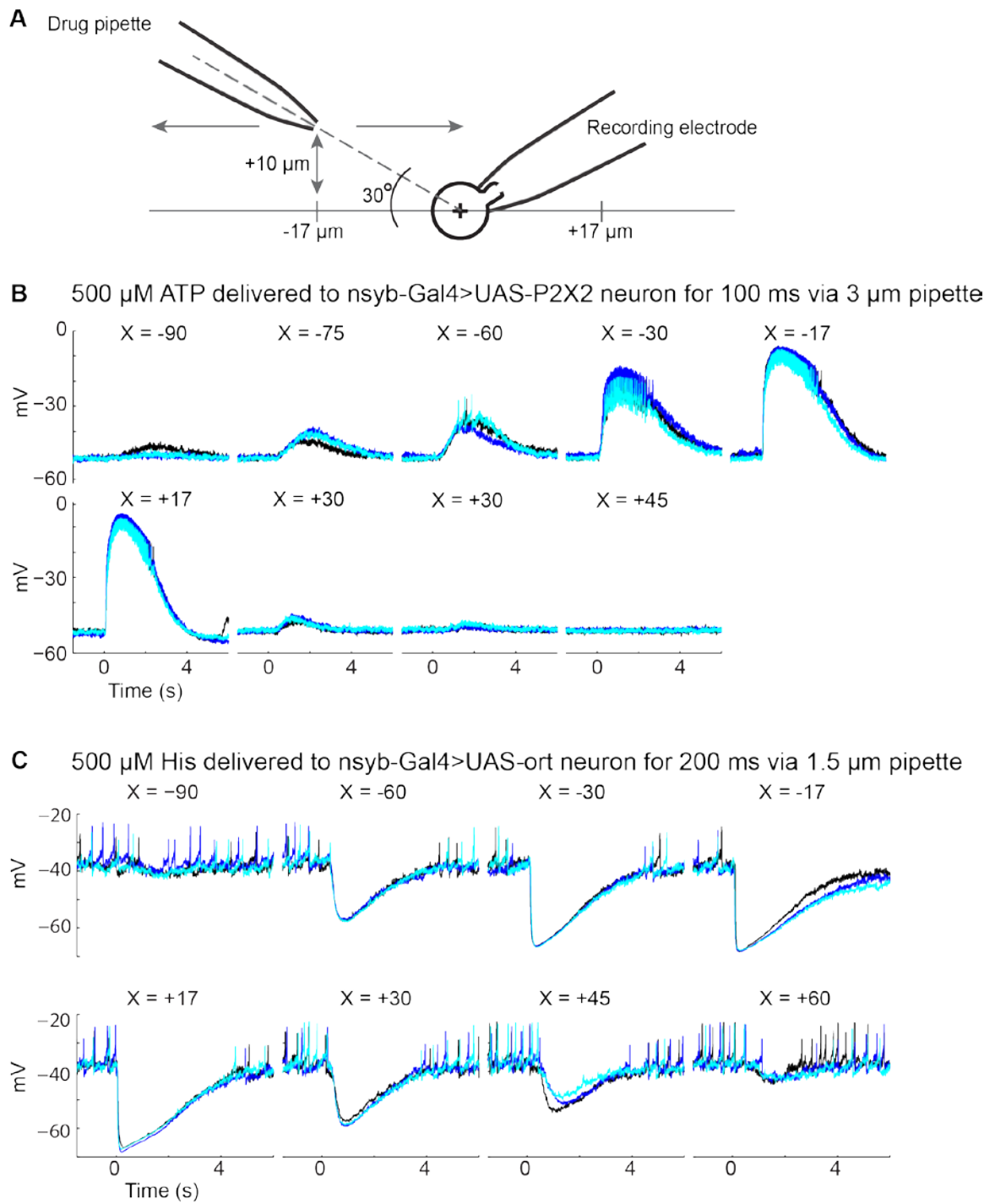


Figure 28 : Representative examples of the effect of (B) ATP and (C) His on neuronal activation and inactivation for a single cell. Each color represents a different trial. The Drug was delivered at time=0. Diagram in (A) illustrates where the position indicated by

the variable X is located relative to the position of the pipette. This schematic is not drawn to scale.

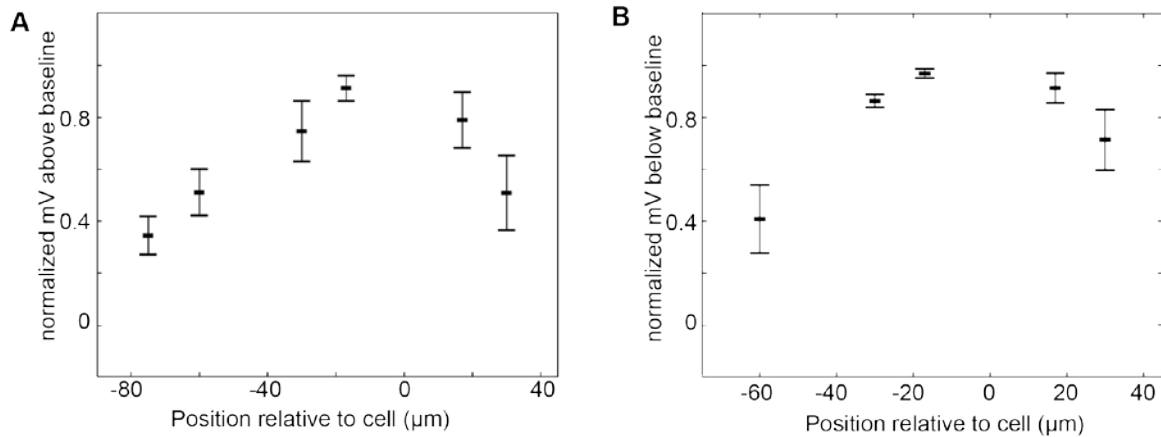


Figure 29 : Mean and SEM data for effects of ATP activation (A) and His inactivation (B). (A) For each neuron (n=6), the average response to ATP over the three trials recorded at each position of the drug pipette was computed. The peak response at each position was then normalized by the peak response overall. (B) Same as for (A), except that the peak refers to the lowest voltage (or the largest magnitude of hyperpolarization). n=5.

Because the number of bursting bouts we observed during the drug delivery conditions described in Figure 27 and Figure 28 was low, we decided to change the conditions for the experiments in which we used the VT50660 Gal4 driver such that the neurons would be activated for a much longer time period. We recorded from one GFP+ neuron in a fly of the genotype *UAS-mCD8-GFP/+; VT50660/UAS-P2X2*, and found that delivering 250 μM ATP through a 2 μM glass pipette ($R_{input}=5-6 \text{ M}\Omega$) 10 μm above the surface of the posterior dorsal surface of the brain was sufficient to produce a depolarization of at least 30 mV and subsequently an increase in firing rate for at least 5 seconds (Figure 29). Based on these results, we chose to deliver ATP to the middle of the

SMP cluster for 10 seconds, and assumed that the neurons were activated for 15 seconds following the onset of drug delivery. This is most likely a conservative assumption.

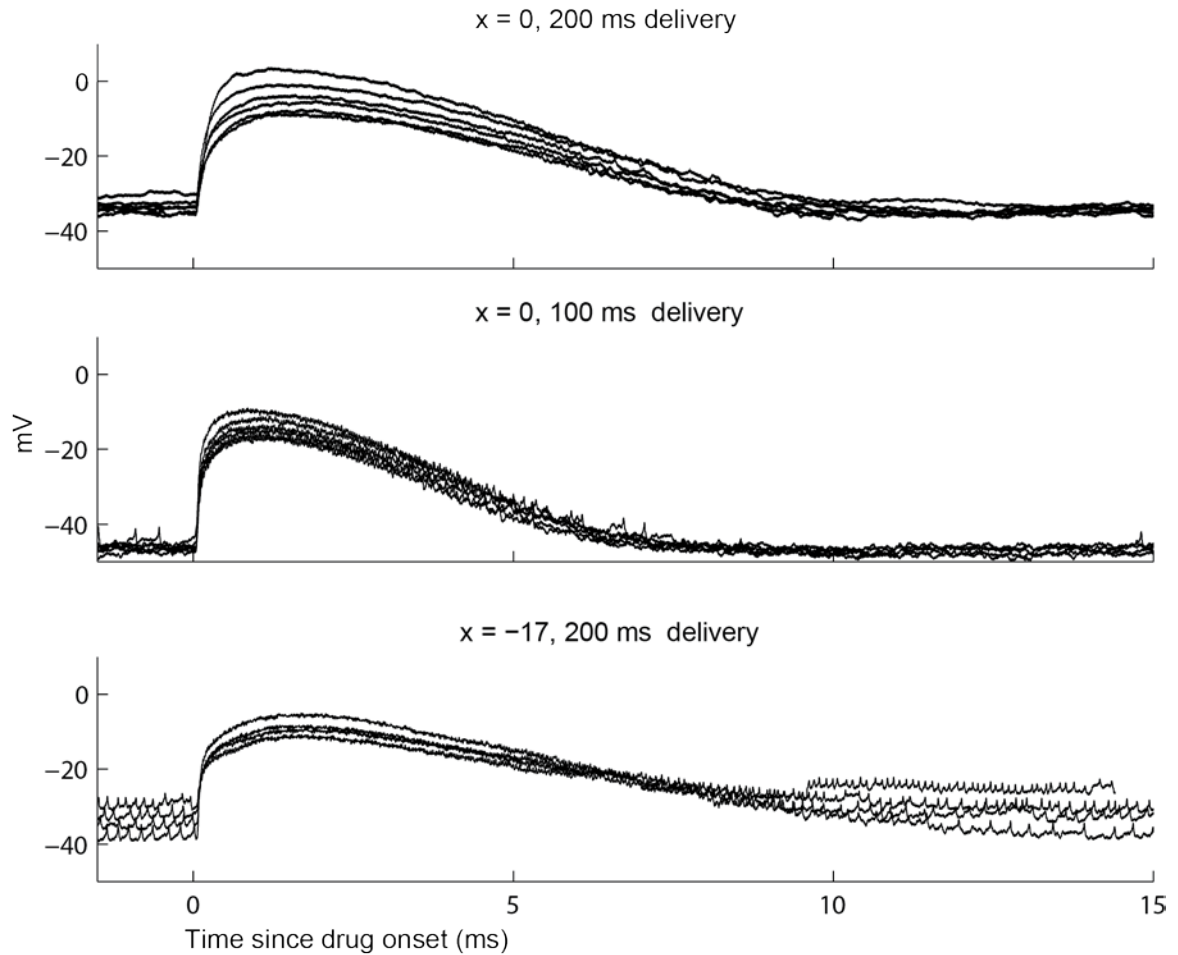


Figure 30 : Response of a GFP+ neuron in a fly of genotype *UAS-mCD8-GFP/+; VT50660/UAS-P2X2* to ATP. Time and position as indicated in the title.

Appendix C: Visual stimuli

To test the visual response of AOTU DNs, stimuli were presented on a paper screen that was 16.5 cm long and 5.5 cm high. The screen was curved such that it formed an arc with an angle of 139° . The center of the screen was 5 cm away from the fly. This resulted in a field of view of 169.8° (Figure 30). Images were projected onto the screen using an Optoma Pico PK301 Projector.

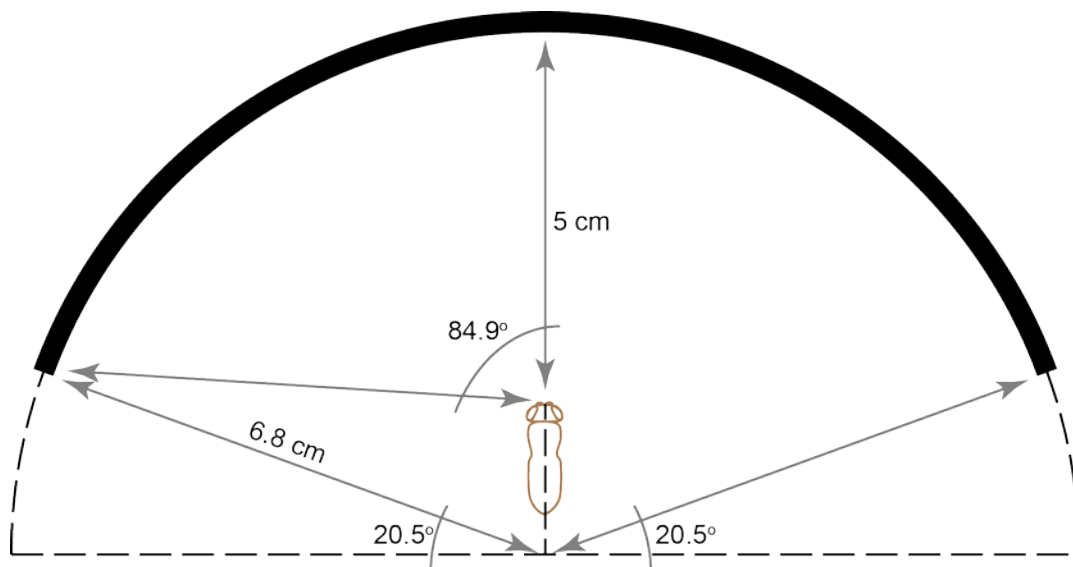


Figure 31 : Schematic showing the position of the screen relative to the fly. The screen is represented by the solid black line. Schematic not drawn to scale.

We tested the response of AOTU DNs to the following stimuli: gratings moving in one of the eight cardinal directions, progressive and regressive optic flow grating, a rotating grating, a small horizontal bar, a tall vertical bar, and visually looming

expanding squares that approach from one of three directions (left 75°, middle, or right 75°).

Grating stimuli were presented with a spatial width of 22.5° and a temporal frequency of 6 Hz, which was chosen to match the stimuli at which the ratio of the calicum response in the Horizontal System neurons of a walking fly relative to that of a stationary fly was at its highest (Chiappe, Seelig et al. 2010). For the visually expanding stimuli, we used size-to-speed ratio $r/v = 50$, since this is midway between the range of size-to-speed used to test the difference between voluntary and involuntary escape (von Reyn, Breads et al. 2014).

References

- Alstermark, B. and C. F. Ekerot (2015). "The lateral reticular nucleus; integration of descending and ascending systems regulating voluntary forelimb movements." Front Comput Neurosci **9**: 102.
- Baek, M. and R. S. Mann (2009). "Lineage and birth date specify motor neuron targeting and dendritic architecture in adult *Drosophila*." J Neurosci **29**(21): 6904-6916.
- Bässler, U. (1983). Neural basis of elementary behavior in stick insects, Springer London, Limited.
- BÄSSLER, U. and U. T. A. WEGNER (1983). "Motor Output of the Denervated Thoracic Ventral Nerve Cord in the Stick Insect *Carausius Morosus*." Journal of Experimental Biology **105**(1): 127-145.
- Belanger, J. H. (2005). "Contrasting tactics in motor control by vertebrates and arthropods." Integr Comp Biol **45**(4): 672-678.
- Bellardita, C. and O. Kiehn (2015). "Phenotypic characterization of speed-associated gait changes in mice reveals modular organization of locomotor networks." Curr Biol **25**(11): 1426-1436.
- Bender, J. A., E. M. Simpson, B. R. Tietz, K. A. Daltorio, R. D. Quinn and R. E. Ritzmann (2011). "Kinematic and behavioral evidence for a distinction between trotting and ambling gaits in the cockroach *Blaberus discoidalis*." J Exp Biol **214**(Pt 12): 2057-2064.
- Berens, P. (2009). "CircStat: A MATLAB Toolbox for Circular Statistics." 2009 **31**(10): 21.
- Berg, E. M., S. L. Hooper, J. Schmidt and A. Buschges (2015). "A leg-local neural mechanism mediates the decision to search in stick insects." Curr Biol **25**(15): 2012-2017.
- Bicker, G., S. Schafer, O. P. Ottersen and J. Storm-Mathisen (1988). "Glutamate-like immunoreactivity in identified neuronal populations of insect nervous systems." J Neurosci **8**(6): 2108-2122.
- Bidaye, S. S., C. Machacek, Y. Wu and B. J. Dickson (2014). "Neuronal control of *Drosophila* walking direction." Science **344**(6179): 97-101.

- Blaesing, B. and H. Cruse (2004). "Stick insect locomotion in a complex environment: climbing over large gaps." J Exp Biol **207**(Pt 8): 1273-1286.
- Borgmann, A., S. L. Hooper and A. Buschges (2009). "Sensory feedback induced by front-leg stepping entrains the activity of central pattern generators in caudal segments of the stick insect walking system." J Neurosci **29**(9): 2972-2983.
- Briggman, K. L., H. D. Abarbanel and W. B. Kristan, Jr. (2005). "Optical imaging of neuronal populations during decision-making." Science **307**(5711): 896-901.
- Busch, S., M. Selcho, K. Ito and H. Tanimoto (2009). "A map of octopaminergic neurons in the Drosophila brain." J Comp Neurol **513**(6): 643-667.
- Buschges, A. (2005). "Sensory control and organization of neural networks mediating coordination of multisegmental organs for locomotion." J Neurophysiol **93**(3): 1127-1135.
- Buschges, A., H. Scholz and A. El Manira (2011). "New Moves in Motor Control." Current Biology **21**(13): R513-R524.
- Chiappe, M. E., J. D. Seelig, M. B. Reiser and V. Jayaraman (2010). "Walking modulates speed sensitivity in Drosophila motion vision." Curr Biol **20**(16): 1470-1475.
- Chittka, L. and J. Niven (2009). "Are Bigger Brains Better?" Current Biology **19**(21): R995-R1008.
- Chrachri, A. and F. Clarac (1990). "Fictive locomotion in the fourth thoracic ganglion of the crayfish, *Procambarus clarkii*." J Neurosci **10**(3): 707-719.
- Clarac, F., D. Cattaert and D. Le Ray (2000). "Central control components of a 'simple' stretch reflex." Trends Neurosci **23**(5): 199-208.
- Cordoba, S. and C. Estella (2014). "The bHLH-PAS transcription factor *dysfusion* regulates tarsal joint formation in response to Notch activity during drosophila leg development." PLoS Genet **10**(10): e1004621.
- Cruse, H. (2002). "The functional sense of central oscillations in walking." Biol Cybern **86**(4): 271-280.
- de Velasco, B., T. Erclik, D. Shy, J. Sclafani, H. Lipshitz, R. McInnes and V. Hartenstein (2007). "Specification and development of the pars intercerebralis and pars

- lateralis, neuroendocrine command centers in the Drosophila brain." Dev Biol **302**(1): 309-323.
- Dietz, V. (2003). "Spinal cord pattern generators for locomotion." Clin Neurophysiol **114**(8): 1379-1389.
- Drew, T., S. Prentice and B. Schepens (2004). "Cortical and brainstem control of locomotion." Prog Brain Res **143**: 251-261.
- Du Beau, A., S. S. Shrestha, B. A. Bannatyne, S. M. Jality, S. Linnen and D. J. Maxwell (2012). "Neurotransmitter Phenotypes of Descending Systems in the Rat Lumbar Spinal Cord." Neuroscience **227**: 67-79.
- Durr, V. (2001). "Stereotypic leg searching movements in the stick insect: kinematic analysis, behavioural context and simulation." J Exp Biol **204**(Pt 9): 1589-1604.
- Enell, L., Y. Hamasaka, A. Kolodziejczyk and D. R. Nassel (2007). "gamma-Aminobutyric acid (GABA) signaling components in Drosophila: immunocytochemical localization of GABA(B) receptors in relation to the GABA(A) receptor subunit RDL and a vesicular GABA transporter." J Comp Neurol **505**(1): 18-31.
- Fotowat, H., R. R. Harrison and F. Gabbiani (2011). "Multiplexing of motor information in the discharge of a collision detecting neuron during escape behaviors." Neuron **69**(1): 147-158.
- Gal, R. and F. Libersat (2006). "New vistas on the initiation and maintenance of insect motor behaviors revealed by specific lesions of the head ganglia." J Comp Physiol A Neuroethol Sens Neural Behav Physiol **192**(9): 1003-1020.
- Garcia-Alonso, L., R. D. Fetter and C. S. Goodman (1996). "Genetic analysis of Laminin A in Drosophila: extracellular matrix containing laminin A is required for ocellar axon pathfinding." Development **122**(9): 2611-2621.
- Gonzalez-Bellido, P. T., H. Peng, J. Yang, A. P. Georgopoulos and R. M. Olberg (2013). "Eight pairs of descending visual neurons in the dragonfly give wing motor centers accurate population vector of prey direction." Proc Natl Acad Sci U S A **110**(2): 696-701.
- Gosgnach, S., G. M. Lanuza, S. J. Butt, H. Saueressig, Y. Zhang, T. Velasquez, D. Riethmacher, E. M. Callaway, O. Kiehn and M. Goulding (2006). "V1 spinal

- neurons regulate the speed of vertebrate locomotor outputs." Nature **440**(7081): 215-219.
- GRAHAM, D. and H. CRUSE (1981). "Coordinated Walking of Stick Insects on a Mercury Surface." Journal of Experimental Biology **92**(1): 229-241.
- Grillner, S. (1973). Locomotion in the Spinal Cat. Control of Posture and Locomotion. R. B. Stein, K. G. Pearson, R. S. Smith and J. B. Redford. Boston, MA, Springer US: 515-535.
- Grillner, S. (2006). "Biological pattern generation: the cellular and computational logic of networks in motion." Neuron **52**(5): 751-766.
- Grillner, S., P. Wallen, K. Saitoh, A. Kozlov and B. Robertson (2008). "Neural bases of goal-directed locomotion in vertebrates--an overview." Brain Res Rev **57**(1): 2-12.
- Homberg, U. and J. G. Hildebrand (1989). "Serotonin-immunoreactive neurons in the median protocerebrum and suboesophageal ganglion of the sphinx moth *Manduca sexta*." Cell Tissue Res **258**(1): 1-24.
- Homberg, U., T. G. Kingan and J. G. Hildebrand (1990). "Distribution of FMRFamide-like immunoreactivity in the brain and suboesophageal ganglion of the sphinx moth *Manduca sexta* and colocalization with SCPB-, BPP-, and GABA-like immunoreactivity." Cell Tissue Res **259**(3): 401-419.
- Hooper, S. L., C. Guschlbauer, M. Blumel, P. Rosenbaum, M. Gruhn, T. Akay and A. Buschges (2009). "Neural control of unloaded leg posture and of leg swing in stick insect, cockroach, and mouse differs from that in larger animals." J Neurosci **29**(13): 4109-4119.
- Hooper, S. L., C. Guschlbauer, G. von Uckermann and A. Buschges (2006). "Natural neural output that produces highly variable locomotory movements." J Neurophysiol **96**(4): 2072-2088.
- Hosie, A. M., K. Aronstein, D. B. Sattelle and R. H. ffrench-Constant (1997). "Molecular biology of insect neuronal GABA receptors." Trends Neurosci **20**(12): 578-583.
- Hsu, C. T. and V. Bhandawat (2016). "Organization of descending neurons in *Drosophila melanogaster*." Scientific Reports **6**: 20259.
- Hsu, C. T. and V. Bhandawat (2016). "Organization of descending neurons in *Drosophila melanogaster*." Sci Rep **6**: 20259.

- Isa, T., Y. Ohki, B. Alstermark, L. G. Pettersson and S. Sasaki (2007). "Direct and indirect cortico-motoneuronal pathways and control of hand/arm movements." Physiology (Bethesda) **22**: 145-152.
- Ito, K., K. Shinomiya, M. Ito, J. D. Armstrong, G. Boyan, V. Hartenstein, S. Harzsch, M. Heisenberg, U. Homberg, A. Jenett, H. Keshishian, L. L. Restifo, W. Rössler, J. H. Simpson, N. J. Strausfeld, R. Strauss, L. B. Vosshall and G. Insect Brain Name Working (2014). "A systematic nomenclature for the insect brain." Neuron **81**(4): 755-765.
- Jung, S. H., C. Hueston and V. Bhandawat (2015). "Odor-identity dependent motor programs underlie behavioral responses to odors." Elife **4**.
- Kamikouchi, A., H. K. Inagaki, T. Effertz, O. Hendrich, A. Fiala, M. C. Gopfert and K. Ito (2009). "The neural basis of *Drosophila* gravity-sensing and hearing." Nature **458**(7235): 165-171.
- Kiehn, O. (2011). "Development and functional organization of spinal locomotor circuits." Curr Opin Neurobiol **21**(1): 100-109.
- Kien, J. and J. S. Altman (1992). "Preparation and execution of movement: parallels between insect and mammalian motor systems." Comp Biochem Physiol Comp Physiol **103**(1): 15-24.
- Kien, J., W. A. Fletcher, J. S. Altman, J. M. Ramirez and U. Roth (1990). "Organization of Intersegmental Interneurons in the Subesophageal Ganglion of *Schistocerca gregaria* (Forsk.) and *Locusta migratoria migratorioides* (Reiche and Fairmaire) (Acrididae, Orthoptera)." International Journal of Insect Morphology & Embryology **19**(1): 35-60.
- Koenig, J. H. and K. Ikeda (2005). "Relationship of the reserve vesicle population to synaptic depression in the tergotrochanteral and dorsal longitudinal muscles of *Drosophila*." J Neurophysiol **94**(3): 2111-2119.
- Kolodziejczyk, A., X. Sun, I. A. Meinertzhagen and D. R. Nassel (2008). "Glutamate, GABA and acetylcholine signaling components in the lamina of the *Drosophila* visual system." PLoS One **3**(5): e2110.
- Kristan, W. B. (2008). "Neuronal decision-making circuits." Curr Biol **18**(19): R928-932.

- Labandeira, C. C. and T. L. Phillips (1996). "A Carboniferous insect gall: insight into early ecologic history of the Holometabola." Proc Natl Acad Sci U S A **93**(16): 8470-8474.
- Lee, C. H., S. J. Blackband and P. Fernandez-Funez (2015). "Visualization of synaptic domains in the Drosophila brain by magnetic resonance microscopy at 10 micron isotropic resolution." Scientific Reports **5**.
- Lemon, R. N. (2008). "Descending pathways in motor control." Annual Review of Neuroscience **31**: 195-218.
- Lima, S. Q. and G. Miesenbock (2005). "Remote control of behavior through genetically targeted photostimulation of neurons." Cell **121**(1): 141-152.
- Liu, G., H. Seiler, A. Wen, T. Zars, K. Ito, R. Wolf, M. Heisenberg and L. Liu (2006). "Distinct memory traces for two visual features in the Drosophila brain." Nature **439**(7076): 551-556.
- Liu, W. W., O. Mazor and R. I. Wilson (2015). "Thermosensory processing in the Drosophila brain." Nature **519**(7543): 353-+.
- Liu, W. W. and R. I. Wilson (2013). "Transient and specific inactivation of Drosophila neurons in vivo using a native ligand-gated ion channel." Curr Biol **23**(13): 1202-1208.
- Ludwar, B., M. L. Goritz and J. Schmidt (2005). "Intersegmental coordination of walking movements in stick insects." J Neurophysiol **93**(3): 1255-1265.
- Marder, E. (2012). "Neuromodulation of Neuronal Circuits: Back to the Future." Neuron **76**(1): 1-11.
- Marder, E. and D. Bucher (2001). "Central pattern generators and the control of rhythmic movements." Curr Biol **11**(23): R986-996.
- Mares, S., L. Ash and W. Gronenberg (2005). "Brain allometry in bumblebee and honey bee workers." Brain Behavior and Evolution **66**(1): 50-61.
- McClellan, A. D. (1988). "Functional regeneration of descending brainstem command pathways for locomotion demonstrated in the in vitro lamprey CNS." Brain Res **448**(2): 339-345.

- Mendes, C. S., I. Bartos, T. Akay, S. Marka and R. S. Mann (2013). "Quantification of gait parameters in freely walking wild type and sensory deprived *Drosophila melanogaster*." Elife **2**: e00231.
- Mishima, T. and R. Kanzaki (1999). "Physiological and morphological characterization of olfactory descending interneurons of the male silkworm moth, *Bombyx mori*." Journal of Comparative Physiology A **184**(2): 143-160.
- Mizunami, M. (1995). "Morphology of higher-order ocellar interneurons in the cockroach brain." J Comp Neurol **362**(2): 293-304.
- Mizunami, M. (1995). "Neural organization of ocellar pathways in the cockroach brain." J Comp Neurol **352**(3): 458-468.
- Mu, L., J. P. Bacon, K. Ito and N. J. Strausfeld (2014). "Responses of *Drosophila* giant descending neurons to visual and mechanical stimuli." The Journal of experimental biology **217**(12): 2121-2129.
- Namiki, S., S. Iwabuchi, P. Pansopha Kono and R. Kanzaki (2014). "Information flow through neural circuits for pheromone orientation." Nat Commun **5**: 5919.
- Nassel, D. R. (1988). "Serotonin and serotonin-immunoreactive neurons in the nervous system of insects." Prog Neurobiol **30**(1): 1-85.
- Nassel, D. R., O. I. Kubrak, Y. Liu, J. Luo and O. V. Lushchak (2013). "Factors that regulate insulin producing cells and their output in *Drosophila*." Front Physiol **4**: 252.
- Neuser, K., T. Triphan, M. Mronz, B. Poeck and R. Strauss (2008). "Analysis of a spatial orientation memory in *Drosophila*." Nature **453**(7199): 1244-1247.
- Nicolai, L. J., A. Ramaekers, T. Raemaekers, A. Drozdzecki, A. S. Mauss, J. Yan, M. Landgraf, W. Annaert and B. A. Hassan (2010). "Genetically encoded dendritic marker sheds light on neuronal connectivity in *Drosophila*." Proc Natl Acad Sci U S A **107**(47): 20553-20558.
- Notvest, R. R. and C. H. Page (1981). "Anatomical Organization of Neurons Descending from the Supraesophageal Ganglion of the Lobster." Brain Research **217**(1): 162-168.
- Ofstad, T. A., C. S. Zuker and M. B. Reiser (2011). "Visual place learning in *Drosophila melanogaster*." Nature **474**(7350): 204-U240.

- Okada, R., M. Sakura and M. Mizunami (2003). "Distribution of dendrites of descending neurons and its implications for the basic organization of the cockroach brain. (vol 458, pg 158, 2003)." Journal of Comparative Neurology **459**(3): 327-+.
- Otsuna, H. and K. Ito (2006). "Systematic analysis of the visual projection neurons of *Drosophila melanogaster*. I. Lobula-specific pathways." J Comp Neurol **497**(6): 928-958.
- Pearson, K. G., H. Acharya and K. Fouad (2005). "A new electrode configuration for recording electromyographic activity in behaving mice." J Neurosci Methods **148**(1): 36-42.
- Poeck, B., T. Triphan, K. Neuser and R. Strauss (2008). "Locomotor control by the central complex in *Drosophila*-An analysis of the tay bridge mutant." Dev Neurobiol **68**(8): 1046-1058.
- Rajashekhar, K. P. and R. N. Singh (1994). "Neuroarchitecture of the tritocerebrum of *Drosophila melanogaster*." J Comp Neurol **349**(4): 633-645.
- Salvaterra, P. M. and T. Kitamoto (2001). "*Drosophila* cholinergic neurons and processes visualized with Gal4/UAS-GFP." Brain Res Gene Expr Patterns **1**(1): 73-82.
- Satoh, D., C. Pudenz and S. Arber (2016). "Context-Dependent Gait Choice Elicited by EphA4 Mutation in Lbx1 Spinal Interneurons." Neuron **89**(5): 1046-1058.
- Sattelle, D. B., S. C. Lummis, J. F. Wong and J. J. Rauh (1991). "Pharmacology of insect GABA receptors." Neurochem Res **16**(3): 363-374.
- Schürmann, F. (1987). "The architecture of the mushroom bodies and related neuropils in the insect brain." Arthropod Brain: Its Evolution, Structure and Functions: 231-264.
- Seelig, J. D. and V. Jayaraman (2013). "Feature detection and orientation tuning in the *Drosophila* central complex." Nature **503**(7475): 262-266.
- Seelig, J. D. and V. Jayaraman (2015). "Neural dynamics for landmark orientation and angular path integration." Nature **521**(7551): 186-191.
- Semmelhack, J. L. and J. W. Wang (2009). "Select *Drosophila* glomeruli mediate innate olfactory attraction and aversion." Nature **459**(7244): 218-223.

- Shenoy, K. V., M. Sahani and M. M. Churchland (2013). "Cortical control of arm movements: a dynamical systems perspective." Annu Rev Neurosci **36**: 337-359.
- Shiga, S., I. Toyoda and H. Numata (2000). "Neurons projecting to the retrocerebral complex of the adult blow fly, *Protophormia terraenovae*." Cell Tissue Res **299**(3): 427-439.
- Staudacher, E. (1998). "Distribution and morphology of descending brain neurons in the cricket *Gryllus bimaculatus*." Cell and Tissue Research **294**(1): 187-202.
- Strausfeld, N. J. (2012). Arthropod brains: evolution, functional elegance, and historical significance, Belknap Press of Harvard University Press Cambridge, MA.
- Strausfeld, N. J. and W. Gronenberg (1990). "Descending neurons supplying the neck and flight motor of Diptera: organization and neuroanatomical relationships with visual pathways." J Comp Neurol **302**(4): 954-972.
- Strausfeld, N. J. and F. Hirth (2013). "Deep homology of arthropod central complex and vertebrate basal ganglia." Science **340**(6129): 157-161.
- Strausfeld, N. J. and J. Y. Okamura (2007). "Visual system of calliphorid flies: organization of optic glomeruli and their lobula complex efferents." J Comp Neurol **500**(1): 166-188.
- Strausfeld, N. J. and H. S. Seyan (1985). "Convergence of visual, haltere, and prosternal inputs at neck motor neurons of *Calliphora erythrocephala*." Cell and Tissue Research **240**(3): 601-615.
- Strauss, R., U. Hanesch, M. Kinkelin, R. Wolf and M. Heisenberg (1992). "No-bridge of *Drosophila melanogaster*: portrait of a structural brain mutant of the central complex." J Neurogenet **8**(3): 125-155.
- Strauss, R. and M. Heisenberg (1993). "A higher control center of locomotor behavior in the *Drosophila* brain." J Neurosci **13**(5): 1852-1861.
- Thuma, J. B., L. G. Morris, A. L. Weaver and S. L. Hooper (2003). "Lobster (*Panulirus interruptus*) pyloric muscles express the motor patterns of three neural networks, only one of which innervates the muscles." J Neurosci **23**(26): 8911-8920.
- Trager, U. and U. Homberg (2011). "Polarization-sensitive descending neurons in the locust: connecting the brain to thoracic ganglia." J Neurosci **31**(6): 2238-2247.

- Tschida, K. and V. Bhandawat (2015). "Activity in descending dopaminergic neurons represents but is not required for leg movements in the fruit fly *Drosophila*." Physiol Rep **3**(3).
- von Philipsborn, A. C., T. Liu, J. Y. Yu, C. Masser, S. S. Bidaye and B. J. Dickson (2011). "Neuronal control of *Drosophila* courtship song." Neuron **69**(3): 509-522.
- von Reyn, C. R., P. Breads, M. Y. Peek, G. Z. Zheng, W. R. Williamson, A. L. Yee, A. Leonardo and G. M. Card (2014). "A spike-timing mechanism for action selection." Nat Neurosci **17**(7): 962-970.
- Weir, P. T. and M. H. Dickinson (2015). "Functional divisions for visual processing in the central brain of flying *Drosophila*." Proc Natl Acad Sci U S A **112**(40): E5523-5532.
- Wertz, A., B. Gaub, J. Plett, J. Haag and A. Borst (2009). "Robust coding of ego-motion in descending neurons of the fly." J Neurosci **29**(47): 14993-15000.
- Wiegmann, B. M., M. D. Trautwein, J. W. Kim, B. K. Cassel, M. A. Bertone, S. L. Winterton and D. K. Yeates (2009). "Single-copy nuclear genes resolve the phylogeny of the holometabolous insects." BMC Biol **7**: 34.
- Wosnitza, A., T. Bockemuhl, M. Dubbert, H. Scholz and A. Buschges (2013). "Inter-leg coordination in the control of walking speed in *Drosophila*." J Exp Biol **216**(Pt 3): 480-491.
- Yang, J. S., T. Awasaki, H.-H. Yu, Y. He, P. Ding, J.-C. Kao and T. Lee (2013). "Diverse neuronal lineages make stereotyped contributions to the *Drosophila* locomotor control center, the central complex." Journal of Comparative Neurology **521**(12): 2645-2662.
- Yasuyama, K. and P. M. Salvaterra (1999). "Localization of choline acetyltransferase-expressing neurons in *Drosophila* nervous system." Microsc Res Tech **45**(2): 65-79.
- Ye, S. and C. M. Comer (1996). "Correspondence of escape-turning behavior with activity of descending mechanosensory interneurons in the cockroach, *Periplaneta americana*." J Neurosci **16**(18): 5844-5853.
- Zhang, Y. Q., C. K. Rodesch and K. Broadie (2002). "Living synaptic vesicle marker: Synaptotagmin-GFP." genesis **34**(1-2): 142-145.

Zill, S., J. Schmitz and A. Buschges (2004). "Load sensing and control of posture and locomotion." Arthropod Struct Dev **33**(3): 273-286.

Zill, S. N., B. R. Keller, S. Chaudhry, E. R. Duke, D. Neff, R. Quinn and C. Flannigan (2010). "Detecting substrate engagement: responses of tarsal campaniform sensilla in cockroaches." J Comp Physiol A Neuroethol Sens Neural Behav Physiol **196**(6): 407-420.

Biography

Cynthia Tien-Cynn Hsu was born June 26, 1986 in Bellevue, Washington. She graduated from University of California, Berkeley in December 2008 with a dual Bachelor of the Arts in Computer Science and in Molecular and Cellular Biology (biochemistry emphasis). After attaining her undergraduate degree, she worked with Dr. Andrew Steele (then at the California Institute of Technology) to study the phenomenon of food anticipatory activity in mice. Her first author papers published from this time include “Daily timed sexual interaction induces moderate anticipatory activity in mice” and “Palatable meal anticipation in mice” (both in *PLoS One*). During her doctoral work with Dr. Vikas Bhandawat at Duke University, she also published an additional paper, “Organization of descending neurons in *Drosophila melanogaster*” (*Scientific Reports*). Awards she has received include the Chancellor’s Scholarship and the James B. Duke Fellowship from Duke University (2010) and a Computational and Systems Neuroscience (COSYNE) Travel Grant (2015). In the fall of 2016 she will be joining Dr. Amita Sehgal’s laboratory at University of Pennsylvania to study how sleep deprivation, stress, and genetics interact to change behavior using the *Drosophila* model.